Biophysical Investigations of the Interactions between Calmodulin and Nitric Oxide Synthase Enzymes

by

John Edmond Lape

A thesis
presented to the University of Waterloo
in fulfillment of the
thesis requirement for the degree of
Masters of Science
in
Chemistry

Waterloo, Ontario, Canada, 2017

AUTHOR'S DECLARATION

I hereby declare that I am the sole author of this thesis. This is a true copy of the thesis, including any required final revisions, as accepted by my examiners.

I understand that my thesis may be made electronically available to the public.

Abstract

Nitric Oxide (•NO) is an essential biomolecule that has physiological functions in neurotransmission, vasodilation and immune response. •NO is produced by a family of enzymes known as nitric oxide synthases (NOS). NOS catalyze the conversion of L-arginine into L-citrulline and •NO. Due to their physiological relevance, abnormal •NO production by NOS has been linked to several disease states. There are three isoforms found in mammalian cells: neuronal (nNOS), endothelial (eNOS), and inducible (iNOS), each involved in different physiological processes. Both nNOS and eNOS are constitutively expressed and are therefore referred to as cNOS enzymes. In contrast, iNOS is transcriptionally regulated by cytokines in macrophages. NOS are homodimeric proteins comprised of an N-terminal heme-oxygenase domain and a C-terminal flavin-binding reductase domain, linked together via a calmodulin (CaM) binding domain. Lastly, NOS activity is regulated by a small ubiquitous Ca^{2+}-binding protein known as Calmodulin (CaM). Interestingly, cNOS isozymes are Ca^{2+}-dependent in terms of CaM binding, whereas iNOS is Ca^{2+}-independent.

The exact mechanism of CaM's control over •NO production is not yet fully understood. Evidence suggests that CaM triggers a large conformational change in NOS to occur that allow for efficient electron transfer. In addition, past studies have investigated how varying different structures and elements within CaM affect NOS catalytic activity through the use of CaM mutants in NOS activity assays. These assay methods have shown to be expensive, lengthy and labour intensive. There is a need for a more facile and robust method to evaluate NOS-CaM interactions.

In this investigation, the NOS-CaM interaction was further characterized by observing the binding kinetics of previously studied CaM mutant proteins binding to peptides that corresponded to the CaM-binding domain of all three NOS isoforms through the use of a spectroscopic technique known as surface plasmon resonance (SPR). SPR is an optical phenomenon that measures and quantifies the adsorption of compounds onto conducting metal surfaces. This SPR study was used to correlate the binding kinetics of mutant CaM proteins with previous enzyme kinetic investigations.

In addition, we attempted to improve current methods to measure NOS activity through the creation of a NOS electrochemical biosensor. Electrochemical biosensors utilize the catalytic activities of redox enzymes immobilized onto electrode surfaces where the biological activities of these enzymes are converted into measurable electrical signals. However, there is evidence of current electrochemical platforms that show denaturation of these redox enzymes when directly immobilized

on electrode surfaces. As a way to circumvent the known denaturation of these electrode immobilized enzymes, we used a modified CaM protein tether to indirectly immobilize NOS enzymes. We used the SPR platform as a preliminary immobilization test for NOS, but overall, we were not able to achieve specific binding. The development of a viable NOS electrochemical biosensor would allow for a high throughput method to measure NOS activity.

Acknowledgements

I would like to thank my supervisor, Dr. Guy Guillemette, for his continual guidance, support, and bountiful patience throughout my studies. I am truly grateful for the opportunity to work in his lab and the tutelage he provided me.

Thank you to my advisory committee members, Dr. Thorsten Dieckmann and Dr. Juewen Liu, for reading and reviewing my thesis.

I am very grateful for all the people, past and present, that I have gotten to know during my time here as a grad at Waterloo. Shout out to the lab members from the Guillemette and Dieckmann labs for making my time at work fun and enjoyable: Dr. Mike Piazza, Erica Lee, Matthew Nguyen, Kyle Piccolo & Cathy Pham. Big thanks to Rona Dong and Bianca Boboc for their help with the SPR data acquisitions. Special mentions to Volition La and Danica Estavillo for the company during those extremely late nights and for all the food runs. To my other friends and colleagues in the surroundings labs and the department, for their support and friendship. A big special thanks to Dr. Laura Marrone for always being available to talk and being my 2nd mom away from home!

Lastly, special thanks to my family and friends, for their love and support during my studies.…and to Hubert, for always reminding me stay hungry and attack life with purpose.

Dedication

To my parents,

Ramonito and Editha,

for their continual love & support throughout my years of education at Waterloo.

Thank you for always believing in me.

Table of Contents

List of Figures

List of Tables

List of Abbreviations

Apo-CaM	Calcium Free Calmodulin
Ca^{2+}	Calcium
$CaCl_2$	Calcium Chloride
CaM	Calmodulin
CD	Circular Dichroism
cGMP	Cyclic Guanosine Monophosphate
cNOS	Constitutive Nitric Oxide Synthase
cryo-EM	Cryo-Electron Microscopy
CV	Cyclic Voltammetry
CYP	Cytochrome P450
CYPOR	Cytochrome P450 oxidoreductase
DTT	Dithiothreitol
EM	Electron Microscopy
eNOS	Endothial Nitric Oxide Synthase
ESI	Electrospray Ionization
ET	Electron Transfer
FAD	Flavin Adenine Dinucleotide
FMN	Flavin Mononucleotide
FPLC	Fast Protein Liquid Chromatography
FRET	Fluorescence Resonance Energy Transfer
H_4B	(6R)-5,6,7,8-tetrahydrobiopterin
Hb	Hemoglobin
Holo-CaM	Calcium Saturated Calmodulin
HuCaM CtermCys	C-terminal cysteine labelled Calmodulin
iNOS	Inducible Nitric Oxide Synthase
ITC	Isothermal Titration Calorimetry
IPTG	Isopropyl B-D-1-thiogalactopyranoside
L-Arg	L-Arginine
LB	Lysogeny Broth
L-NOHA	N-ω-hydroxy-L-arginine
L-SPR	Localized Surface Plasmon Resonance
metHb	Oxidized Hemoglobin
MS	Mass Spectrometry
NANC	Nonadregernic-Noncholinergenic
•NO	Nitric Oxide
NOS	Nitric Oxide Synthase
NOSoxyCaM	Truncated Nitric Oxide Synthase Oxygenase Domain with the Calmodulin binding-site Domain
NSB	Non-specific Binding
O_2^-	Superoxide
OD	Optical Density
$ONOO^-$	Peroxynitrite
oxyHb	Reduced Hemoglobin
nNOS	Neuronal Nitric Oxide Synthase
PDZ	PSD-95 Discs Large/ZO-1 Homology
PSD	Post Synaptic Density Protein
QTOF	Quadrupole Time of Flight
RNS	Reactive Nitrogen Species

ROS	Reactive Oxygen Species
SPR	Surface Plasmon Resonance
TB	Terrific Broth
TnC	Troponin
XRD	X-ray Diffracti

Chapter 1
Literature Review

1.1 Nitric Oxide in Biological Organisms

The works of R. Furchgott, L. Ignarro and F. Murad in the 1980's led to the discovery, identification and characterization of nitric oxide (•NO) as an important signalling molecule. •NO is a gaseous, highly reactive, free-radical species that is an essential biological regulator involved in a plethora of physiological processes: neurotransmission, vasodilation and immune response (Alderton et al., 2001). •NO's functions in neurons range from synaptogenesis, sensory input processing, synaptic plasticity and learning, and most importantly as a nonadregernic-noncholinergenic (NANC) neurotransmitter (Meffert et al., 1994; Schmidt & Walter, 1994). Additionally, •NO can activate soluble guanylyl cyclase in smooth muscle cells that surround blood vessels. This increases cellular cyclic guanosine monophosphate (cGMP), a secondary messenger that activates the lowering of intracellular calcium (Ca^{2+}) levels, resulting in the vasodilation of blood vessels (Schmidt et al., 1993; Schmidt & Walter, 1994). Lastly, as a reactive nitrogen species (RNS), it can be used as a cytotoxic agent as a means for immunological defense through cell-mediated immune response against microbes, tumour cells and alloantigens (Kroncke et al., 1998; Nathan & Hibbs, 1991).

1.2 Nitric Oxide Synthase

The production of •NO in tightly regulated by a family of enzymes knows as nitric oxide synthases (NOS; EC 1.14.13.39). NOS catalyze the mono-oxygenation reaction of L-arginine (L-Arg) to an intermediate, N-ω-hydroxy-L-arginine (L-NOHA), with a subsequent second mono-oxygenation reaction converting L-NOHA into L-citrulline and •NO (Figure 1.1). Each step of this reaction consumes a nicotinamide adenine dinucleotide phosphate (NADPH) as the electron donor in the presence of molecular oxygen (O_2) (Daff, 2010).

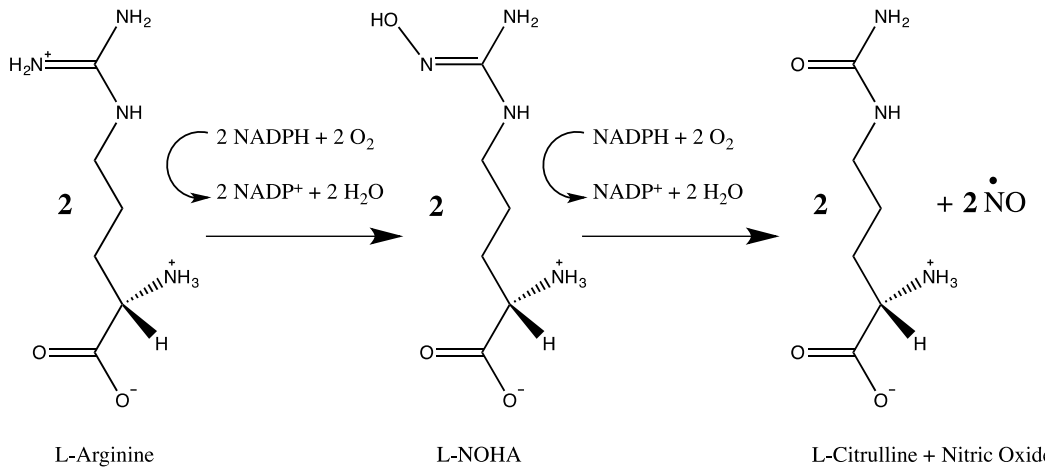

Figure 1.1 - The enzyme catalyzed reaction of L-arginine conversion into L-citrulline and •NO by NOS
NADPH provides reducing equivalents for the conversion of L-arginine to L-citrulline and •NO by NOS catalysis. This figure is adapted from a previous review (Daff, 2010), using ChemBioDraw.

Three different isoforms of NOS have been identified in mammalian tissues: neuronal NOS (nNOS; NOS1), endothelial NOS (eNOS; NOS III) and inducible NOS (iNOS; NOS II) (Alderton et al., 2001). nNOS, eNOS and iNOS were each primarily found to be expressed in nervous tissues, epithelium tissues and macrophages, respectively, but are now known to be expressed in several different tissues throughout the body (Bachetti et al., 2004; Kroncke et al., 1998). All three isozymes are catalytically active only when in their dimeric form and bound to a small protein known as calmodulin (CaM), in a 1:1 ratio (Alderton et al., 2001; Daff, 2010).

1.2.1 Importance of Studying Nitric Oxide Synthase

The production of •NO is important for maintaining normal physiological conditions. However, the aberrant production of this diatomic molecule has been linked to several pathological conditions. The uncoupling of the NOS enzymatic reaction (Figure 1.1) can produce superoxide (O_2^-) instead of •NO. O_2^- can react in turn with any surrounding •NO to generate more reactive nitrogen species (RNS), such as peroxynitrite ($ONOO^-$). These RNS and other reactive oxygen species (ROS) can cause oxidative damage to surrounding biomolecules (Roe & Ren, 2012; Schmidt & Walter, 1994). Overproduction of •NO due to increased iNOS activity has been associated with immune response-related and inflammatory diseases such as immune-type diabetes, arthritis and Crohn's disease (Kroncke et al., 1998; Schmidt & Walter, 1994). Overproduction of •NO due to increased nNOS activity has been associated with neurodegenerative disorders such as Parkinson's and Alzheimer's disease (Xue et al., 2010; Zhang et al., 2006). In contrast, •NO produced by eNOS mainly plays a physiological role and is important for blood

pressure regulation. Thus, the underproduction of •NO due to the lack of eNOS activity has been associated with cardiovascular diseases such as hypertension and atherosclerosis (Förstermann & Münzel, 2006; Roe & Ren, 2012).

Developing isoform-selective inhibitors for nNOS and iNOS isozymes over eNOS is of great interest due to the pathological diseases arising from •NO overproduction mentioned above. Nonetheless, finding isoform-selective inhibitors has proven to be difficult for several reasons. Firstly, the high conservation of the L-arg substrate binding pocket within the oxygenase dimer between all three isozymes make isoform selectivity a challenge for structure-based design (Alderton et al., 2001; Xue et al., 2010). Secondly, inhibitor studies are usually done using non-mammalian NOS isoforms such as rat nNOS and murine iNOS. Rat nNOS is the most thoroughly investigated nNOS isoform due to its 90% sequence homology to human nNOS and its reliable expression and purification. However, the slight difference in sequences has caused discrepancies in inhibitor sensitivity between human and non-human isoforms. This makes pharmacokinetic and pharmacodynamic studies hard to analyze and compare inhibitor efficacies (Fang et al., 2009; Joubert & Malan, 2011; Xue et al., 2010). Lastly, current *in vitro* inhibitor-enzyme assays for NOS are limited in that they are lengthy and use expensive regents. With these factors in mind, there is a need for a convenient, high-throughput analysis method to study NOS enzymatic activity.

1.2.2 Nitric Oxide Synthase Expression

Both nNOS and eNOS isozymes are constitutively expressed and are referred to as constitutive NOS (cNOS) isoforms. These isoforms are activated by elevated intracellular Ca^{2+} concentrations through the binding of CaM and are thus classified as Ca^{2+}-dependent (Ghosh, Dipak, 2003). Unlike the cNOS enzymes, iNOS is transcriptionally regulated by endotoxins and cytokines in macrophages, although, there are reports of specific epithelial cell types that can constitutively express iNOS (Geller & Billiar, 1998; Guo et al., 1995). iNOS binds CaM tightly regardless of the Ca^{2+} concentration, and is thus referred to as Ca^{2+}-independent. The dependence of iNOS viability to CaM binding is so high it is usually expressed and purified in the CaM-bound state (Geller & Billiar, 1998; Stevens-Truss & Marletta, 1995).

1.2.3 Nitric Oxide Synthase Structure

The nNOS, eNOS and iNOS isozymes share approximately 50-60% sequence homology in humans and have molecular weights of 165kDa, 134kDa and 130kDa, respectively. All three enzymes are homodimeric, where each monomer is composed of 2 main domains: an N-terminal oxygenase domain and a multi-subdomain C-terminal reductase domain (Figure 1.2). The 2 domains are linked together via a

CaM-binding site domain (Figure 1.2; Section 1.3.1) (Alderton et al., 2001; Daff, 2010). There are currently no full-length crystal structures of any NOS enzymes, however several individual domains have been characterized and reported (Fischmann et al., 1999; Garcin et al., 2004; Li et al., 2001; Matter et al., 2005).

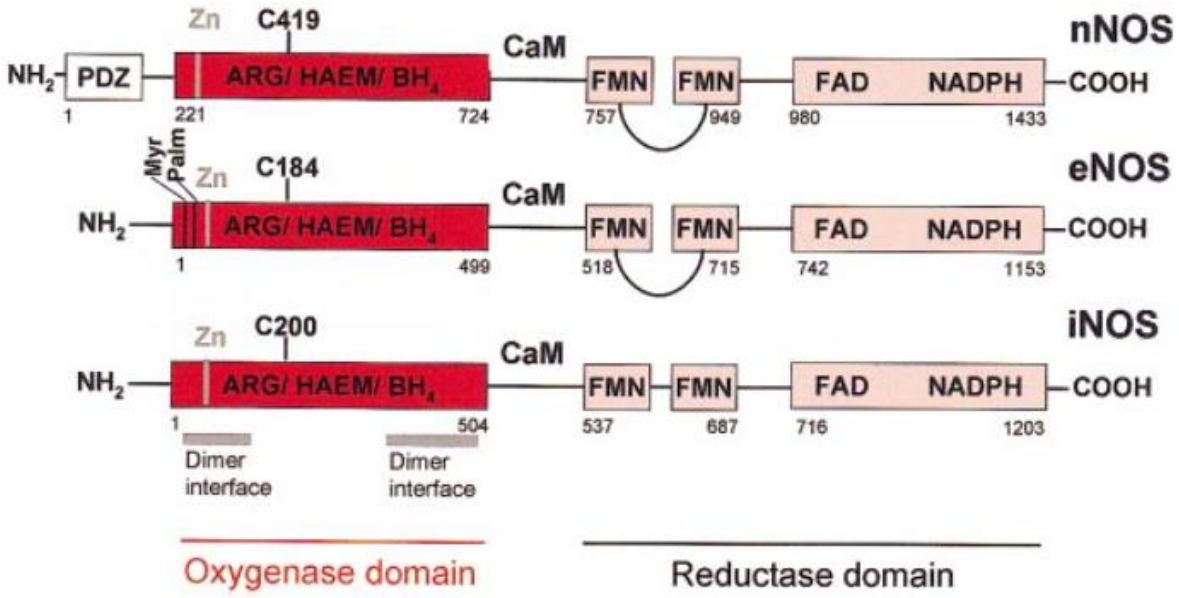

Figure 1.2 - Monomeric nNOS, eNOS & iNOS Domain Structure
The oxygenase and reductase domain are shown in red and pink respectively. The numbers represent the amino acid residues at the start and end of each respective NOS's oxygenase domain, and the reductase FMN and FAD/NADPH subdomains. Figure reprinted with permission from (Alderton et al., 2001).

1.2.3.1 Nitric Oxide Synthase Oxygenase Domain

The oxygenase domain contains the catalytic site and has binding sites for the substrate, L-arg, molecular oxygen (O_2), iron protoporphyrin (heme) and the cofactor (6R)-5,6,7,8-tetrahydrobiopterin (H_4B). The heme domain in NOS can be compared to those in cytochrome P450 (P450; EC 1.14.-.-) enzymes, in that both catalyze the oxidations of substrate molecules bound close, but not directly ligated, to a penta-coordinated thiolate ligated heme iron. The heme groups between each enzyme however have fundamental structural and functional differences (Alderton et al., 2001; Daff, 2010). All of these binding sites are highly conserved between NOS isoforms, although nNOS has a unique binding domain called the post synaptic density protein 95 (PSD-95) discs large/ZO-1 homology (PDZ) domain (Figure 1.2). The PDZ domain is located in the 220 amino acid N-terminal extension of nNOS, attributing to the larger size of this enzyme compared to the other isoforms. The PDZ domain is used for the localization and targeting of nNOS to specific areas in the cell (Brenman et al., 1996; Zhou & Zhu, 2009). Several crystal

structures of the oxygenase domain of all NOS isoforms have been published (Figure 1.4) (Fischmann et al., 1999; Li et al., 2001; Matter et al., 2005). They show that the dimer interface of NOS occurs between the two oxygenase domains and contain a structural zinc ion tetra-coordinated to 2 conserved cysteine residues from each monomer (Li et al., 2001; Raman et al., 1998).

1.2.3.2 Nitric Oxide Synthase Reductase Domain

The reductase domain is comprised of the flavin adenine dinucleotide/nicotinamide adenine dinucleotide phosphate (FAD/NADPH) and the flavin mononucleotide (FMN) subdomains and each has binding sites for the respective cofactors (Alderton et al., 2001). Notably, the FAD/NADPH subdomain has structural and functional homology to cytochrome p450 oxidoreductases (CYPOR; EC 1.6.2.4.) but not the FMN subdomain (J. Zhang et al., 2001). Currently, solved structural data on the reductase domain is limited to only the nNOS isoform (Figure 1.3) (Garcin et al., 2004).

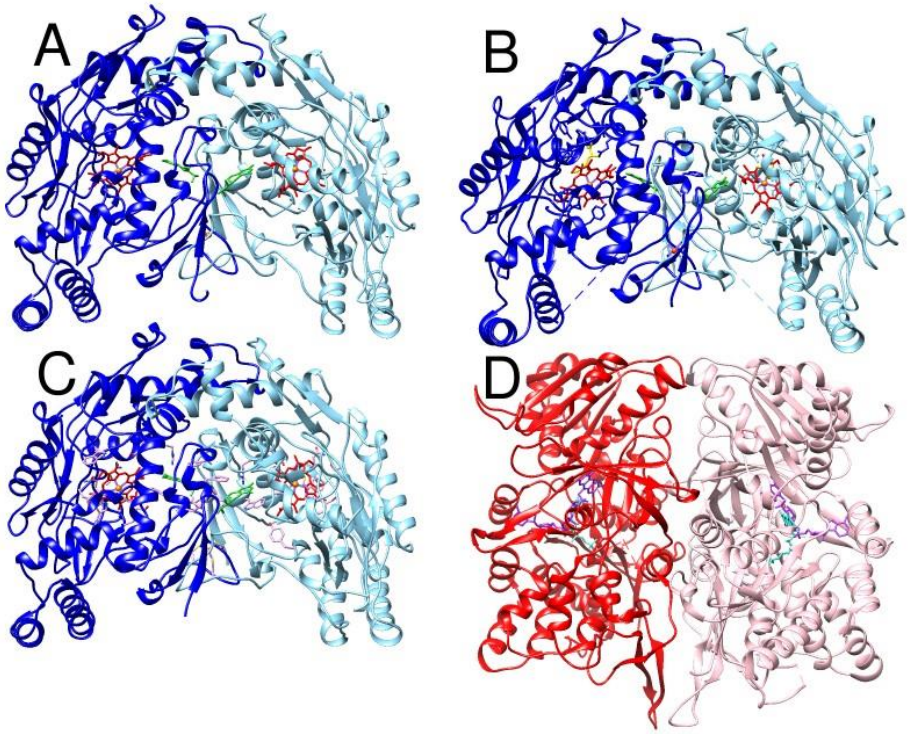

Figure 1.3 - Structures of NOS Oxygenase Domains & NOS Reductase Domain
(A) rat nNOS oxygenase domain **(B)** human eNOS oxygenase domain **(C)** human iNOS oxygenase domain **(D)** rat nNOS reductase domain. All solved structures depict domain dimers. NOS oxygenase monomers are shown in blue and sky blue. nNOS reductase monomers are shown in red and pink. H_4B, heme, L-Arg, FAD, FMN, Fe, & Zn^{2+} are shown in light green, red, yellow, purple and turquoise sticks and orange and magenta balls respectively. Models were derived from PDB 1ZVL, 3NOS, 4NOS and 1TLL respectively (Fischmann et al., 1999; Garcin et al., 2004; Li et al., 2001; Matter et al., 2005), and viewed using UCSF Chimera.

1.3 Calmodulin

CaM is a ubiquitous cytosolic calcium (Ca^{2+})-binding protein that can be found in all eukaryotic organisms. It is involved in the regulation of many different proteins, one of them being NOS. CaM is known to acts as a signal transducer for a wide variety of physiological processes (Babu et al., 1988). CaM is a relatively small protein with a length of 148-amino acids (16.7 kDa) and it is made up of globular N- and C-terminal domains tethered by a central flexible linker region (Figure 1.4). CaM has been reported to bind to approximately 300 target proteins (Ikura & Ames, 2006). This protein can chelate up to a total of 4 Ca^{2+} ions through 2 pairs of EF-hand motifs, found in each terminal domain. Ca^{2+} binds cooperatively within each domain, where the C-terminal lobe has approximately 10-fold greater affinity for Ca^{2+} than the N-terminal lobe (Bayley et al., 1996). Although CaM can exist in various Ca^{2+} bound states, it is primarily found in two states: the Ca^{2+}-free state (apo-CaM) and the Ca^{2+}-saturated state (holo-CaM).

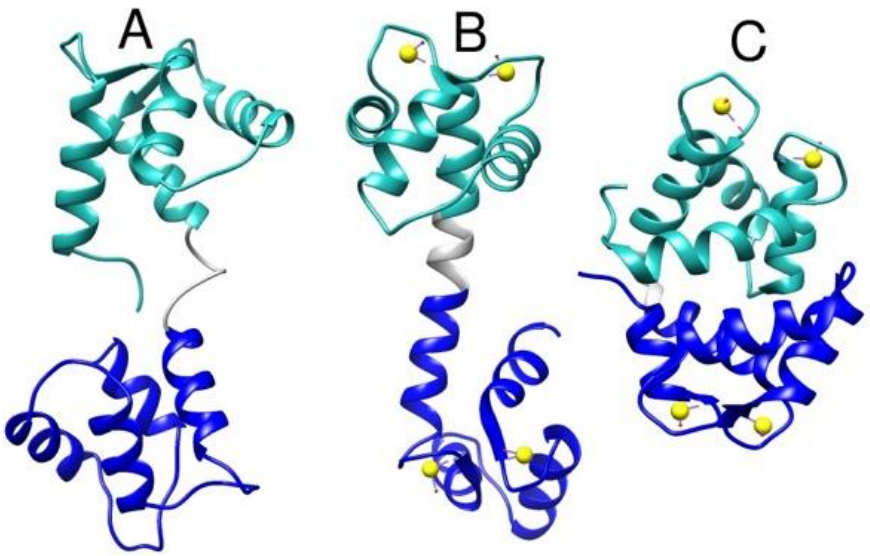

Figure 1.4 - Calmodulin in various Ca^{2+}-bound states
(**A**) Apo-CaM (Kuboniwa et al., 1995) (**B**) Holo-CaM (Chattopadhyaya et al., 1992) (**C**) Holo-CaM in compact form (Fallon & Quiocho, 2003). The N-terminal, C-terminal and linker region are colored in cyan, blue and grey, respectively. Ca^{2+} ion are colored in yellow. Models were derived form PDB 1CFD, 1CLL, 1PRW, respectively and viewed using UCSF Chimera.

Apo-CaM has a relatively compact conformation, whereas holo-CaM appears to be more dynamic and can range from an extended state (dumbbell-shaped) to a compact state, with various intermediate conformations in between (Figure 1.4) (Finn & Forsén, 1995). This flexibility can be attributed to the

central linker region, which can be readily bent and unravelled, allowing the N- and C-terminal domains to change orientation, giving CaM the ability to bind several different target proteins (Chou et al., 2001). Additionally, the amino acid composition of these domains contains a significant amount of hydrophobic and acidic residues. The C-terminal domain has slightly higher hydrophobic and acidic character, giving CaM the ability to accommodate a wider variety of amino acids in the target peptide (Ikura & Ames, 2006).

1.3.1 The Nitric Oxide Synthase Calmodulin-Binding Domain

As mentioned previously, CaM can bind target proteins in a Ca^{2+}-dependent and -independent manner, in the holo and apo forms respectively. It recognizes peptide sequences that are approximately 20 amino acids long and can form basic, amphipathic α-helical secondary structure. Although sequences between target proteins can vastly differ in sequence identity, positions of bulky hydrophobic amino acids are highly conserved (Yap et al., 2000). CaM can bind in a Ca^{2+}-dependent manner to the CaM-binding domains of target proteins that contain a recognition motif in the form 1-5-8-14, 1-8-14 or 1-5-10, where the amino acids at these positions are either F-A-I-L-V or W, with some exceptions (Figure 1.5). CaM can also bind in a Ca^{2+}-independent manner to target proteins that have the IQ motif, a consensus sequence of IQ-XXX-RG-XXX-R, where X can be any amino acid. However, the IQ motif can be found in some Ca^{2+}-dependent proteins (Rhoads & Friedberg, 1997).

The CaM-binding domain of all NOS isozymes all share the 1-5-8-14 CaM binding motif, where the residue at position 1 is usually an aromatic amino acid, 5 & 8 are hydrophobic, and 14 is bulky and hydrophobic (Figure 1.5) (Aoyagi, 2003; Venema et al., 1996).

	1 5 8 14	
Human nNOS	**RRA I G FKKLAEAVKFSA KLMGQAMAKRV**	**(731-758)**
Human eNOS	**TRK KT FKEVANAVKI SA S LMGTVMAKRV**	**(491-518)**
Human iNOS	**RRE I P LKVLVKAVLFACMLMRKTMAS RV**	**(510-537)**

Figure 1.5 - Sequence alignment of the human NOS CaM-binding region
Alignment was taken from a previous study (Aoyagi, 2003). Basic residues are shown in blue and acidic residues in red.

Structural studies of CaM binding to peptides of the NOS CaM-binding domain reveal that CaM wraps tightly around the peptides in an antiparallel orientation, where the N-terminal residues of CaM interact with the C-terminal residues of the NOS and vice versa (Aoyagi, 2003).

1.4 Nitric Oxide Synthase Electron Transfer

During NOS catalysis, it is generally understood that upon initiation of CaM binding to the CaM-binding domain, electrons are shuttled from the reductase domain of one monomer of the quaternary structure to the heme oxygenase domain of the opposite monomer (Volkmann et al., 2014). However, the exact mechanism of the electron transport within NOS is still under investigation. Research using electron microscopy (EM) has demonstrated that NOS adopts several different structural conformations during electron transport (Campbell et al., 2014; Leferink et al., 2014). The binding of NADPH in the FAD/NADPH subdomain reduces FAD by two electrons. Through interaction with the FMN subdomain, which is buried within the reductase domain, FAD donates one electron to FMN, but the FMN remains inaccessible to the heme in the oxygenase domain. This is known as the "input" or "closed state" (Figure 1.6). A significantly large conformational change occurs that releases the FMN subdomain from the reductase domain closer towards the oxygenase domain where FMN can donate the electron to the heme cofactor. This is known as the "output" or "open state" (Figure 1.6) (Campbell et al., 2014; Ghosh & Salerno, 2003; Roman & Masters, 2006; Smith et al., 2013; Volkmann et al., 2014).

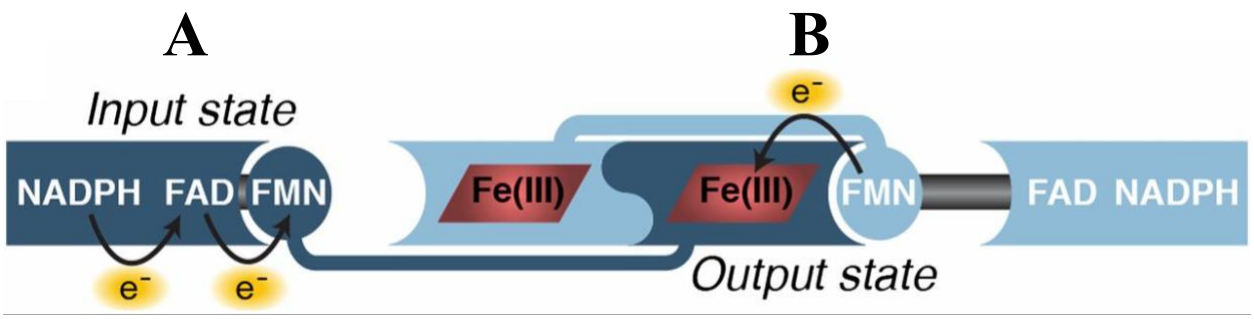

Figure 1.6 - Electron transport in NOS
Individual monomers are depicted in light and dark blue. **(A)** depicts the input state showing the interaction between the FAD/NADPH and FMN subdomains (electron transport between NADPH→FAD→FMN). **(B)** depicts the output state showing the interaction of the FMN subdomain with the opposite heme oxygenase domain (electron transport between FMN→heme). This figure was reprinted and adapted with permission from Proc. Natl. Acad. Sci. (PNAS) U. S. A, 111 (35) (Campbell et al., 2014).

1.4.1 Calmodulin's Role In Activation of Nitric Oxide Synthase Electron Transport

Due to the lack of structural data of the full NOS holoenzymes, the exact mechanism and role of CaM activation of NOS for •NO catalysis is not yet fully understood and is still being elucidated. Several different models have been proposed but there is yet to be a consensus as to which model is correct. Interestingly, the EM research mentioned in in Section 1.4 suggest an actual multi-step mechanism for the CaM activation of electron transport in NOS.

Campbell et al. (2014) propose that upon CaM binding, the input state is destabilized and releases the FMN subdomain from its interaction with the FAD/NADPH subdomain (Figure 1.7). This mechanism accounts for the large conformational change in NOS that minimizes the distance between the FMN subdomain to the heme oxygenase domain for electron transport. Due to the tight binding of CaM by iNOS at basal levels, this mechanism is unique to the cNOS isoforms (Campbell et al., 2014; Nishida & de Montellano, 1998; Smith et al., 2013). The second step proposes that CaM stabilizes the interaction between the FMN subdomain to the heme oxygenase domain by binding directly to the oxygenase dimer interface, forming a calmodulin-docked intermediate (Figure 1.7). This constricts the rotational movement of the FMN subdomain, locking it into the output state, causing the rapid and efficient transfer of electrons (Campbell et al., 2014; Smith et al., 2013).

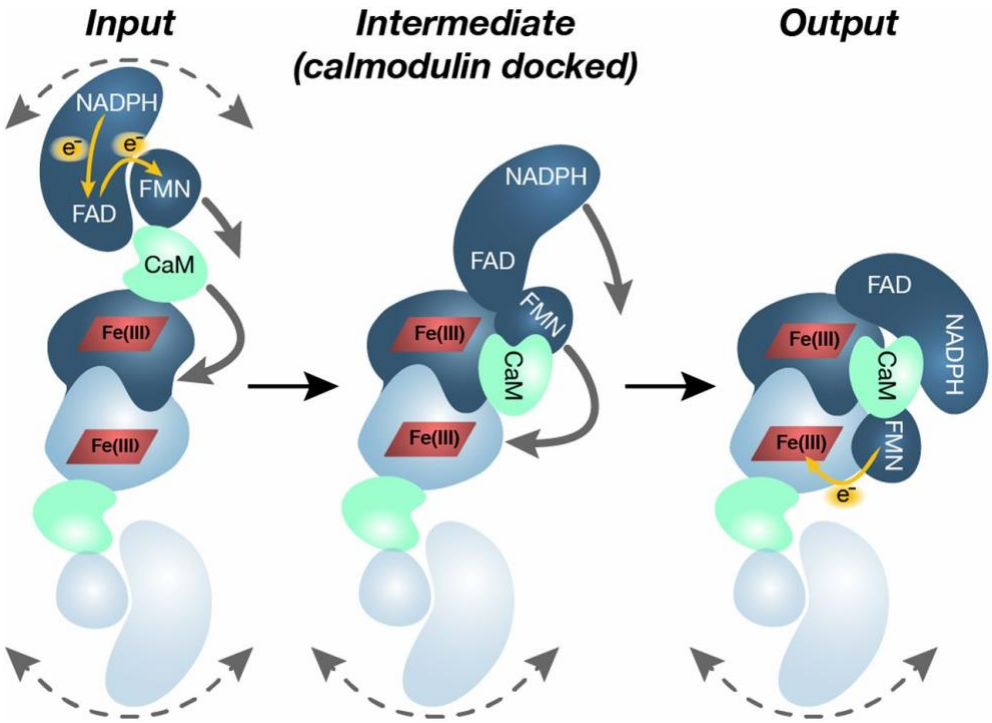

Figure 1.7 - Proposed conformational changes during NOS electron transport
Individual NOS monomers are depicted in light and dark blue, and CaM in light green. Yellow arrows suggest direction of electron transfer. Dashed grey arrows on the ends suggest both of the reductase domain are highly flexible with respect to the oxygenase domain, adopting a range of conformations when the enzyme is in a resting state. Grey arrows suggest the conformational changes instigated upon CaM binding, where the FMN subdomain is pulled away from the NADPH/FAD subdomain (input state). Another conformational change occurs where CaM is able to bind to the oxygenase dimer (calmodulin-docked intermediate), promoting a second FMN transition that brings it closer to the oxygenase domain of the opposite monomer, allowing for efficient electron transfer (output state). Only one FMN domain participates in electron transfer at a time, where the opposite reductase domain remains in the input state, unaffected by the large conformational changes occurring in the opposite monomer. This figure was reprinted with permission from Proc. Natl. Acad. Sci. (PNAS) U. S. A, 111 (35) (Campbell et al., 2014).

1.5 Reasons for Studying the Nitric Oxide Synthase – CaM Interaction

Understanding the molecular mechanisms and interactions that govern the processes and reactions of enzymes within biological organisms is of major interest in many fields of science, with importance in areas of molecular biology, biochemistry, medicine and proteomics. To achieve this goal, it is essential to identify and characterize how they interact with their regulating protein partners to fully understand their roles and functions.

More specifically, over the last few decades, there has been much interest in fully understanding the dynamic interplay between NOS enzymes and their regulation by CaM proteins. There are two main questions about this protein-protein interaction that are currently under investigation:

(1) How does CaM bind NOS enzymes, and;

(2) How does CaM activate NOS enzymes

Interestingly, there are two emerging techniques that could be used to study the NOS-CaM interaction. These techniques include surface plasmon resonance and bioelectrochemistry.

1.5.1 Surface Plasmon Resonance

Surface plasmon resonance (SPR) spectroscopy is an analytical technique that can be used to monitor the adsorption of compounds onto diaelectric metal surfaces such as gold. With vast advances in the past decade for the development of SPR technology and its applications, SPR biosensors have become a central tool for characterizing and quantifying bimolecular interactions.

1.5.1.1 Surface Plasmon Resonance Theory

The surface plasmon polariton, also known as propagating plasmons, is an electromagnetic wave that runs parallel to the metal surface and is sensitive to changes in the surface composition (Homola et al., 1999). A beam of plane-polarized light is directed onto the surface and reflected back into a detector (Figure 1.8). Upon stimulation of polarized light onto the surface, energy is absorbed by free electrons in the metal layer causing a resonant oscillation and thus, the phenomenon known as SPR (Piliarik et al., 2009). The absorption of energy causes a decrease in the intensity and the detector can measure the change in the angle of intensity decrease (Figure 1.8). Any change onto the surface due to binding will affect the surface plasmon, shifting the resonance angle, which is linearly proportional to the mass of the bound material (Homola et al., 1999). With this is mind, advances in SPR technology have gained popularity in

the past few years for becoming a widely used tool for its ability in biological and chemical sensing (Pattnaik, 2005).

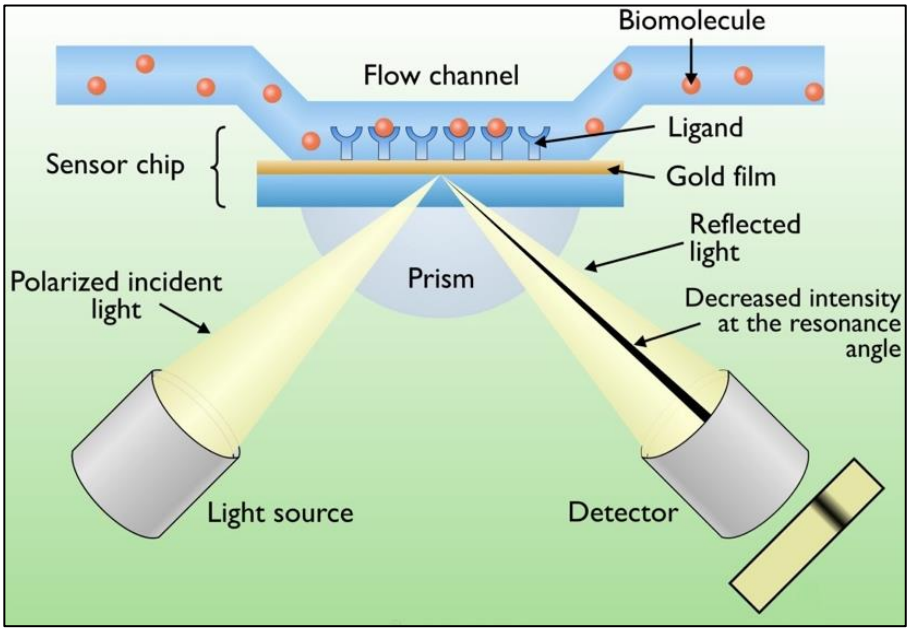

Figure 1.8 - Principles of SPR Detection
A cartoon depiction highlighting that principles of SPR sensor optical detection. This figure was reprinted from (Hegyi et al., 2013) [Open Source].

1.5.1.2 Surface Plasmon Resonance Kinetic Analysis

A typical SPR kinetic analysis consists of 3 phases: the immobilization phase, the association/dissociation phase, and lastly, the regeneration phase. During immobilization, the ligand is usually bound to the surface of the chip using the gold-thiol covalent link, which is very stable and usually does not require the modification of the ligand other than the addition of a thiol group. The ligand must contain some reactive groups (such as –NH2, –SH, –COOH). Most often, thiol and amino groups are used for immobilization; however, the streptavidin-biotin linkage is also popular when studying protein complexes (Homola et al., 1999).

The next phase consists of the association and dissociation phase in conjunction with the regeneration phase (Figure 1.9). A predetermined concentration of analyte in running buffer can be titrated into the flow channel, thus interacting and binding with the immobilized ligand, causing a change in the resonance angle that is displayed as a Resonance Unit (RU) (Figure 1.9; association phase) (Piliarik et al., 2009). A steady state is reached when the amount of analyte molecules binding is equal to the amount of analyte bonds breaking, where this response corresponds to the concentration of the bound sample (Figure 1.9). Subsequently, the system is allowed to flow with running buffer in the absence of

analyte, removing any weakly associated analyte molecules (Figure 1.9; dissociation phase). Over time, the analyte–ligand complex will eventually dissociate, although very slow. Therefore, a regeneration solution is injected, usually containing harsh conditions, such as low pH, high salt concentration or a solution that has been predetermined to break apart the interaction, to instantly break apart the analyte-ligand complex (Figure 1.8; regeneration phase;). This cycle of association/dissociation and regeneration can be repeated several times with varying concentrations of analyte to get a robust data set that can be analyzed for binding kinetics (Piliarik et al., 2009).

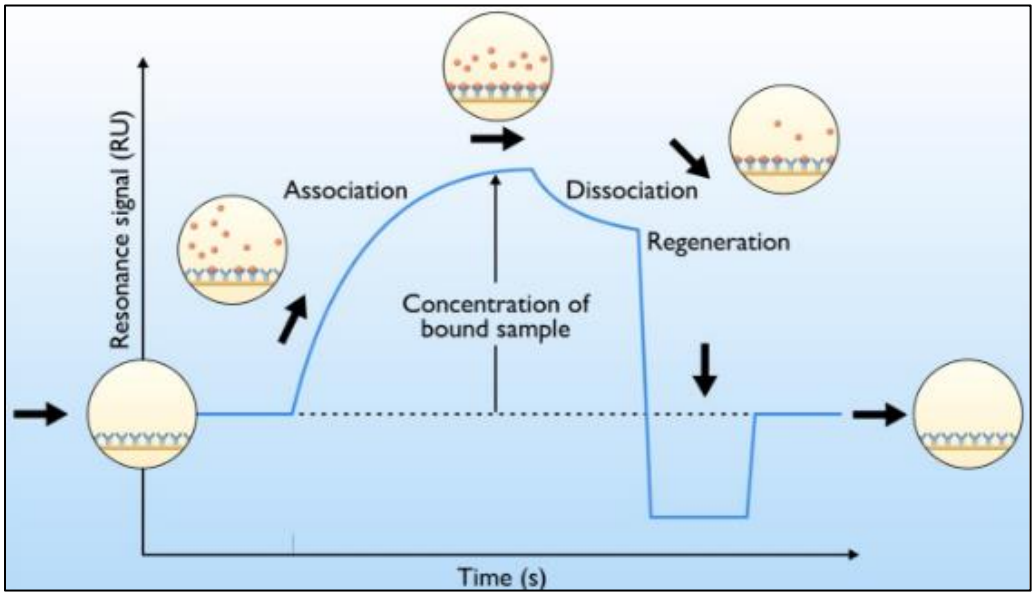

Figure 1.9 - SPR kinetic analysis
A typical response curve, also known as a sensogram, observed for a real-time SPR analysis of ligand-analyte bimolecular interactions. This figure was reprinted from (Kardos, 2013) [Open Source].

The last phase concludes with post-analysis of SPR data. The sensograms can be analyzed using tracing software that fit the data according to pre-determined mathematical binding models. The fitting model outputs the rate constants for association and dissociation, k_a & k_d, along with the binding affinity constant, K_D (Zoche, Bienert, et al., 1996).

1.5.1.3 Surface Plasmon Resonance Advantages and Disadvantages

A big advantage of using SPR is that the binding kinetics can be followed in real-time on the sensogram. Furthermore, the analyte of interest does not require modification or labelling keeping their properties unchanged, which is important in trying to understand *in vivo* interactions (Homola et al., 1999). The chip can be regenerated with the bound ligand and can be reused several times, allowing for measurements of different binding partners. In addition, a turbid analyte sample does not affect the measurement as the

interaction of the ligand and analyte should have been pre-selected for specificity. Lastly, SPR systems are quite sensitive and have low detection limits, often times in the nanomolar range, therefore low amounts of material can be used (Piliarik et al., 2009).

On the other hand, SPR is severely limited in that the immobilization of the ligand could interfere with the binding reaction by orienting the binding region toward the chip surface or if the immobilization occurs through the same groups as those involved in ligand interactions (O'Shannessy & Winzor, 1996). However, this problem can be avoided through the use of linkers or functionalized surfaces. Another main disadvantage is that binding interactions occur on a surface and not in solution phase, thus interactions might differ from those observed under *in vivo* conditions (Karlsson & Fält, 1997). Furthermore, artificial increased binding affinity can occur due to increased localized concentration. In the case of multiple binding sites, the interpretation of results could become complicated (Nieba et al., 1997; O'Shannessy & Winzor, 1996). Molecules of molecular weight that are <300-500 Da might be too small for a quantitative measurement. And lastly, the binding orientation of the immobilized ligand is not well-defined as it cannot be observed (Homola et al., 1999; O'Shannessy & Winzor, 1996).

1.5.2 Bioelectrochemistry

The study of any enzyme protein, such as NOS, usually requires the measurement of its ability to carry out its enzymatic reaction. Due to the physiological relevance of NOS activity (Section 1.2.2.), it is crucial to understand how this enzyme is regulated. Fully comprehending the protein-protein interactions that govern this particular enzymatic process could give us more control in clinical design, such as developing new isoform-selective inhibitors that could be used to treat pathological disease states arising from irregularities in NOS expression (Section 1.2.2).

Current methods to measure NOS activity are kinetic and end-point determination assays, which measure the enzymatic rate of product formation from a substrate and quantify the total amount of product formed. Some specific examples of assay methods that monitor NOS activity are the hemoglobin (Hb) assay and the NADPH assay. Both assays are labor intensive methods that require frequent time-point measurements (Kelm et al., 1997). Additionally, they extensively require expensive reagents such as NADPH. Although these methods are sensitive and accurate, the time requirement, amount of work and monetary costs are great limiting factors when one needs to analyze several samples (Kelm et al., 1997) . Therefore, the development of an efficient, high throughput method that can measure NOS enzymatic activity is of great importance.

As a developing field in science, bioelectrochemistry attempts to use electro and biophysical chemistry concepts to better understand and manipulate biological systems. A popular application of this area of research is direct electrochemistry of redox enzymes and the development of new biosensors (Armstrong et al., 1988). Intriguingly, in these studies, electrode surfaces provide a stable source of electrons for the enzymatic activity of immobilized redox proteins, thus eliminating the need for expensive and limiting substrates such as NADPH (Schneider & Clark, 2013). These new biosensing platforms have proven to be fast, relatively easy to complete and are also highly repeatable (Schneider & Clark, 2013), showing some potential for the development of a brand new platform to study NOS activity.

1.6 Research Objectives

The purpose of this Masters study is to further improve our understanding of CaM's control over NOS function by investigating how different structural and regulatory elements of CaM affect its binding to NOS enzymes and correlate how those elements affect NOS enzymatic activity.

Furthermore, we are trying to improve current methods to measure NOS activity by developing a brand new electrochemical NOS biosensor that will make the clinical design and screening of new isoform-selective inhibitors easier to accomplish.

These goals will be achieved by:

(1) Investigating the binding kinetics of various CaM mutants binding to immobilized peptides that represent the canonical CaM-binding domain of NOS enzymes through the use of SPR spectroscopic methods.

(2) Correlating the binding kinetics with the NOS activity profiles determined by activation of the same CaM mutants & elucidate the relationship between mutant CaM binding and activation.

(3) Using the principles of bioelectrochemistry, we plan to directly immobilize NOS enzymes onto a gold electrode surface, eliminating the need for expensive reducing equivalents for the development of a robust and efficient NOS biosensor. We will circumvent the known denaturing effect of electrode fouling of proteins through the use of a CaM protein tether. We will first use optical SPR methods to test the immobilization of our CaM tether construct onto a gold surface, and observe if we can specifically bind NOS enzymes before the use of an electrochemical platform.

Chapter 2
A Localized Surface Plasmon Resonance Study on Mutant CaM Binding with NOS Target Peptides

2.1 Introduction

There have been numerous experiments done in previous years that have looked at the dynamic interplay between CaM and NOS enzymes. A range of biophysical methods have been utilized in attempts to understand CaM's control over •NO production by characterizing CaM binding and activation of NOS enzymes. Characterization of this protein-protein interaction has been done by analyzing the structure with methods such as cryo-electron microscopy (cryo-EM), x-ray diffraction (XRD) and nuclear magnetic resonance (NMR) (Alderton et al., 2001; Campbell et al., 2014; Piazza et al., 2012), as well as analyzing the binding kinetics with methods such as affinity chromatography, gel filtration and isothermal titration calorimetry (ITC) (Piazza et al., 2017; Spratt et al., 2006)

Other binding experiments that have also been completed used methods such as SPR, competition assays, and fluorescence resonance energy transfer (FRET) and stopped-flow spectroscopy to determine rate constants for the binding of CaM proteins to target peptides that represent the CaM-binding domains of each of the NOS enzymes (Table 2.1). The differences in values for the binding rate parameters seen in Table 2.1 can be attributed to the differences in the techniques used. Despite these differences, these studies have showed a general trend in which CaM binding to cNOS peptides is Ca^{2+} dependent with respect to cNOS enzymes at all concentrations, whereas CaM binding to the iNOS peptide is Ca^{2+} independent, relatively irreversible and has a higher affinity compared to the cNOS peptides. Furthermore, the order of CaM affinity for the associated peptides can be noted as iNOS>>eNOS>nNOS. Overall, CaM is essential for NOS activity, and by understanding how it binds, we can understand more about its role in the regulation of NOS enzymes.

Table 2-1 - CaM binding kinetics of NOS peptides

NOS Peptide	k_a ($M^{-1}s^{-1}$)	k_d (s^{-1})	K_D (nM)
nNOS	1.58×10^5 [(a)]	7.87×10^{-4} [(a)]	5.0 [(a)]
	6.6×10^8 [(b)]	3.7 [(b)]	5.6 [(b)]
iNOS	3×10^4 [(a)]	$< 10^{-6}$ [(a)]	< 0.10 [(a)]
	---	---	1.5 [(c)]
	6.1×10^8 [(b)]	0.063 [(b)]	0.1 [(b)]
eNOS	---	---	4.0 [(c)]
	2.9×10^8 [(b)]	4.5 [(b)]	1.6 [(b)]

[(a)] SPR studies of CaM binding to nNOS and iNOS target peptides (Zoche et al., 1996)
[(b)] FRET and stopped-flow spectroscopy studies on Alexa-350 labelled T34C/T110W CaM binding to NOS target peptides (Wu et al., 2011)
[(c)] Competition assays of nNOS activity inhibition by eNOS and iNOS peptides (Venema et al., 1996)

2.1.1 CaM Mutants

A common strategy used in binding studies is the comparison of native proteins with mutated versions to observe how different modifications affect the protein-protein interactions. The use of CaM mutants in this particular binding study can help us understand and characterize the overall control that CaM structures play in terms of NOS activity. We conducted three different studies using three different mutant constructs which include CaM chimeric hybrids (Newman et al., 2004), CaM truncations (Spratt et al., 2006) and CaM single-point mutations (Spratt et al., 2008). All mutant constructs are described in more detail below (Section 2.1.1.2).

2.1.1.1 Measuring Mutant CaM-Dependent Activation of NOS Enzymes

A series of spectrophotometric kinetic assays were completed to observe mutant CaM-NOS interactions and assess which structural elements within CaM are important for electron transfer. The assays used measured three distinct activities associated with NOS: NADPH oxidation, cytochrome c reduction and •NO production. These activities were measured using the NADPH oxidation assay, the cytochrome c oxidation assay, and the oxyhemoglobin assay, respectively (Figure 2.4).

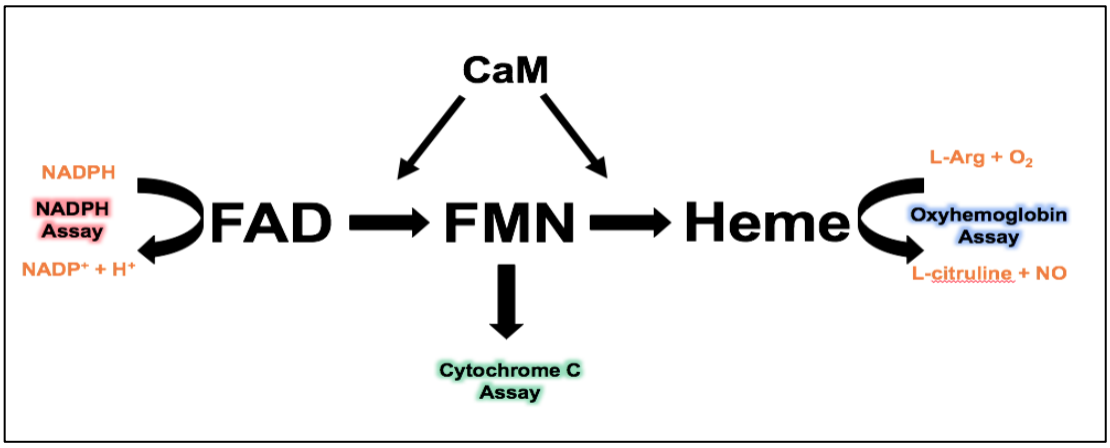

Figure 2.1 - Spectrophotometric kinetic assay methods for NOS activity
The NADPH oxidation assay (red) measures NADPH utilization through monitoring initial rates of NADPH oxidation to $NADP^+$ and H^+ in the terminal end of the reductase domain by monitoring the decrease in absorbance at 340 nm. *The cytochrome c assay* (green) measures the initial rates of electron transfer from the FAD subdomain to the FMN subdomain via cytochrome c reduction by monitoring increase in absorbance at 550 nm. Lastly, *the oxyhemoglobin capture assay* (blue) can be used to indirectly measure the efficiency of electron transfer from the FMN subdomain to the heme catalytic site via monitoring the reduction of oxyhemoglobin into methemoglobin observed at an absorbance of 401 nm. This image is adapted from Spratt (2008).

In these experiments, controls using wt CaM were completed for each assay and activity rates were expressed as a percentage normalized to 100%. The 3 sets of CaM mutants were tested under the same conditions as wt CaM controls, where results were expressed as a percentage of relative activity compared to CaM controls. Interestingly, the cumulative results from these activity studies revealed how different regions within CaM play an important role in NOS enzymatic activity. These studies revealed major differences between CaM control over cNOS isozymes vs. iNOS enzymes.

2.1.1.2 Calmodulin Troponin C Chimera Mutants

As mentioned in Section 1.3, CaM binds Ca^{2+} through 4 highly conserved EF-hand motifs. The binding and activation of CaM's protein targets are regulated through the binding of Ca^{2+}. A structurally similar Ca^{2+}-binding protein akin to CaM is cardiac troponin C (TnC), a protein responsible for the activation of thin filament cardiac muscle (Schreier et al., 1990). Although both proteins consist of 2 globular domains linked by a central helix region, TnC has seven more N-terminal and three more central helix residues than CaM (George et al., 1993). CaM and TnC share approximately 70% sequence homology, where the local structures within EF-hands 1, 3 and 4 are highly conserved but the difference in sequence found in EF-hand 2 of TnC causes a difference in overall structure of the protein (Figure 2.2.A) (Sia et al., 1997; Su et al., 1995).

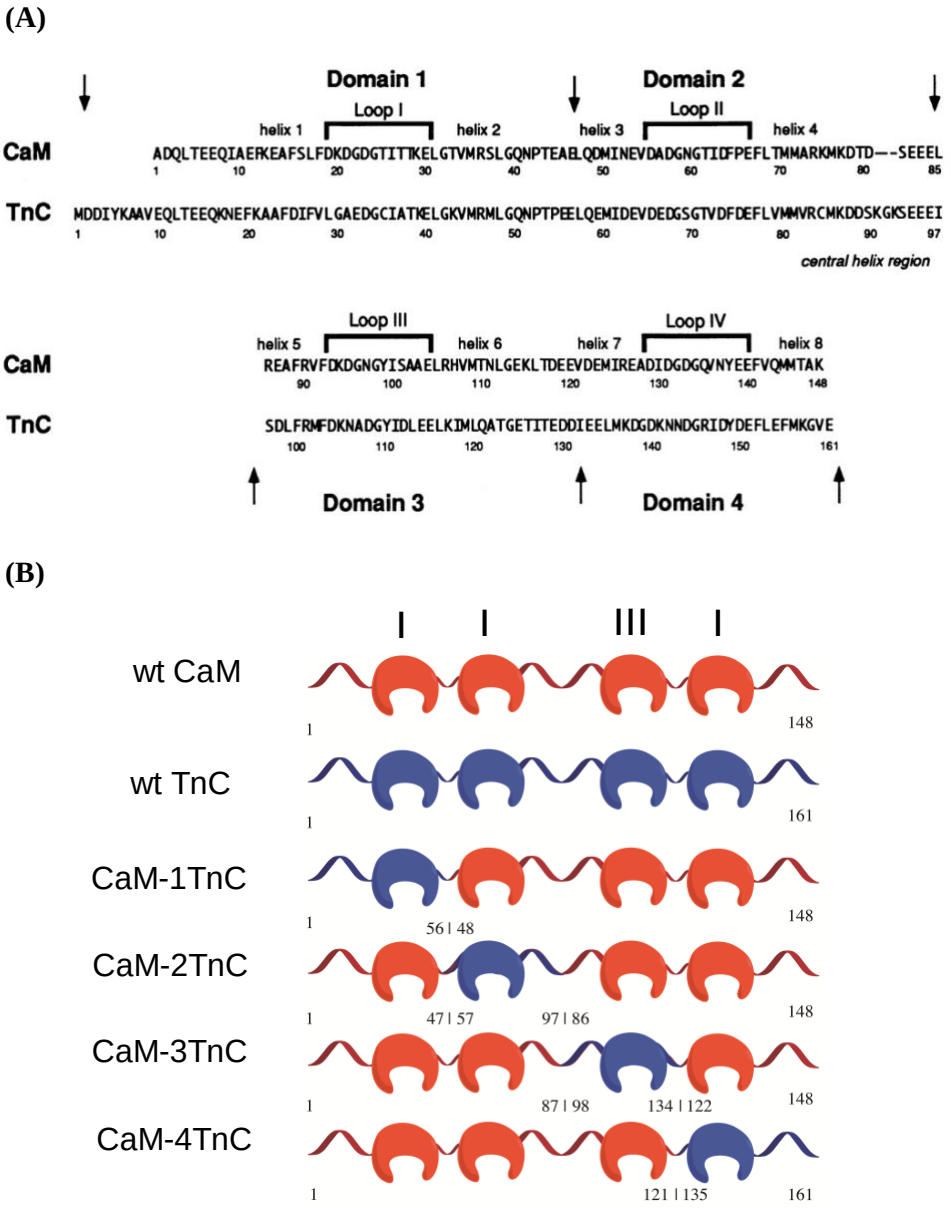

Figure 2.2 - CaM-TnC chimera constructs
(**A**) A sequence alignment of CaM and TnC according to similarities in primary amino acid sequence and secondary structure. Locations of the EF-Hand domains, subdomain loops and helices are indicated. Residue numbers are indicated below the sequences. The central helices of CaM and TnC are indicated. The arrows indicate splice points used to make chimeric mutants. Reprinted from Su et al. 1995. (**B**) A cartoon depiction of chimeric CaM-TnC mutant proteins aligned according to EF-Hand domains (in roman numerals). CaM portions are shown in red and TnC portions in blue. EF hands motifs are shown as crescents. The small numbers show the corresponding amino acid residues from each respective protein. This figure is adapted from Spratt (2008).

Another major difference observed is the affinities of each EF-hand for Ca^{2+}; most notable is the 1 order of magnitude greater Ca^{2+} affinity of TnC EF-hand 4 compared to the same EF-hand in CaM.

Importantly, TnC proteins are unable to activate CaM-dependent enzymes (George et al., 1993). Due to their overall EF-hand structural similarities, chimeric proteins were developed, replacing individual EF-hand domains from CaM with the corresponding EF-hand domains from TnC (Figure 2.2.B). This set of mutants was constructed by Su et al. (1995). Through the replacement of each domain within each specific construct, the function of the specific EF-hand was effectively removed. To investigate the role and importance of each individual EF-hand during NOS catalysis, Newman et al. (2004) studied the CaM-TnC dependent activation of NOS enzymes (Table 2.2). Presented below is the summary of the activity kinetic results from the CaM-TnC activation of NOS enzymes

Table 2-2 - Activity Profiles of CaM-TnC Binding to NOS Enzymes

CaM Construct	**Neuronal NOS**			**Endothelial NOS**		
	NADPH oxidation (%)	Cyt c reduction (%)	•NO production (%)	NADPH oxidation (%)	Cyt c reduction (%)	•NO production (%)
wt CaM	100 ± 3	100 ± 4	100 ± 5	100 ± 4	100 ± 3	100 ± 3
wt CaM (EDTA)	NAA	NAA	NAA	4 ± 1	6 ± 1	8 ± 2
CaM-1TnC	12 ± 1	5 ± 1	7 ± 4	28 ± 2	67 ± 3	17 ± 2
CaM-2TnC	89 ± 3	102 ± 2	108 ± 5	101 ± 3	27 ± 1	56 ± 1
CaM-3TnC	22 ± 3	75 ± 2	20 ± 2	47 ± 4	87 ± 3	31 ± 1
CaM-4TnC	23 ± 4	102 ± 4	17 ± 2	47 ± 3	71 ± 1	39 ± 3
	Inducible NOS					
	NADPH oxidation (%)		Cyt c Reduction (%)		•NO Production (%)	
	200 μM $CaCl_2$	250 μM EDTA	200 μM $CaCl_2$	250 μM EDTA	200 μM $CaCl_2$	250 μM EDTA
wt CaM	100 ± 2	79 ± 6	100 ± 3	92 ± 1	100 ± 2	66 ± 2
CaM-1TnC	131 ± 1	76 ± 3	160 ± 7	131 ± 7	123 ± 4	71 ± 4
CaM-2TnC	79 ± 3	35 ± 5	141 ± 5	161 ± 4	58 ± 4	4 ± 1
CaM-3TnC	93 ± 6	38 ± 8	145 ± 6	98 ± 2	109 ± 5	18 ± 1
CaM-4TnC	90 ± 3	89 ± 6	113 ± 6	101 ± 2	115 ± 3	72 ± 4

A study of CaM-TnC chimera activation of NOS enzymes (Newman et al., 2004).
All assays were performed @ 25 °C, in the presence of 2 μM wt CaM or CaM mutant and either 200 μM $CaCl_2$ or 250 μM EDTA as indicated, unless otherwise specified. All values are expressed as a % relative to wt CaM controls for each set of mutants. NAA = No Apparent Activity.

Activities of **nNOS** bound to wt CaM were **148 min^{-1}** (NADPH oxidation), **1163 min^{-1}**(Cyt c reduction), **40 min^{-1}** (•NO production).
Activities of **eNOS** bound to wt CaM were **31 min^{-1}** (NADPH oxidation), **70 min^{-1}**(Cyt c reduction), **10 min^{-1}** (•NO production).
Activities of **iNOS** bound to wt CaM were **77 min^{-1}** (NADPH oxidation), **1395 min^{-1}**(Cyt c reduction), **47 min^{-1}** (•NO production).
Data is adapted and summarized from Newman et al. (2004).

2.1.1.3 Calmodulin EF-Hand Pair Mutants

CaM is made up of 2 globular N- and C-terminal domains with an EF-hand pair within each domain. To investigate the contribution of each EF-hand pairs in regards to the binding and activation of various target proteins, including NOS enzymes, a set of mutants was developed by the Persechini group (1994; 1996) containing 4 different constructs (Figure 2.2). This includes single EF hand pairs (nCaM and cCAM) and duplicated EF Hand pairs (CaMNN and CaMCC).

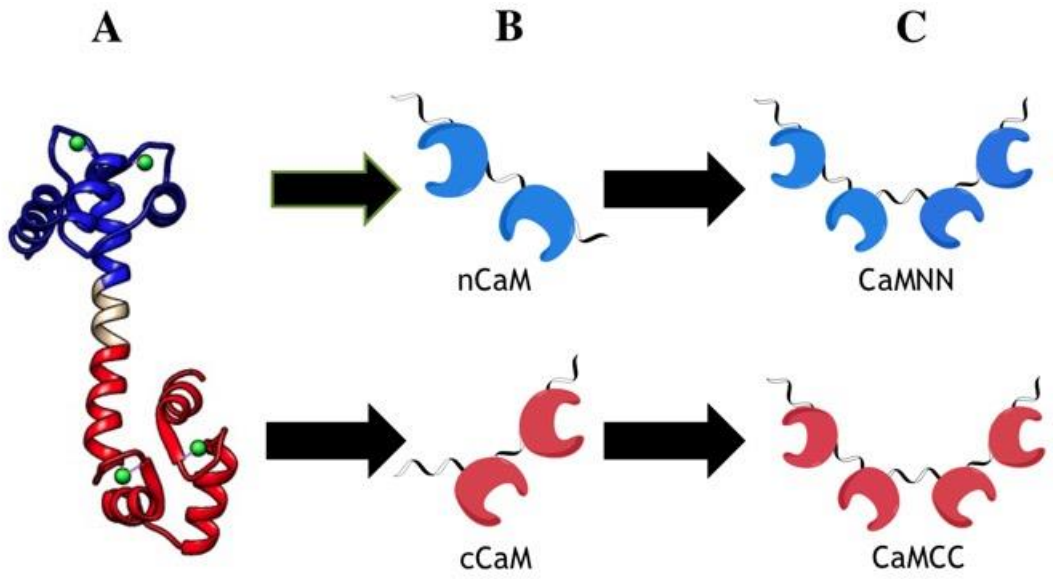

Figure 2.3 - CaM EF-hand pair constructs
(A) A ribbon structure showing holo CaM (1CLL). The N-terminal, C-terminal and linker region are colored in blue, red and grey, respectively. **(B)** A cartoon depiction of single EF-hand pair mutants, nCaM in blue (residues 1-81) and cCaM in red (residues 76-148) (Anthony Persechini et al., 1994). EF-Hand motifs are shown as crescents. **(C)** A cartoon depiction of duplicated EF-hand pair mutants, CaMNN in blue (residues 1-81, 76-81, 9-75) and CaMCC in red (1-8, 82-148, 76-81, 76-148) (Persechini et al., 1996). EF-Hand motifs are shown as crescents.

Single EF-hand pair mutants (Figure 2.2.B) are truncations of the wt CaM protein (Figure 2.2.A) where the name denotes the respective globular domain. The nCaM construct employed in these studies has a slight modification where the central linker region has been included (i.e. residues 1-81) whereas the original nCaM construct used by Persechini et al. (1994) did not contain the central linker region (i.e. residues 1-75). However, previous work from our lab has shown that the addition of the central linker region does not affect the ability of the nCaM to bind to its target (Spratt et al., 2006). The duplicated EF-hand pair mutants in Figure 2.2.C are the result of the fusion of the single EF-hand pair mutants.

Unlike the CaM-TnC constructs, this set of mutants was used to investigate the role and importance of the associated EF-hand pairs within the 2 terminal globular domains. Similar to the previous

investigation, Spratt et al. (2006) studied the CaM EF-hand pair dependent activation of NOS enzymes Table 2.3). Presented below is the summary of the activity kinetic results from the CaM EF-hand pair activation of NOS enzymes.

Table 2-3 - Activity Profiles of CaM EF-Hand Pairs Binding to NOS Enzymes

CaM Construct	Neuronal NOS			Endothelial NOS		
	NADPH oxidation (%)	Cyt c reduction (%)	•NO production (%)	NADPH oxidation (%)	Cyt c reduction (%)	•NO production (%)
wt CaM	100 ± 2	100 ± 6	100 ± 5	100 ± 4	100 ± 2	100 ± 2
wt CaM (EDTA)	6 ± 3	NAA	NAA	NAA	NAA	NAA
nCaM	6 ± 2	37 ± 3	NAA	5 ± 3	17 ± 1	5 ± 1
cCaM	4 ± 3	NAA	NAA	NAA	NAA	NAA
CaMNN	93 ± 4	90 ± 5	81 ± 3	115 ± 4	111 ± 3	98 ± 4
CaMCC	5 ± 2	NAA	NAA	4 ± 3	43 ± 1	17 ± 3
	Inducible NOS					
	NADPH oxidation (%)		Cyt c Reduction (%)		•NO Production (%)	
	200 μM $CaCl_2$	250 μM EDTA	200 μM $CaCl_2$	250 μM EDTA	200 μM $CaCl_2$	250 μM EDTA
wt CaM	100 ± 4	96 ± 6	100 ± 2	94 ± 1	100 ± 2	66 ± 2
nCaM	80 ± 7	28 ± 3	109 ± 3	115 ± 2	71 ± 2	NAA
cCaM	44 ± 3	20 ± 3	62 ± 1	77 ± 2	12 ± 1	NAA
CaMNN	48 ± 3	58 ± 3	133 ± 4	133 ± 1	74 ± 7	23 ± 1
CaMCC	75 ± 1	38 ± 3	69 ± 2	82 ± 3	54 ± 1	7 ± 1

A study of EF-hand pair mutant activation of NOS enzymes (Spratt et al., 2006).
All assays were performed @ 25 °C, in the presence of 2 μM wt CaM or CaM mutant and either 200 μM $CaCl_2$ or 250 μM EDTA as indicated, unless otherwise specified. All values are expressed as a % relative to wt CaM controls for each set of mutants. NAA = No Apparent Activity.

Activities of **nNOS** bound to wt CaM were **142 min^{-1}** (NADPH oxidation), **917.5 min^{-1}**(Cyt c reduction), **45.5 min^{-1}** (•NO production).
Activities of **eNOS** bound to wt CaM were **30 min^{-1}** (NADPH oxidation), **50.7 min^{-1}**(Cyt c reduction), **11 min^{-1}** (•NO production).
Activities of **iNOS** bound to wt CaM were **101 min^{-1}** (NADPH oxidation), **1397min^{-1}**(Cyt c reduction), **47 min^{-1}** (•NO production).
Data is adapted and summarized from Spratt et al. (2006).

2.1.1.4 Calmodulin Phosphomimetic Mutants

CaM has been found to be phosphorylated within the central linker *in vivo* by casein kinase II (CK-II) (Quadroni et al., 1994). The central linker is believed to be important in the activation of various target

proteins (Persechini et al., 1989). Post-translational modifications at these sites are important in the regulation of CaM's activity, and thus, the regulation of NOS enzymes. Studying these modifications however are hard due to the difficulty individually phosphorylating single amino acids. Therefore, to study the role of post-translational modifications of CaM and its effect on NOS function, specific amino acids were mutated into an aspartic or glutamic acid residues to mimic the effects of post-translational phosphorylation, yielding the phosphomimetic CaM mutants (Figure 2.3).

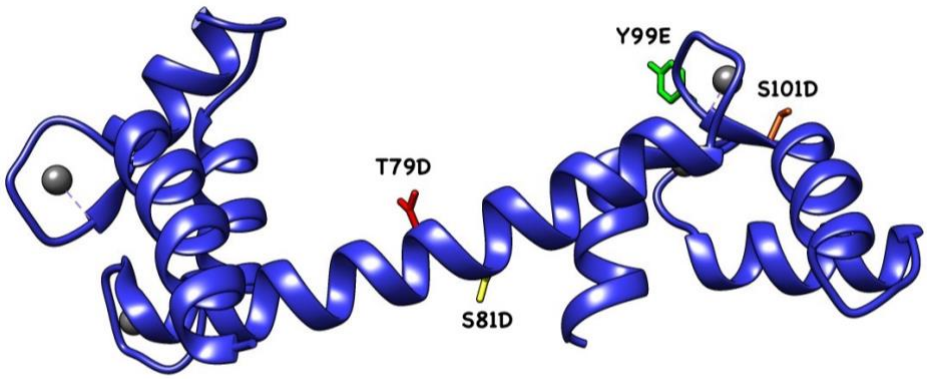

Figure 2.4 - CaM phosphomimetic constructs
A ribbon structure displaying the peptide backbone of holo CaM (PDB 1CLL) with the mutation sites used to yield phosphomimetic CaM constructs highlighted to demonstrate their respective locations: T79D (red), S81D (yellow), Y99E (green) and S101D (orange). The protein backbone is shown in blue and Ca^{2+} atoms are depicted as grey spheres. This image was created and viewed using UCSF Chimera and adapted from Spratt et al. (2008).

The amino acid residues threonine 79 and serine 81, two of the residues within the central linker modified by CK-II (Quadroni et al., 1994), were mutated into aspartic acid residues. These yielded the phosphomimetic mutants, CaM T79D and CaM S81D, along with a combination of the two, CaM T79D/S81D (Spratt et al., 2008). Interestingly, phosphorylation of 2 sites flanking the central linker, tyrosine 99 (Mishra et al., 2010) and serine 101(Greif et al., 2004), were reported to affect the activity of NOS specifically and therefore, phosphomimetic mutant constructs Y99E and S101D were also developed and studied. Similar to the previous sets of mutants, Spratt et al. (2008) studied the phosphomimetic CaM-dependent activation of NOS enzymes (Table 2.4). Presented below is the summary of the activity kinetic results from the phosphomimetic CaM activation of NOS enzymes.

Table 2-4 - Activity Profiles of Phosphomimetic CaM Mutants Binding to NOS Enzymes

CaM Construct	Neuronal NOS			Endothelial NOS		
	NADPH oxidation (%)	Cyt c reduction (%)	•NO production (%)	NADPH oxidation (%)	Cyt c reduction (%)	•NO production (%)
wt CaM	100 ± 4	100 ± 3	100 ± 2	100 ± 1	100 ± 4	100 ± 2
wt CaM (EDTA)	13 ± 4	9 ± 1	NAA	15 ± 3	9 ± 3	NAA
CaM-1TnC	93 ± 3	105 ± 3	94 ± 3	105 ± 3	86 ± 4	108 ± 3
CaM-2TnC	89 ± 5	106 ± 5	89 ± 3	107 ± 4	84 ± 5	106 ± 2
CaM-3TnC	97 ± 2	111 ± 2	76 ± 3	99 ± 2	80 ± 1	102 ± 3
CaM-4TnC	80 ± 3	99 ± 3	80 ± 2	100 ± 2	86 ± 4	82 ± 5
	Inducible NOS					
	NADPH oxidation (%)		Cyt c Reduction (%)		•NO Production (%)	
	200 μM $CaCl_2$	250 μM EDTA	200 μM $CaCl_2$	250 μM EDTA	200 μM $CaCl_2$	250 μM EDTA
wt CaM	100 ± 3	86 ± 4	100 ± 4	84 ± 5	100 ± 4	87 ± 2
T79D	106 ± 1	95 ± 2	120 ± 4	131 ± 7	123 ± 4	71 ± 4
S81D	104 ± 1	103 ± 3	169 ± 3	161 ± 4	58 ± 4	4 ± 1
T79D S81D	102 ± 1	98 ± 3	149 ± 1	98 ± 2	109 ± 5	18 ± 1
S101D	103 ± 3	97 ± 3	153 ± 3	101 ± 2	115 ± 3	72 ± 4

All assays were performed @ 25 °C, in the presence of 2 μM wt CaM or CaM mutant and either 200 μM $CaCl_2$ or 250 μM EDTA as indicated, unless otherwise specified. All values are expressed as a % relative to wt CaM controls for each set of mutants. NAA = No Apparent Activity.

A study of CaM phosphomimetic mutant activation of NOS enzymes (Spratt et al., 2008).
Activities of **nNOS** bound to wt CaM were **132 min^{-1}** (NADPH oxidation), **1253 min^{-1}**(Cyt c reduction), **36 min^{-1}** (•NO production).
Activities of **eNOS** bound to wt CaM were **27 min^{-1}** (NADPH oxidation), **71.1 min^{-1}**(Cyt c reduction), **9 min^{-1}** (•NO production).
Activities of **iNOS** bound to wt CaM were **1486 min^{-1}** (NADPH oxidation), **82.4 min^{-1}**(Cyt c reduction), **50 min^{-1}** (•NO production).
Data is adapted and summarized from Spratt et al. (2008).

2.1.2 Using Surface Plasmon Resonance to Investigate the CaM-NOS Interaction

The previous studies from Section 2.1.1 have suggested possible effects different regions within CaM have on the activation of •NO production in NOS isozymes by observing activation rates. These studies gave more insight about the dynamic interplay that can occur between CaM and NOS. Binding rate constants and affinities for the mutant CaM proteins detailed in Section 2.1.1 interacting with CaM-binding site peptides of NOS enzymes, have not yet been determined.

A study by Zoche et al. (1995) investigated the binding of wt CaM to peptides representing the CaM-binding domains nNOS and iNOS and determined both binding rate constants and dissociation constants for both isozymes using traditional SPR. Similarly, this current study will aim to determine the same binding parameters as those determined by Zoche et al. (1995) for the aforementioned CaM mutants (Section 2.1.1) binding to all 3 NOS peptide sites of all three NOS isozymes using a modified SPR method known as localized SPR (L-SPR) spectroscopy (Figure 2.6) (2.1.2.1). The results from this SPR study will be used to supplement the activity data acquired from past activity experiments (Section 2.1.1). We hope to correlate the binding kinetics from this SPR study with the activity profiles from the assay studies and see if there is a direct relationship between the affinity of CaM protein and the activation of NOS activity.

2.1.2.1 Localized Surface Plasmon Resonance

SPR is an emerging technique to study the thermodynamics and kinetics of biological binding processes (Piliarik et al., 2009). The most popular commercially available SPR instrument used today is the BIAcore®. With traditional SPR experiments, continuous metal films are used as the sensing platform for propagating plasmons (Section 1.3). However, with recent advances in science and engineering, the ability to control the fabrication and manipulation of metallic structures on the nanoscale has paved the way for the development of new sensing platforms that utilize small metal nanoparticles instead of continuous films (Haes & Van Duyne, 2004).

Compared to metal films, the light used to stimulate the surface interacts with nanoparticles much smaller than the incident wavelength, leading to plasmons that oscillate locally around the particle with a frequency known as the L-SPR (Haes & Van Duyne, 2004). Similar to its traditional predecessor, L-SPR spectroscopy can provide thermodynamic and real-time kinetic data for bimolecular interactions. Although traditional SPR sensors provide higher sensitivity to changes in the bulk refractive index than L-SPR sensors (Figure 2.5), the response from both methods are comparable. This is a result of smaller sensing volumes offered in L-SPR sensors due to a 40-50 times reduction in the electromagnetic (EM)-field-decay length (Figure 2.5) (Willets & Van Duyne, 2007).

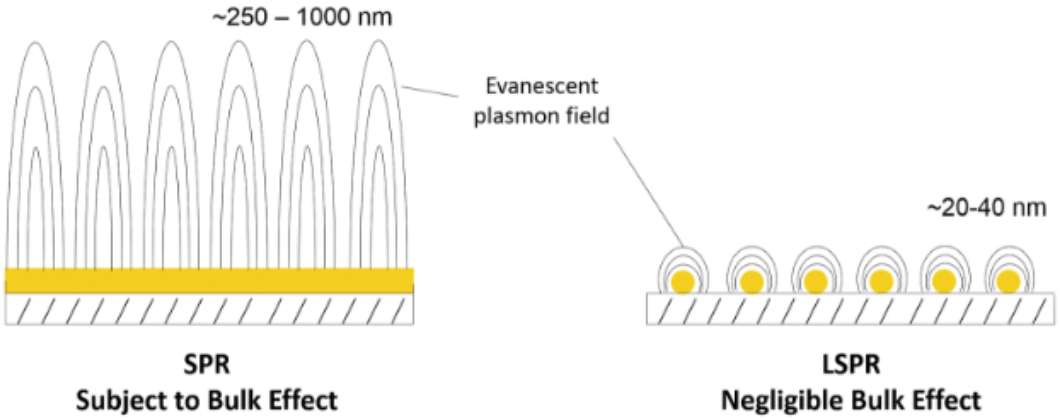

Figure 2.5 - SPR sensors VS. L-SPR sensors
Schematic diagram illustrating the benefits of L-SPR, highlighting the key differences in terms of metal surface composition, response sensitivity to bulk effects and the length of electromagnetic field decay. This figure was reprinted with permission from Nicoya Lifesciences Inc. ©2016.

Moreover, L-SPR produces a strong resonance absorbance peak in the visible range of light, with its position highly sensitive to the local refractive index surrounding the particle (Figure 2.5). Therefore, L-SPR typically senses small changes in the wavelength of the absorbance position, rather than the angle as with traditional SPR (Willets & Van Duyne, 2007). Another advantage that LSPR sensors offer is that they can be manufactured at a more affordable price than current commercial SPR instruments on the market (Haes & Van Duyne, 2004). The hardware needed for L-SPR sensors is less complex as no prism is needed to couple the light, as well as no strict temperature control. This simplifies the instrument as it can be made smaller as well as making them more robust against vibrational and mechanical noise. Furthermore, the utilization of nanoparticles instead of continuous metal films leads to cheaper manufacturing costs of sensor chips (Willets & Van Duyne, 2007). With this is mind, this SPR study was completed in partnership with Nicoya Lifesciences Inc., developers and manufacturers of the benchtop L-SPR biosensing platform, OpenSPR™ (Appendix B).

2.2 Experimental Procedures

2.2.1 Expression of Wild-Type CaM

pET9dCaM plasmid (Appendix B) was transformed into BL21 (DE3) *E. coli* cells using electroporation with Eppendorf Electroporator (insert specifics here). Transformants were plated onto ampicillin-selective lysogeny broth (LB) media and grown overnight for 16 hrs. Individual colonies from overnight plates were used to inoculate 2 x 50 mL ampicillin-selective terrific broth (TB) media in 250 mL flasks and grown overnight at 37 °C, 200 rpm. 25 mL of overnight starter culture was used to inoculate 2 x 1 L ampicillin-selective TB media. 1 L cultures were grown at 37 °C, 200 rpm, to an optical density (OD) at 600 nm of 0.6 - 0.8 and protein expression was induced with 500 μM isopropyl B-D-1-thiogalactopyranoside (IPTG). Cells were harvested after 3 – 4 hours of expression by centrifugation at 6000 x g at 4 °C for 5 minutes, flash frozen and stored at -80 °C.

2.2.2 Purification of Wild-Type CaM

Cells were thawed on ice and resuspended in 4 volumes of 50 mM Tris-HCl, 100 mM NaCl, 1 mM dithiothreitol (DTT) with an addition of a cOmplete protease inhibitor cocktail tablet (Roche). Cells were lysed by homogenization using an Avestin EmulsiFlex-C5 homogenizer (Ottawa, ON). Extra cellular debris was clarified by centrifugation at 48,000 x g for 30 mins at 4 °C and the supernatant was collected. The protein was purified using a phenyl sepharose column (GE Healthcare Life Science) on the AKTAFPLC (GE Healthcare Life Science). The column was equilibrated with 5 column volumes of Buffer A (50 mM Tris-HCl, 1 mM $CaCl_2$, pH 7.5, 4 °C). Calcium chloride ($CaCl_2$) was added to the supernatant to a concentration of 5mM to saturate CaM with Ca^{2+} and expose hydrophobic patches and ensure interaction with the phenyl sepharose resin. The Ca^{2+}-saturated solution was loaded fully onto the column at a rate of 1 mL/min and the column was washed using Buffer A. This was followed with 2 rounds of washes using Buffer B (50 mM Tris-HCl, 500 mM NaCl, 1 mM $CaCl_2$, pH 7.5, 4 °C) to remove any non-specific proteins binding to the resin and then Buffer A again to remove NaCl. The CaM proteins were then eluted from the phenyl sepharose column using Buffer C (10 mM Tris-HCl, 10 mM EDTA, pH 7.5, 4 °C) and 1 mL fractions were collected and pooled.

Pooled fractions were scanned from 350 – 250 nm on a Cary 4000 UV-visible spectrophotometer (Varian, Mississauga, ON). The collected fraction should show characteristic absorbance peaks of CaM at 277 nm (tyrosine residues) and 269, 265, 259 and 253 (phenylalanine residues). The pooled fractions were dialysed overnight against 1 L of Buffer A using 6-8000 MWCO dialysis tubing (VWR

International, Mississauga, ON). Dialysis tubing was prepared in boiling MQH_2O with addition of sodium bicarbonate and a pinch of EDTA for 10-15 minutes and rinsed thoroughly with MQH_2O. Dialyzed fractions were scanned once again to determine the concentration of the purified CaM using the ε_{277} of 3029 $M^{-1}cm^{-1}$ for CaM saturated with Ca^{2+}. The purified CaM was aliquoted in 100 µL fractions, flash frozen and stored at -80 °C.

2.2.3 Expression and Purification of EF-Hand Pair CaM Mutants

EF Hand mutant proteins were expressed in BL21 (DE3) *E.coli cells* transformed with pnCaMChlor, pcCaMKan, pCaMNNKan and pCaMCCKan Appendix A) plasmids prepared by previous members of our lab. Protein sequences are outlined in Figure 2.2. The expression procedure was the same as previously described for wild-type CaM (section 2.2.1).

2.2.4 Expression and Purification of CaM-TnC Chimeras

CaM-TnC proteins were expressed in BL21 (DE3) *E.coli cells* transformed with pCaM-1TNCKan, pCaM-2TNCKan, pCaM-3TNCKan and pCaM-4TNCKan plasmids subcloned by previous members of our lab (Appendix B). The expression procedure was the same as previously described for wild-type CaM (section 2.2.1).

EF Hand mutant CaM proteins were purified as previously described for wild-type CaM (section 2.2.2).

2.2.5 Expression and Purification of CaM Phosphomimetic Mutants

CaM phosphomimetic mutant proteins were retrieved from stocks expressed and purified by previous members of our lab. These mutants were expressed and purified as previously described in Spratt et al. (2008)

2.2.6 Characterization of CaM Mutants

All CaM proteins were characterized using ultraviolet-visible (UV-Vis) spectroscopy (Section 2.2.1), sodium dodecyl sulfate polyacrylamide gel electrophoresis (SDS-PAGE), electrospray ionization - mass spectrometry (ESI-MS) (Section 2.2.6.1) and circular dichroism (CD)

2.2.6.1 Mass Spectrometry

ESI-MS was done using a Quadrupole Time-OF-Flight (QTOF) spectrometer (Micromass, Mancheser, UK) on all purified CaM mutants as well as retrieved CaM phosphomimetic mutants to ensure the absence of posttranslational modifications on CaM proteins and the correct size of protein. CaM mutants were prepared for ESI-MS by buffer transfer into water using a Y3000 centrifugual filter device (Millipose, Millerica, MA, USA) and then diluted using a 1:1 CH_3OH:H_2O containing 0.1% formic acid to a concentration of approximately 5-10 pmol in 300 µL. The samples were infused at 10 µL/min. Raw data (m/z) was collected and then run through deconvolution software to yield spectra with a true molecular mass scale.

2.2.7 Surface Plasmon Resonance Spectroscopy of CaM Proteins with NOS Peptides

SPR analysis was completed using the OpenSPR by Nicoya LifeSciences (Waterloo, ON, Canada) (Appendix B) at 25 °C with a 100 µL loading loop.

2.2.7.1 SPR Chip Preparation for cNOS Peptide Immobilization on Standard Gold Chips

The interaction of CaM proteins with cNOS peptides were completed using a standard gold sensor chip (Appendix B). Gold chips were rinsed with ethanol, followed with acetone and finally isopropanol. The gold chip was soaked in an isopropanol (IPA) bath in a petri dish for 5 minutes and subsequently dried with filtered air using a syringe filter. The chip was then treated with a 7:3 piranha acid solution[1] (sulfuric acid to 30% hydrogen peroxide) for 10 minutes in another petri dish. The reaction was quenched with MQH_2O. The chip was rinsed with MQH_2O to remove any traces of acid on the surface, followed with an ethanol rinse. Lastly, the chip was submerged in an ethanol bath for a minimum of 2 hours before use.

2.2.7.2 SPR Chip Preparation for iNOS Peptide Immobilization on Streptavidin-Functionalized Gold Chips

The interaction of CaM proteins with iNOS peptides were completed using a streptavidin functionalized sensor chip. The streptavidin chip was rinsed with cold MQH_2O and dried with filtered air using a syringe filter.

[1] ***WARNING***: Piranha acid is a strong oxidizer. Both liquid and vapour forms are highly corrosive to skin and respiratory tract. Direct contact can be extremely destructive to mucous membranes, upper respiratory tract, eyes and will cause skin burns. Review MSDS and ensure proper safe work practices and training before use.

2.2.7.3 Binding Kinetic Analysis of CaM Proteins and Immobilized cNOS Peptides

nNOS & eNOS CaM-binding domain peptides were ordered (CanPeptide, Quebec) containing an –SH terminal (Table 2.2). The OpenSPR was run at 150 µL/min with phosphate-buffered saline (PBS) (1X PBS, pH 7.5) equilibration buffer and a dark/light reference was taken with a blank gold chip. A newly prepared chip (Section 2.1.7.1) was loaded into the sample holder for equilibration for approximately 10 minutes to stabilize the baseline. 80% IPA was loaded and injected for 10 seconds (referred to as a pulse injection) to remove any air bubbles in the system. The pump speed was reduced to 50 µL/min. cNOS peptides were immobilized onto the gold surface by injecting a solution of 5:1 cysteamine to cNOS peptide in PBS equilibration buffer.[2] Cysteamine was added as a blocking agent to ensure adequate spacing between peptides.

Table 2-5 - NOS CaM-binding domain peptide sequences

NOS Peptide	Sensor Chip	Protein Sequence ($N_{terminal}$ → $C_{terminal}$)
nNOS	Standard Gold	KRRAI – GFKKL – AEAVK – MGQAM – AKRV**C**
eNOS	Standard Gold	TRKKT – FKEVA – NAVKI – SASLM - **C**
iNOS	Streptavidin	**Biotin** – GSGGG- GRRWI –PLKVL –VKAVL – FACML –MRK

This table displays the protein sequences of the 3 peptide ligands used in this SPR study. The binding elements used to bind onto the sensor chip surface are highlighted in red. Sensor chips were provided by Nicoya Lifesciences.

Several injections of 1 mM cysteamine in equilibration buffer were done to saturate the rest of the surface and prevent non-specific binding (NSB). After each injection, equilibration buffer was pumped for approximately 10 minutes or until the response signal was stabilized. The inlet line was switched into PBS analyte buffer (1X PBS, pH 7.5 + 0.1 mM $CaCl_2$) and buffer was allowed to flow until the signal reached a new baseline. A range of decreasing wt CaM concentrations (500-25 nM) were prepared and injected in analyte buffer (association phase). After each injection of sample, analyte buffer was pumped for approximately 8-12 minutes or until the response signal was stabilized (dissociation phase). An injection of regeneration buffer (1X PBS, pH 8.0 + 10 mM EDTA) in between analyte concentrations was done to fully dissociate any remaining bound CaM proteins from the peptide surface and to bring the signal back to baseline (regeneration phase). A blank injection of analyte buffer was done at the end to measure the background signal. Analysis of the the data and calculations of the kinetic parameters were done using TraceDrawer software as recommended by the manufacturer. The system was cleaned as recommended by the manufacturer.

[2] NOTE: The sample line was purged with buffer and air after each injection to prevent the contamination and diffusion of the succeeding injections into the new sample being loaded.

2.2.7.4 Binding Kinetic Analysis of CaM Proteins and Immobilized iNOS Peptide

iNOS CaM-binding domain peptide was ordered with a biotin label (CanPeptide Inc., Quebec, Canada) (Table 2.2). The OpenSPR was run at 150 µL/min with 3-*N*-morpholinopropane-1-sulfonic acid (MOPS) analyte buffer (30 MOPS, 100 mM KCl, 0.1 mM $CaCl_2$, pH 7.5) and a dark/light reference was taken with a blank gold chip. A newly prepared chip (Section 2.1.7.2) was loaded into the sample holder for equilibration for approximately 10 minutes to stabilize the baseline. A pulse injection of 80% IPA was done to remove any air bubbles in the system. The pump speed was reduced to 50 µL/min and a 50 µg/µL solution of iNOS peptide was prepared and injected for immobilization. The analyte buffer was pumped for approximately 10 minutes or until the response signal was stabilized. A range of decreasing wt CaM concentrations (500-25 nM) were prepared and injected in analyte buffer (association phase). After each injection of sample, analyte buffer was pumped for approximately 8-12 minutes or until the response signal was stabilized (dissociation phase). An injection of regeneration buffer (10 mM HCl) in between analyte concentrations was done to fully dissociate any remaining bound CaM proteins from the peptide surface and to bring the signal back to baseline (regeneration phase). A blank injection of analyte buffer was done at the end to measure the background signal. Analysis of the the data and calculations of the kinetic parameters were done using TraceDrawer software as recommended by the manufacturer. The system was cleaned as recommended by the manufacturer.

2.3 Results

2.3.1 Protein Expression, Purification, And Characterization

Each of the CaM proteins were expressed and purified with the exception of CaM phosphomimetic mutants, which were retrieved from old stocks from Spratt et al, (2008). Purified CaM proteins were analyzed by SDS-PAGE.

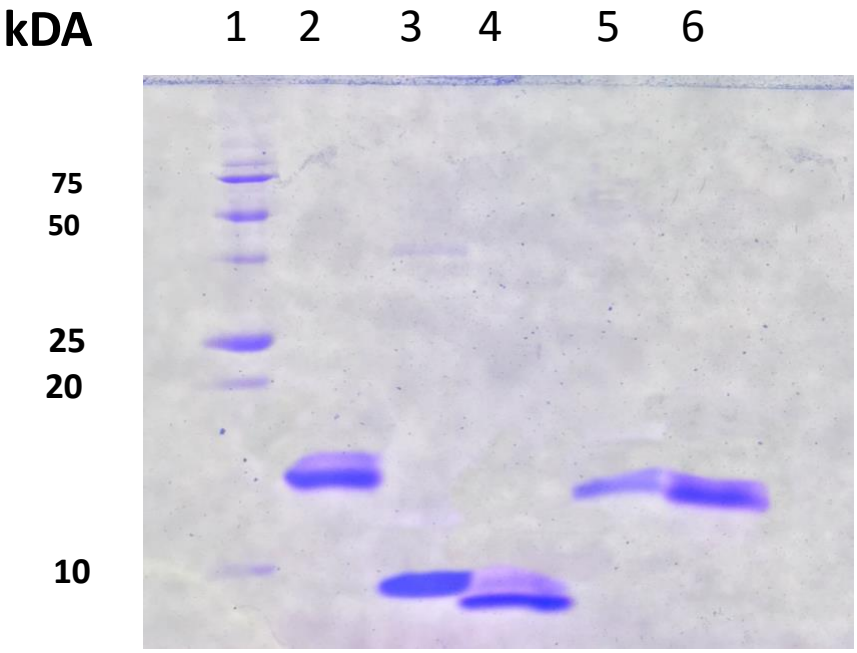

Figure 2.6 - SDS-PAGE of CaM EF-hand pair mutants
The purified EF-hand CaM mutants were run on a 15% SDS-polyacrylamide gel. 10 ug of each protein was loaded into an SDS buffer containing 5% BME. *Lane 1*: Low molecular mass protein standard (Bio Rad); *Lane 2*: wt CaM; *Lane 3:* nCaM; *Lane 4:* cCaM; *Lane 5:* CaMNN; Lane 6: CaMCC. Key protein size markers are labelled on the side

SDS-PAGE analysis of CaM EF-Hand pairs displayed the proper size and were judged to be >95% homogenous. Smudging seen on wt CaM and cCaM can be attributed to artifacts from running the procedure.

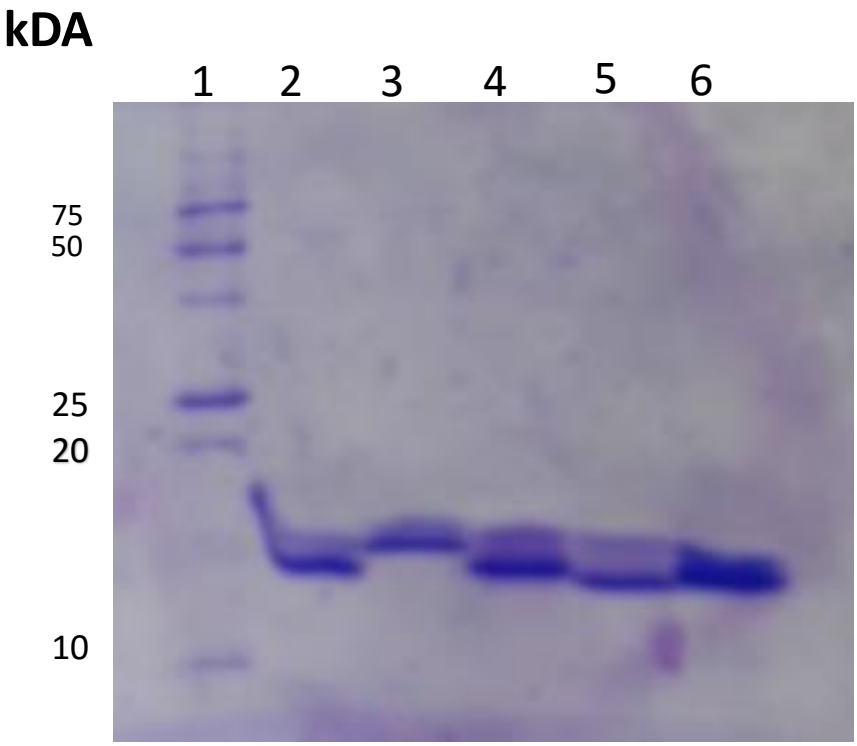

Figure 2.7 - SDS-PAGE of CaM-TnC chimeric mutants
The purified TNC Chimeric mutants were run on a 15% SDS-polyacrylamide gel. 10 ug of each protein was loaded into an SDS buffer containing 5% BME. *Lane 1*: Low molecular mass protein standard (Bioshop); *Lane 2*: wt CaM; *Lane 3:* 1TnC; *Lane 4:* 2TnC; *Lane 5:* 3TnC Lane 6: 4TnC. Key protein size markers are labelled on the side

SDS-PAGE analysis of TnC chimeric proteins displayed the proper size were judged to be >95% homogenous. Smudging of proteins on the gel is an artifact from running the procedure.

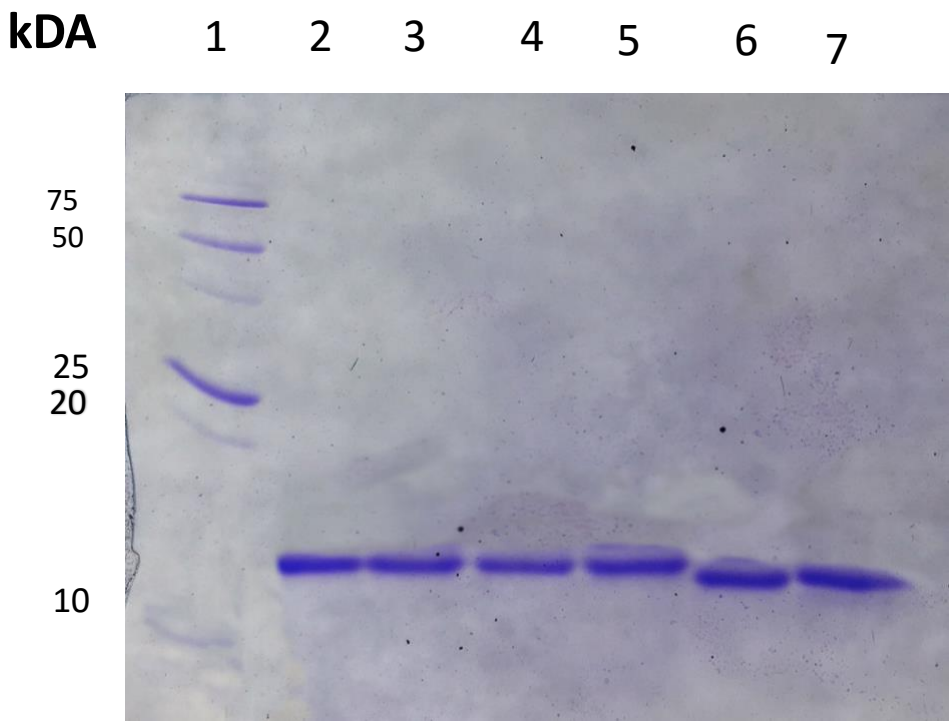

Figure 2.8 - SDS-PAGE of CaM phosphomimetic mutants
The purified central linker mutants were run on a 15% SDS-polyacrylamide gel. 10 ug of each protein was loaded into an SDS buffer containing 5% BME. *Lane 1*: Low molecular mass protein standard (Bio Rad); *Lane 2*: wt CaM; *Lane 3*: CaM T79D; *Lane 4*: CaM T79D/CaM S81D; *Lane 5*: CaM S81D; *Lane 6*: CaM S101D; *Lane 7*: Y99E. Key protein size markers are labelled on the side

SDS-PAGE analysis of retrieved phosphomimetic CaM mutants displayed appropriate banding patterns and CaM proteins were judged to be >95% homogenous. Splaying of the ladder in Lane 1 is an artifact from running the procedure.

All CaM proteins sizes were further verified using ESI-MS to rule out any modifications (Table 2.3). All proteins were verified to be the correct size with the exception of nCaM.

Table 2-6 - ESI-MS analysis of CaM proteins

CaM Protein	Mass (kDa)[a]	
	Theoretical[b]	Observed
wt CaM	16.706	16.705
nCaM	8.317	---[c]
cCaM	8.408	8.407
CaMNN	16.379	16.378
CaMCC	17.033	17.032
1-TnC	17.796	17.794
2-TnC	17.273	17.269
3-TnC	16.732	16.731
4-TnC	16.894	16.893
T79D	16.720	16.719
S81D	16.734	16.733
T79D / S81D	16.748	16.747
Y99E	16.672	16.674
S101D	16.734	16.733

(a) – Masses of deconvoluted ESI-MS spectra are accurate to within 4-5 Da.
(b) – Calculated mass based on amino acid sequence
(c) – Spectra could not be deconvoluted. Analysis of size was confirmed through SDS-PAGE.

As a secondary test to confirm the validity of retrieved phosphomimetic CaMs, spectropolarimetry was employed. All CaM proteins displayed α-helical content expected of CaM proteins, indicated by peaks at 208 and 222 nm. (Results not shown).

Due to the differences observed in Ca^{2+} dependency and immobilization methods between cNOS enzymes vs. iNOS enzymes, the L-SPR binding kinetic analysis of CaM binding to iNOS peptide was done separately (Section 2.3.3) from CaM binding to cNOS peptides (Section 2.3.2) as seen below.

2.3.2 L-SPR Binding Kinetic Analysis of CaM Mutant Proteins with cNOS Peptides

L-SPR was used to monitor real-time binding kinetics of CaM mutant proteins binding with immobilized cNOS peptides. The L-SPR response was observed via a sensogram, which monitors the wavelength of the maximum resonance peak vs. time (Figure 2.9). As a set of controls, L-SPR analysis was first completed for wt CaM binding to both nNOS and eNOS peptides.

The first step involved the immobilization of the cNOS peptide ligand onto the sensor surface. The immobilization of cNOS peptides was most optimal when injecting a 5:1 solution of cysteamine blocker to NOS peptide into the flow cell, producing a large and rapid response, with an average λ shift of at least 0.8 nm – 1 nm. This response indicated a strong and successful binding of the peptide to the gold sensor surface as a new stable baseline was achieved. Cysteamine was added to ensure adequate spacing in between peptides and allow enough space for CaM protein binding. Multiple injections of cysteamine was subsequently done to ensure full saturation of all gold nanoparticle sites on the surface (Figure 2.8.A).

Once the surface was functionalized with the appropriate ligand, the buffer was switched to a Ca^{2+} containing running buffer, ensuring all CaM proteins would be Ca^{2+} saturated for binding cNOS peptides. L-SPR binding analysis occurred in 3 phases: an association phase, a dissociation phase and a regeneration phase. wt CaM prepared in the Ca^{2+} running buffer was injected in decreasing concentrations from 500 nM – 50 nM for the association phase. The rapid response upon exposure of wt CaM on the surface indicated strong 1:1 CaM:cNOS peptide complex formation (Figure 2.8.B). For the dissociation phase, the sensor surface was washed and equilibrated with Ca^{2+} running buffer removing any non-specific and/or weakly bound CaM protein first. The dissociation of the CaM-peptide complex is illustrated by the slow decrease in response over time (Figure 2.8.B). Lastly, 10 mM EDTA was injected for the regeneration phase, chelating all Ca^{2+} ions from remaining bound CaM, disrupting CaM's ability to bind the peptide and completely regenerating the ligand-bound surface as seen by the return of the sensogram back to baseline. The association, dissociation and regeneration phases were repeated for all concentrations of CaM (Figure 2.8.B). For both cNOS peptides CaM binding, a concentration-dependent response was observed.

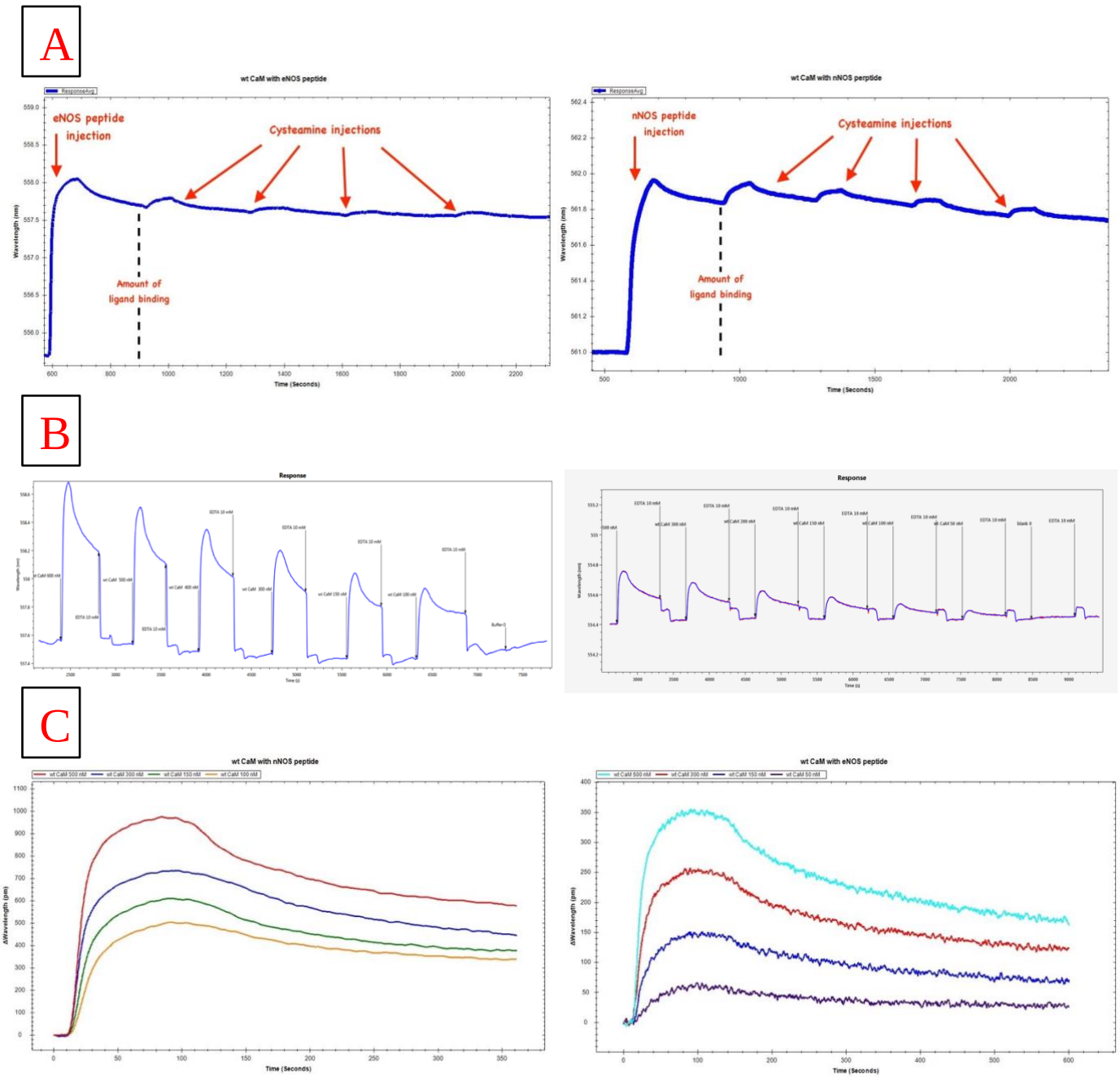

Figure 2.9 - L-SPR Analysis of wt CaM

A typical L-SPR analysis of CaM proteins with immobilized cNOS peptides (**A)** Immobilization of peptide ligands on a nanogold chip. Amount of ligand binding is assessed by the change in baseline. **(B)** CaM analyte injections at decreasing concentrations. Association, dissociation and regeneration phases are seen in real-time. **(C)** Kinetic analysis of L-SPR data using Tracedrawer. Data was fit according to a 1:1 binding model

Lastly, the kinetic parameters were determined by post-analysis of L-SPR data. The sensogram was exported into Tracedrawer software, a curve-fitting program, (Figure 2.8.C). The average measured wavelength of all analyte injections were set to a value of 0 and overlayed on top of each other to compare the phases of SPR binding. The datasets were fit according to a 1:1 binding model, unless otherwise stated, where the binding rate parameters, k_a and k_d, the association and dissociation rate constants (also known as k_{on} and k_{off}) and K_D, the dissociation constant, were determined. For conventional purposes, we will now refer to rate constant parameters as k_{on} and k_{off} for the remainder of this thesis.

We determined k_{on} = 9.77 (± 0.03) x 10^4 $M^{-1}s^{-1}$ and k_{off} = 14 (± 0.003) x 10^{-4} s^{-1} for wt CaM bound to the nNOS peptide. The dissociation constant K_D, a ratio of k_d / k_a, was 14.4 (±0.09) nM. Changes in cNOS peptide concentration immobilized on the surface did not overtly affect the kinetic parameters. These results were not consistent with traditional SPR experiments observed by Zoche et al, (1996) where they determined k_{on} = 1.58 x 10^5 $M^{-1}s^{-1}$, k_{off} = 17.87 x 10^{-4} s^{-1} and K_D = 5.0 for wt CaM bound to the nNOS peptide (Table 2.1). In comparison, traditional SPR analysis yielded a larger k_{on}, resulting in an overall smaller K_D, with a difference of approximately 9 nM compared with the L-SPR value. However, the difference in kinetic parameters between the traditional vs localized methods can be attributed to the longer EM-field-decay length of metal films in traditional SPR sensors vs. the shorter EM-field-decay length of nanoparticles in L-SPR sensors (Section 2.1.2.1). The decrease in surface height of nanoparticles vs. continuous metal films is also known to increase the overall sensitivity of the SPR response (Yonzon et al., 2004).

This is the first time kinetic parameters have been reported for CaM bound to the eNOS peptide using an L-SPR method. We report the values of k_{on} = 15.8 (± 0.02) x 10^4 $M^{-1}s^{-1}$, k_{off} = 18.9 (±0.001) x 10^{-4} s^{-1}, and a dissociation constant K_D of 12.0 (±0.17) nM for wt CaM bound to the eNOS peptide. The binding parameters determined here for CaM and eNOS peptide via L-SPR are largely different than those determined through fluorescence experiments by Wu et al. (2011), where they reported: k_{on} = 2.9 x 10^8 $M^{-1}s^{-1}$, k_{off} = 4.5 s^{-1} and a K_D of 1.6. The difference in values between these two methods is most likely due to different experimental methods. Despite the differences between different methods, the order of binding affinity is the same: CaM binds the eNOS peptide tighter than the nNOS peptide (eNOS > nNOS).

2.3.3 Binding Interactions Between CaM Mutants and cNOS Peptides

After wt CaM controls were established, the procedure was repeated for all CaM mutant proteins binding to both cNOS peptides. This study is the first report of kinetic parameters derived for TnC chimeras, EF-hand pair and phosphomimetic CaM mutants binding to cNOS peptides. The kinetic rate constants, k_{on} & k_{off}, as well as the dissociation constant K_D, calculated from fitting sensogram data with Tracedrawer software, are displayed and summarized in Appendix C. Overall, we measured the quality of binding according to the binding dissociation constant, K_D, which is inversely proportionate to binding affinity, K_A. Furthermore, we used the binding rate constants, k_{on} and k_{off}, as supplementary values to help explain the quality of binding.

In addition, as part of our binding interaction analysis, we compared our experimentally determined kinetic rate parameters of CaM mutant proteins binding to immobilized cNOS peptides to previously determined activity profiles of the same mutant CaM proteins and their ability to activate full cNOS activity, using the assay methods mentioned in Section 2.1.1.1 (Newman et al., 2004; Spratt et al., 2006, 2008). This comparison is further explained in Section 2.3.3.1. and displayed in bar graphs in Section 2.3.3.2 – Section 2.3.3.3.

2.3.3.1 Comparative Analysis of Kinetic Rate Parameters and CaM Mutant Activation Profiles

For our binding analysis, we compared the relative binding and relative activation of mutant CaM proteins with respect to wt CaM binding and activation, where binding and activation of wt CaM was made to be 100%. The values for relative activation of cNOS enzymes were previously determined (Newman et al., 2004; Spratt et al., 2006, 2008) and were attained using Formulas 1-3.

Formula 1 - Relative Activity: NADPH Oxidation

$$\left(\frac{\text{NADPH oxidation}_{mutant}}{\text{NADPH oxidation}_{wt\ CaM}} \times 100\%\right)$$

Formula 2 - Relative Activity: Cytochrome c Reduction

$$\left(\frac{\text{Cytochrome } c \text{ reduction}_{mutant}}{\text{Cytochrome } c \text{ reduction}_{wt\ CaM}} \times 100\%\right)$$

Formula 3 - Relative Activity: •NO production

$$\left(\frac{\bullet\ \text{NO Production}_{mutant}}{\bullet\ \text{NO PRoduction}_{wt\ CaM}} \times 100\%\right)$$

Using L-SPR, we were able to determine the binding rate parameters: k_{on}, k_{off}, and K_D. We expressed our binding results in terms of relative binding, similar to the relative activity outlined in Formulas 1-3. Formula 4 was used to determine relative binding in terms of association rate constant, k_{on}, whereas formula 5 was used to determine relative binding in terms of dissociation rate constant k_{off}. Naturally, a high k_{off} signifies weaker binding, but to display a positive relationship, the inverse of k_{off} values were used. Therefore, for our analysis, higher relative binding in terms of k_{off} signifies stronger binding as it represents slower dissociation rates. Lastly, our overall quality of binding was assessed by comparing relative binding in terms of affinity, K_A, where $\left(K_A = {}^{1}/_{K_D}\right)$ (Formula 6).

Formula 4 - Relative Binding: k_{on}

$$\left(\frac{\mathrm{k}_{on-mutant}}{\mathrm{k}_{on-wt\ CaM}} \times 100\%\right)$$

Formula 5 - Relative Binding: k_{off}

$$\left(\frac{\frac{1}{k_{off-mutant}}}{\frac{1}{k_{on-wt\ CaM}}} \times 100\%\right)$$

Formula 6 - Relative Binding: K_D

$$\left(\frac{\mathrm{K}_{A-mutant}}{\mathrm{K}_{A-wt\ CaM}} \times 100\%\right)$$

2.3.3.2 Binding interactions between CaM-TnC Chimeric Mutants and cNOS peptides

The CaM-TnC proteins displayed varying binding profiles for immobilized nNOS and eNOS peptides. Ranking the overall quality of binding in terms of CaM-TnC mutant affinity for immobilized nNOS peptides were: 4TnC > wt CaM > 1TnC > 2TnC > 3TnC. Rankings for the affinities of CaM-TnC mutants for the immobilized eNOS peptide were: 2TnC > 1TnC > wt CaM > 3TnC >> 4TnC (Figure 2.10).

Figure 2.10 – Comparing CaM-TnC Chimera cNOS Activation and cNOS Peptide Binding
The relative activities for the 3 types are NOS assays are displayed in different shades of blue: NADPH oxidation (light blue), cytochrome c reduction (blue), •NO production (navy blue). Relative binding is displayed in red: k_{on}(diagonal lines), k_{off} (vertical lines), K_D (shaded). nNOS activity and binding are displayed at the top and eNOS activity and binding on the bottom. Relative activities were determined using Formulas 1-3 and details on activity assays are found in Section 2.1.1.2. Relative binding values were determined using Formulas 4-6 and SPR raw data is located in Appendix C and analyzed using Tracedrawer software. All TnC protein binding was completed in duplicate. Bar values represent the standard mean deviation.

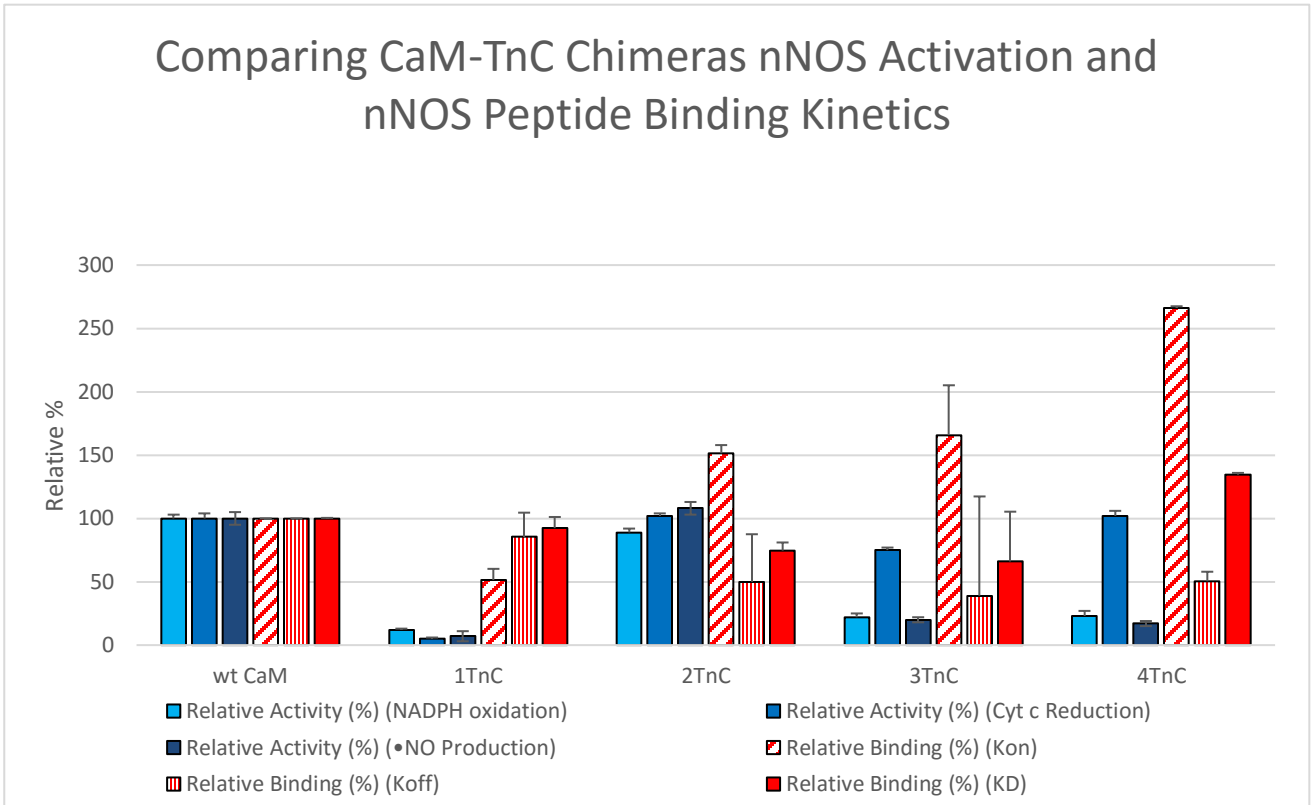
Comparing CaM-TnC Chimeras nNOS Activation and nNOS Peptide Binding Kinetics
Relative %
300
250
200
150
100
50
0
wt CaM
1TnC
2TnC
3TnC
4TnC
Relative Activity (%) (NADPH oxidation)
Relative Activity (%) (Cyt c Reduction)
Relative Activity (%) (•NO Production)
Relative Binding (%) (Kon)
Relative Binding (%) (Koff)
Relative Binding (%) (KD)

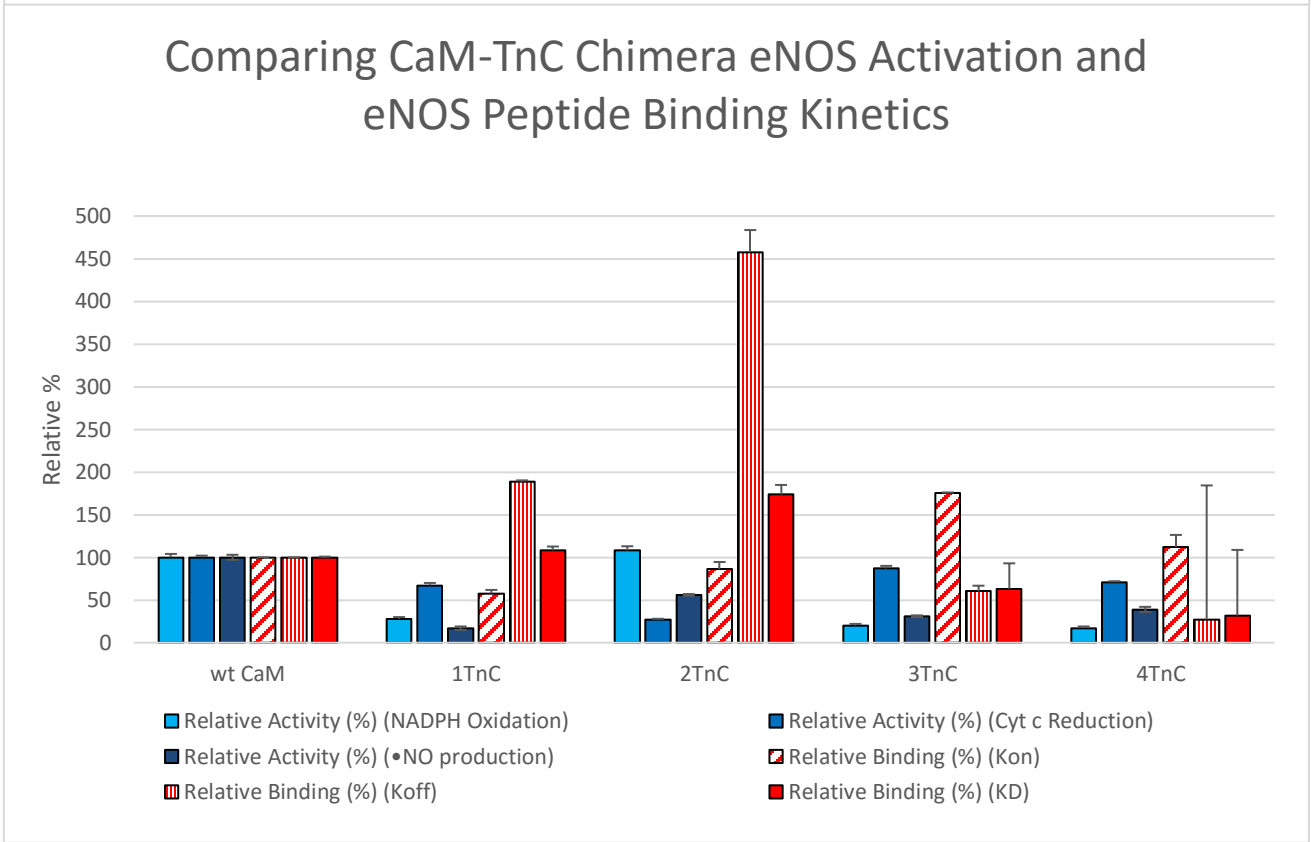
Comparing CaM-TnC Chimera eNOS Activation and eNOS Peptide Binding Kinetics
Relative %
500
450
400
350
300
250
200
150
100
50
0
wt CaM
1TnC
2TnC
3TnC
4TnC
Relative Activity (%) (NADPH Oxidation)
Relative Activity (%) (Cyt c Reduction)
Relative Activity (%) (•NO production)
Relative Binding (%) (Kon)
Relative Binding (%) (Koff)
Relative Binding (%) (KD)

We predicted that for the interactions yielding greater relative affinity, we would yield an association rate constant to dissociation rate constant ratio (k_{on} : k_{off}) <1. The slower the NOS-CaM complex dissociates, or the closer the ratio is closer to 0, the stronger the affinity is for that CaM construct to the associated peptide. With regards to nNOS peptide binding, we see that the 4TnC mutant had greater relative affinity compared to wt CaM, whereas the other TnC mutants displayed weaker relative affinity. Contrary to our prediction, we observed k_{on} : k_{off} ratios of 0.6, 3, 4.2 and 5.2 for 1TnC, 2TnC, 3TnC and 4TnC, respectively. For eNOS peptide binding, 1TnC and 2TnC displayed higher overall relative affinity, where 1TnC displayed similar affinity to wt CaM and 2TnC displayed 1.7x greater affinity. With respect to the k_{on} : k_{off} rate constant ratio, we determined values of 0.3 and 0.2. On the other hand, both 3TnC and 4TnC displayed a substantial decrease in affinity compared to wt CaM. Comparing the k_{on} : k_{off} rate constants ratios, we get values of 2.9 and 4.1. Overall, the protein interactions of TnC constructs with the eNOS peptide follow the expected trend but not with the nNOS peptide. These interactions are further examined in Section 2.4.1.

Comparing our CaM-TnC mutant protein binding data with the activity profiles determined by Newman et al. (2004), we observed no overall underlying correlation between the relative strength of binding of TnC proteins and their relative activities determined in NOS activity assays. For example, the 2TnC construct displayed diminished binding in terms of the nNOS peptide and greater binding in terms of the eNOS peptide. However, we see greatly diminished activities of eNOS enzyme when activated by the same CaM mutant and greater relative activity in the nNOS enzyme. We see this mismatch in binding and activity throughout all 4 of the CaM-TnC mutants. These results can be explained by the fact that we are specifically only looking at CaM protein binding in terms of a small portion of the NOS enzyme, and not the full holoenzyme. In other words, there are elements of the NOS enzyme and CaM outside the specific interactions in the NOS-CaM binding domain that could stabilize/destabilize the interaction of CaM with NOS that could affect both activity and binding. The relationship between cNOS peptide binding and cNOS activation for CaM TnC chimeras is further explored in Section 2.4.

2.3.3.3 Binding Interactions Between CaM EF-Hand Pair Mutants and cNOS Peptides

Compared to the CaM-TnC mutants, the EF-hand proteins showed similar binding profiles for nNOS and eNOS peptides. Ranking the overall quality of binding in terms of CaM mutants for immobilized nNOS peptides were: CaMNN > wt CaM/CaM CC >> nCaM/cCaM. On the other hand, ranking the affinities of EF-hand CaM mutants for the eNOS peptide were: CaMCC > CaMNN > wt CaM >> nCaM/cCaM (Figure 2.11).

Figure 2.11 – Comparing CaM EF-Hand Mutant cNOS Activation and cNOS Peptide Binding The relative activities for the 3 types are NOS assays are displayed in different shades of blue: NADPH oxidation (light blue), cytochrome c reduction (blue), •NO production (navy blue).). Relative binding is displayed in red: k_{on}(diagonal lines), k_{off} (vertical lines), K_D (shaded). nNOS activity and binding are displayed at the top and eNOS activity and binding on the bottom. Relative binding is displayed in red: k_{on}(diagonal lines), k_{off} (vertical lines), K_D (shaded). Relative activities were determined using Formulas 1-3 and details on activity assays are found in Section 2.1.1.2. Relative binding values were determined using Formulas 4-6 and SPR raw data is located in Appendix C and analyzed using Tracedrawer software. All TnC protein binding was completed in triplicate. Bar values represent the standard mean deviation. *= No Apparent Activity (NAA)/ No Apparent Binding (NAB).

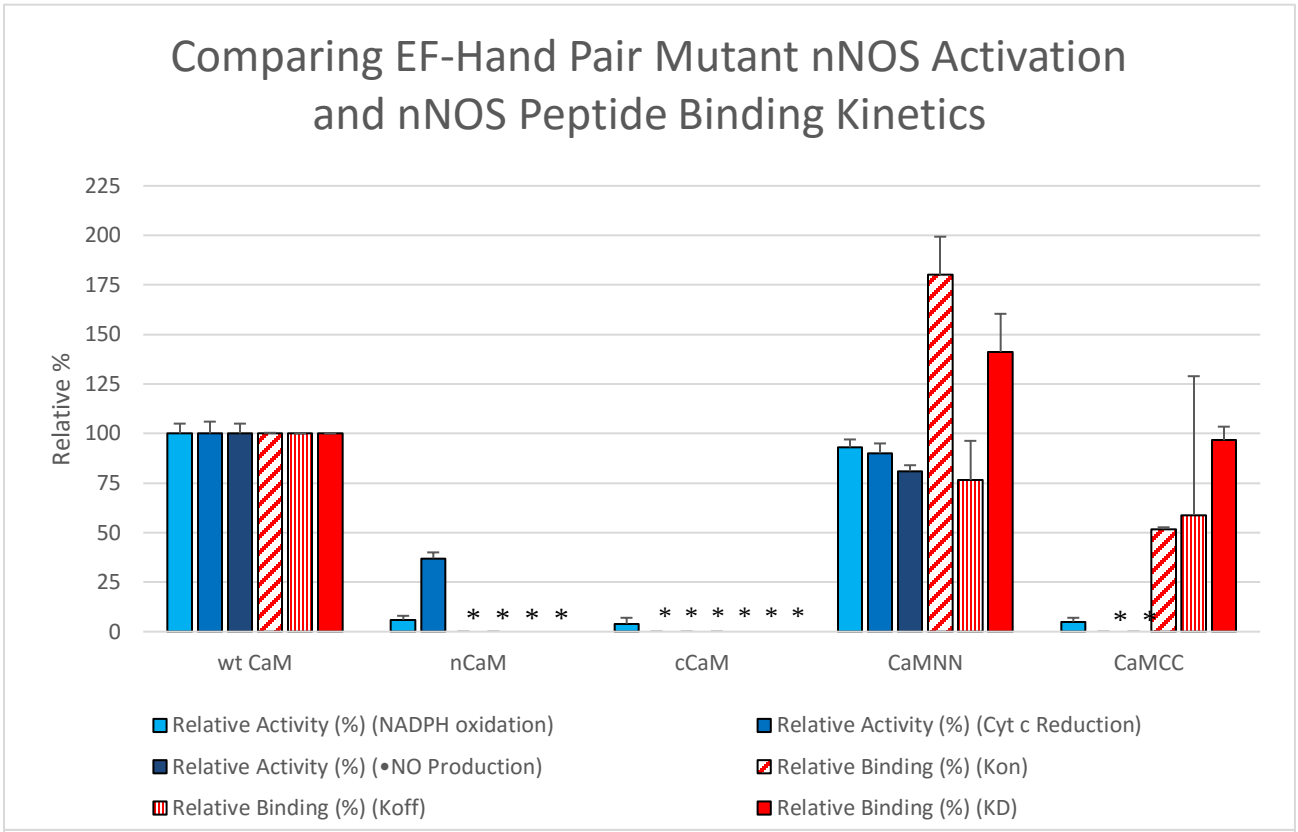
Comparing EF-Hand Pair Mutant nNOS Activation and nNOS Peptide Binding Kinetics
Relative %
225
200
175
150
125
100
75
50
25
0
wt CaM
nCaM
cCaM
CaMNN
CaMCC
Relative Activity (%) (NADPH oxidation)
Relative Activity (%) (Cyt c Reduction)
Relative Activity (%) (•NO Production)
Relative Binding (%) (Kon)
Relative Binding (%) (Koff)
Relative Binding (%) (KD)

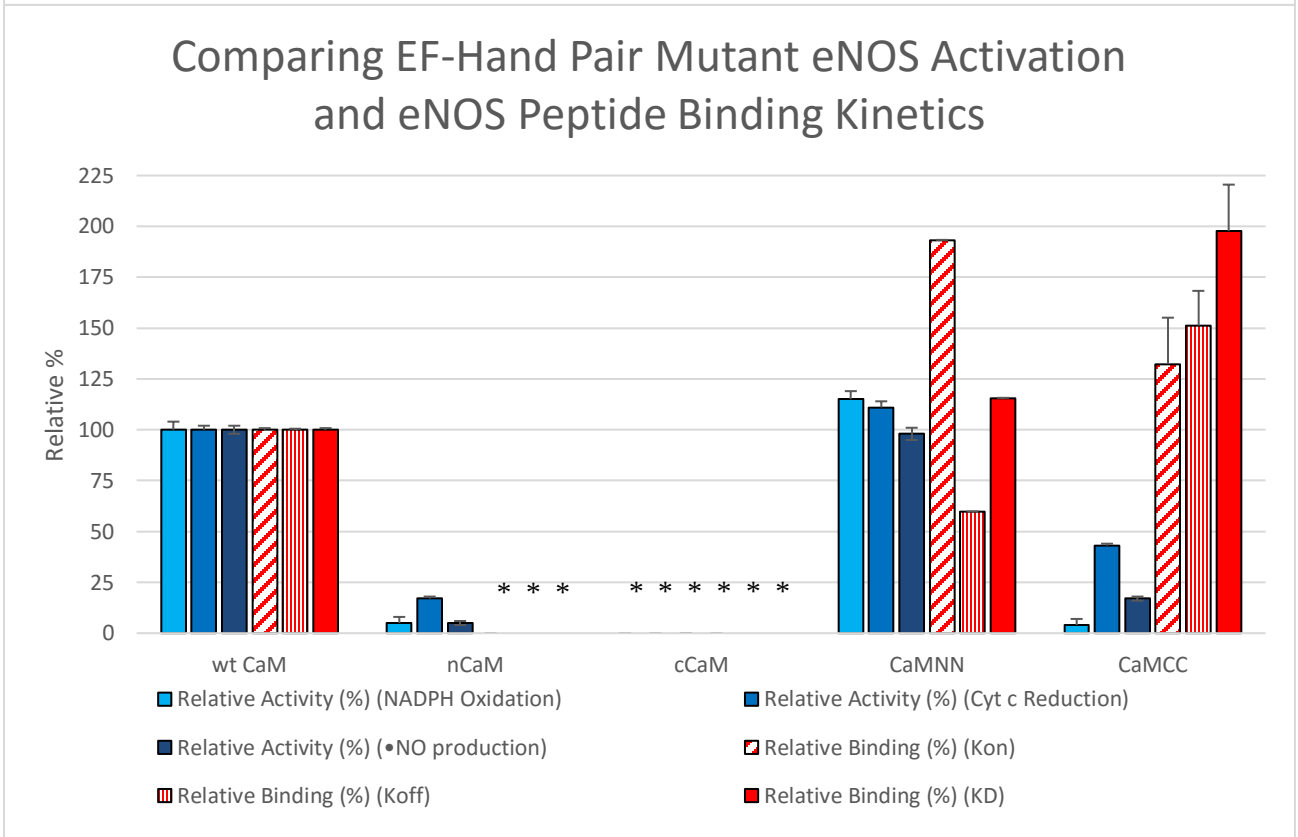
Comparing EF-Hand Pair Mutant eNOS Activation and eNOS Peptide Binding Kinetics
Relative %
225
200
175
150
125
100
75
50
25
0
wt CaM
nCaM
cCaM
CaMNN
CaMCC
Relative Activity (%) (NADPH Oxidation)
Relative Activity (%) (Cyt c Reduction)
Relative Activity (%) (•NO production)
Relative Binding (%) (Kon)
Relative Binding (%) (Koff)
Relative Binding (%) (KD)

Interestingly, both single EF-hand mutant constructs, nCaM and cCaM, displayed no significant relative binding with both cNOS peptides. In contrast, duplicate EF-hand pair constructs, CaMNN and CaMCC, showed significant relative binding. In terms of the nNOS peptide, CaMNN had 1.4x greater affinity for the peptide, whereas CaMCC had comparable affinity when compared to wt CaM with k_{on} : k_{off} ratios of 2.4 and 0.87. The opposite is observed for the eNOS peptide where we see that CaMNN had comparable affinity for the peptide compared to wt CaM, whereas CaMCC displayed 2x greater affinity than wt CaM with k_{on} : k_{off} ratios of 3.2 and 0.87. CaMCC followed the expected trend where the greater relative affinity is due to having a slower dissociation rate. On the contrary, the CaMNN construct displayed strong affinity for both peptides but displayed a higher rate of dissociation. These interactions are further examined in sections 2.4.2.

Comparing our CaM EF-hand pair mutant binding data with the activity profiles determined by Spratt et al. (2006), we see a strong correlation between the single EF-hand pair constructs wherein the lack of apparent cNOS activity across all 3 assays is associated by the weak affinity of these constructs for the peptide. Analysis of the single EF-hand pairs on the SPR displayed initial binding during the association phase, but dissociated rapidly as indicated by a very steep drop in response. This interaction was almost identical to a bulk shift response and thus could not be properly fitted and evaluated using the TraceDrawer software. Therefore, the binding of these constructs was noted as NAB (Figure 2.11). Conversely, we do not see the same correlation for the duplicate EF-Hand pairs. The mismatch in relative binding compared to relative activity similar to that seen in CaM TnC chimeras is observed for the CaMCC construct, but not CaMNN. Similar to the TnC proteins in Section 2.3.3.2., we see that for CaMCC, high affinity does not translate into high activity. The same caveat applies in this investigation where the binding interactions is limited to only a small portion of the cNOS holoenzyme. The relationship between cNOS peptide binding and cNOS activation for CaM EF-hand mutants are further explored in Section 2.4.2.

2.3.3.4 Binding interactions between Phosphomimetic CaM Mutants and cNOS peptides

Similar to the TnC mutants, the phosphomimetic mutants showed varying binding profiles for cNOS peptides. Ranking the affinities of phosphomimetic mutants for the nNOS peptide were: wt CaM > S81D > S101D / [T79/S81D] > T79D/Y99E. Ranking the affinities of phosphomimetic mutants for eNOS peptide were: wt CaM > Y99E > T79D > S81D / S101D >> [T79D/S81D] (Figure 2.12).

Figure 2.12 - Comparing Phosphomimetic CaM Mutant cNOS Activation and cNOS Peptide Binding

The relative activities for the 3 types are NOS assays are displayed in different shades of blue: NADPH oxidation (light blue), cytochrome c reduction (blue), •NO production (navy blue). nNOS activity and binding are displayed at the top and eNOS activity and binding on the bottom. Relative binding is displayed in red: k_{on}(diagonal lines), k_{off} (vertical lines), K_D (shaded). Relative activities were determined using Formulas 1-3 and details on activity assays are found in Section 2.1.1.2. Relative binding values were determined using Formulas 4-6 and SPR raw data is located in Appendix C and analyzed using Tracedrawer software. All TnC protein binding was completed in triplicate. Bar values represent the standard mean deviation.

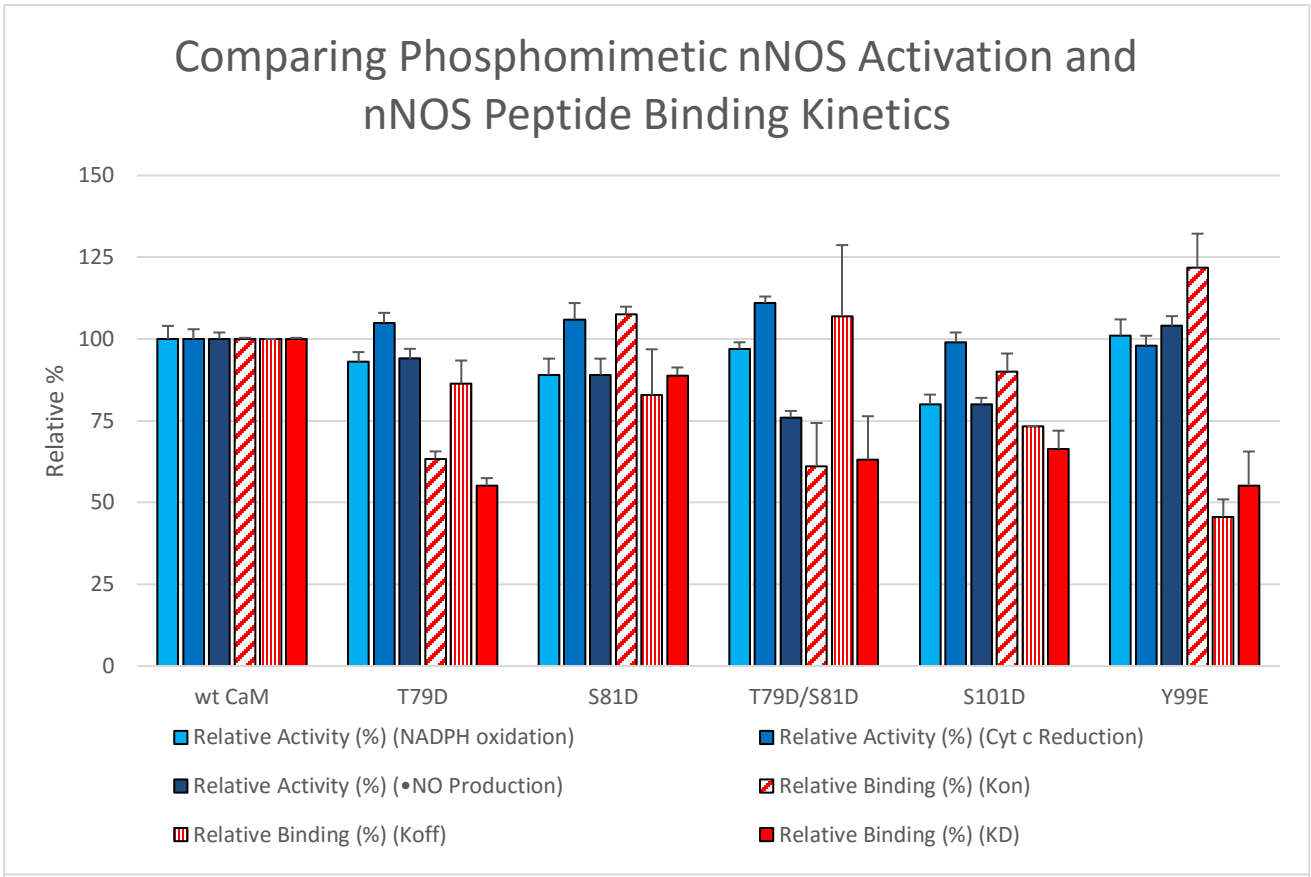
Comparing Phosphomimetic nNOS Activation and nNOS Peptide Binding Kinetics
Relative %
150
125
100
75
50
25
0
wt CaM
T79D
S81D
T79D/S81D
S101D
Y99E
Relative Activity (%) (NADPH oxidation)
Relative Activity (%) (Cyt c Reduction)
Relative Activity (%) (•NO Production)
Relative Binding (%) (Kon)
Relative Binding (%) (Koff)
Relative Binding (%) (KD)

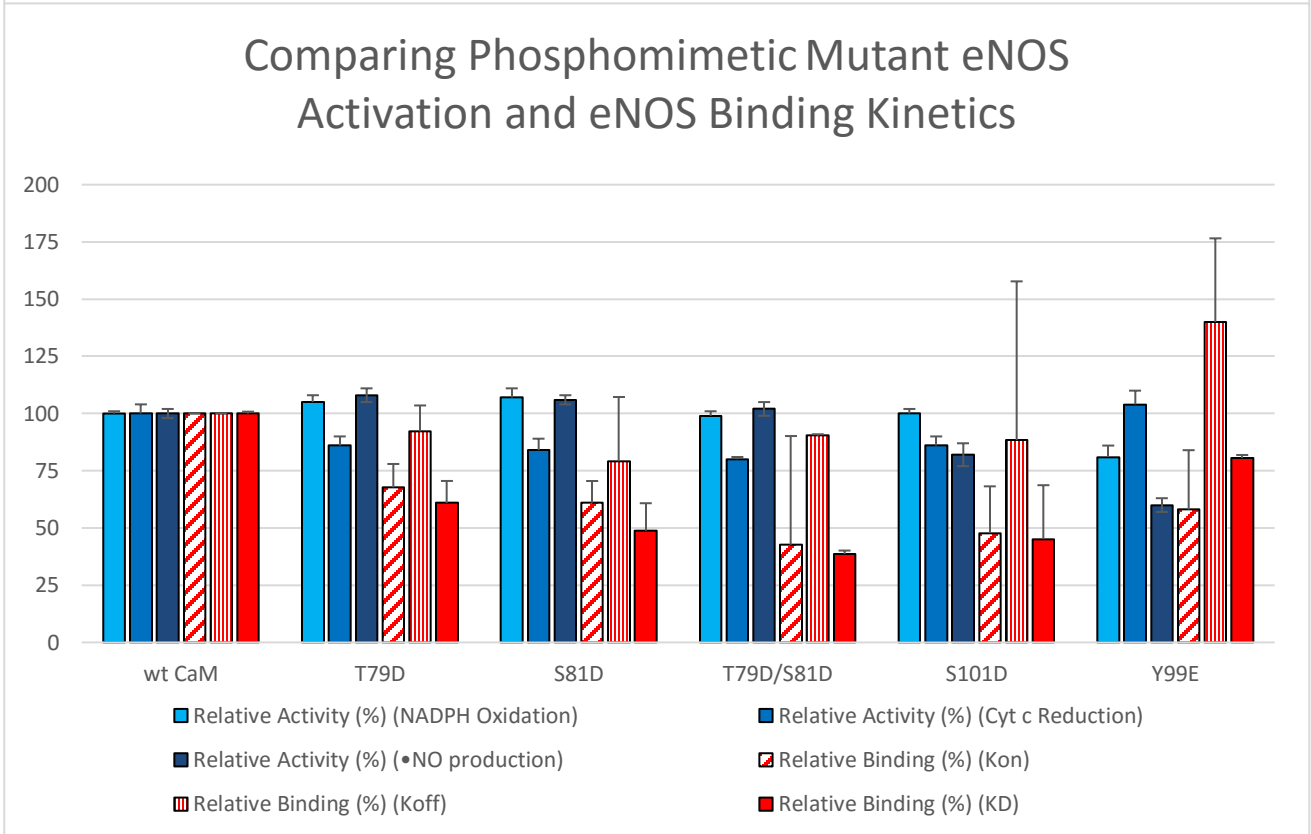
Comparing Phosphomimetic Mutant eNOS Activation and eNOS Binding Kinetics
200
175
150
125
100
75
50
25
0
wt CaM
T79D
S81D
T79D/S81D
S101D
Y99E
Relative Activity (%) (NADPH Oxidation)
Relative Activity (%) (Cyt c Reduction)
Relative Activity (%) (•NO production)
Relative Binding (%) (Kon)
Relative Binding (%) (Koff)
Relative Binding (%) (KD)

All phosphomimetic proteins in this study displayed lesser relative affinity for both nNOS and eNOS peptides suggesting that the introduction of a negative charge at these sites weakly disrupt the electrostatic interactions that stabilize CaM binding to the canonical nNOS and eNOS CaM-binding domain and implying that phosphorylation at these sites inhibit NOS activity. These results are in agreement with past phosphorylation studies (Greif et al., 2004; Mishra et al., 2010; Piazza et al., 2012; Spratt et al., 2008). Taking a look at the k_{on} : k_{off} ratios, we observed ratio values for nNOS peptide of 0.73, 1.29, 0.57, 1.23 and 2.65 for phosphomimetic mutants T79D, S81D, T79D/S81D, S101D and Y99E, respectively. For eNOS peptide binding, we observed ratios of 0.72, 0.77, 0.47, 0.54 and 0.41 for the same phosphomimetic mutants. These ratio values did not match our expected results where lesser relative affinity should correlate to ratio values of >1, suggesting that the dissociation of the NOS-CaM complex is favored due to higher dissociation rates compared to the rate of association. These interactions are further examined in Section 2.4.3.

Comparing the binding results with the activity profiles determined by Spratt et al. (2008), the diminished amount of binding correlated well with diminished activity observed for CaM central linker phosphomimetic proteins T79D, S81D, T79D/S81D as well as the phosphomimetic mutant S101D (Figure 2.12). As previously mentioned, the phosphorylation of Y99 was observed to induce hypoxia in newborn piglets due to increased nNOS activity (Mishra et al., 2010). Although our binding study shows that there is overall, lesser relative affinity for our phosphomimetic Y99E compared to wildtype for both peptides, we do observe a corresponding large increase in the rate of association in binding the nNOS peptide compared with the eNOS peptide. This discrepancy is most likely the reason for the induction of detrimental effects observed in piglets. The relationship between cNOS peptide binding and cNOS activation for phosphomimetic mutants are further examined in Section 2.4.3.

2.3.4 L-SPR Binding Kinetic Analysis of CaM Mutant Proteins with iNOS Peptide

Unlike the cNOS peptides, the immobilization of iNOS peptide required the use of a special functionalized sensor chip. In contrast with the cysteine modified cNOS peptides, the iNOS peptide contained a cysteine in the middle of the sequence (Table 2.2). Although it would have been beneficial to use the inherent traits of the peptide for immobilization to reduce the amount of modifications needed, one of the disadvantages of using immobilization techniques is ensuring proper orientation of the ligand on the surface (O'Shannessy & Winzor, 1996). With the cysteine in the middle, the orientation of the peptide could not be controlled. A non-uniform surface could lead to

errors in readings and misinterpretation of results (O'Shannessy & Winzor, 1996). Therefore, the strong streptavidin-biotin bond was employed.

Streptavidin is a 52.8 kDa protein that has an extremely high affinity for biotin, a water-soluble B-vitamin. Streptavidin's affinity for biotin has a reported K_D on the order of 10^{-14} mol/L, making this bond one of the strongest non-covalent interactions known in nature. This interaction is heavily used in molecular biology and biotechnology due to the streptavidin-biotin complex being resistant to a multitude of organic solvents, denaturants, detergents, proteolytic enzymes, and extreme temperatures and pH. Only extremely harsh conditions are able to break this interaction, which can oftentimes denature the protein analyte being studied.

With this in mind, the iNOS peptide was synthesized with a biotin label at the N-terminus (Table 2.2) and a gold sensor chip functionalized with streptavidin was provided by Nicoya Lifesciences. Initial immobilization tests using 20 ug/mL of biotinylated iNOS peptide showed strong binding to the streptavidin functionalized sensor chip as indicated by an average λ shift of at least 0.7 nm. Titration of 500 nM wt CaM sample produced a very small response. However, the CaM-iNOS peptide complex did not dissociate during the dissociation phase and could not be removed using EDTA regeneration solution. iNOS enzymes are known to have a high affinity for CaM. These results correlate with previous SPR studies by Zoche et al (1996) and reinforce the fact that the binding of CaM to iNOS is Ca^{2+}-independent.

A harsher method was employed using strong acidic conditions to dissociate wt CaM from the iNOS peptide. A solution of 10 mM HCl (pH 2) was used in attempts to dissociate the CaM-iNOS peptide complex. Initial tests showed full dissociation of wt CaM. However, the acidic conditions were too harsh and disrupted the streptavidin-biotin interaction on the surface, displayed as an approximate 60% reduction in the baseline after each subsequent injection of HCL. The incomplete reduction of the response back to the original baseline heavily indicated that not all of the streptavidin-biotin bonds were broken. Originally thought to be stable over a wide range pH, strong evidence from affinity studies revealed that the streptavidin-biotin bond is actually disrupted at acidic conditions of $\leq pH4$. Milder regeneration conditions were attempted using 100 uM HCl (pH 4), but it was not enough to dissociate CaM from the peptide, indicated by the plateau in the response signal.

We attempted to solve the approximate 60% loss of peptide on the surface after injection of HCl regeneration solution by adapting the method to try and regenerate the ligand surface through supplemental injections of iNOS peptide after the regeneration phase. The same initial steps were carried out: immobilization of the iNOS peptide, immediately followed by a 50 nM CaM association phase, a dissociation phase in running buffer and then a regeneration phase by injection of 10 mM

HCl. Unlike the previous experiments, another 20 ug/mL iNOS peptide injection was completed before the next [CaM] association. This process was repeated for 150, 450 and 1350 nM CaM samples. The response signals for all concentrations of CaM were inconsistent, non-uniform and did not follow a concentration-dependency like that seen with CaM and cNOS peptides, therefore the data was unsuitable for kinetic rate analysis. Furthermore, repeated disruption and regeneration of ligand on the surface is not recommended because the quality of ligand binding and the uniformity of the surface cannot be confidently ascertained. A non-uniform surface could lead to misinterpretation of the results and false binding interaction analysis (O'Shannessy & Winzor, 1996).

Due to the harsh acidic requirements needed to dissociate the NOS-CaM complex and the disruption of the streptavidin-biotin interaction under those conditions, a new regeneration solution was tested. Urea, a chaotropic denaturant, was used. Urea is known for its ability to denature several proteins such as CaM, by destabilizing internal, non-covalent bonds between atoms, but is not known to disrupt the streptavidin-biotin complex. The original method was employed with the variation of using 1M Urea as the regeneration solution[3]. This test showed that the urea did not affect the streptavidin-biotin interaction but no dissociation of CaM and iNOS peptide was observed.

Overall, we were not able to find a method that can regenerate the surface with full dissociation of the CaM-iNOS peptide interaction without disrupting the streptavidin-biotin complex. We hope to explore other techniques and strategies to accomplish our goal of monitoring CaM protein binding with the iNOS peptide.

2.4 Discussion

The goal of this chapter was to increase our understanding of the NOS-CaM interactions by investigating the binding interactions of CaM mutants and CaM constructs to peptides corresponding to the canonical CaM-binding domains of all 3 NOS isozymes through the determination of the binding kinetics. Using SPR, an optical bioanalytical method used to measure bimolecular interactions, we could determine the parameters we set out in our goal. These binding parameters would be used to compare with past activity profile studies using the same CaM mutants to activate full NOS enzymes. We set out to determine if there is a relationship between elements and structures of CaM binding and their ability to activate NOS catalysis.

The binding kinetics were derived with the use of an L-SPR platform. NOS peptides were immobilized onto a surface and the different CaM proteins were allowed to bind in a concentration

[3] The system was washed with injections of running buffer several times to remove any traces of urea before any other analyte samples were added.

dependent manner. This is the first time SPR kinetic parameters have been determined for EF-hand pairs, TnC chimeras and phosphomimetic CaM mutants. Initial SPR analysis using traditional techniques was previously done on wt CaM binding with nNOS and iNOS peptides (Zoche et al., 1996). Comparison of our binding parameters with those from Zoche et al (1996) show that the values derived from traditional SPR vs. L-SPR are comparable. The discrepancies can be attributed to the longer EM-field-decay length of metal films in traditional SPR sensors vs. the shorter EM-field-decay length within nanoparticles in L-SPRs. The decrease of the metal surface height from the use of nanoparticles compared to continuous metal film is also known to increase the overall response of the sensogram (Yonzon et al., 2004).

Past studies have shown that the binding of CaM plays a key role in the activation of electron transport within cNOS enzymes, however its role in activation of iNOS is not well understood (Campbell et al., 2014). This is attributed to the Ca^{2+}-independent nature of iNOS with respect to CaM binding. With this in mind, it is extremely unfortunate that the binding kinetics could not be observed for any of the CaM proteins with iNOS peptide due to the inability to fully dissociate the iNOS peptide/CaM complex without disrupting the sensor surface. This set of data would have been very insightful in understanding more of the NOS-CaM interaction.

As demonstrated in the results section (Section 2.3), the use of mutant CaM proteins displayed varying binding profiles for both cNOS peptides within each set of mutants and demonstrated that by changing different elements of CaM affect different elements of its interaction with NOS enzymes. These specific interactions are further explained in the following subsections below.

2.4.1.1 Analyzing the Binding Interactions Between CaM-TnC Mutants and cNOS Peptides

Using the TnC mutants, we were able to observe the importance of each specific EF-hand domain in cNOS binding and activation by effectively changing the functionality of individual EF-hands while retaining structure (Su et al., 1995). With respect to TnC protein activation of nNOS enzyme, only the 2TnC construct was able to fully activate overall NOS activity in terms of •NO production, cytochrome c reduction and NADPH oxidation (Figure 2.10). Exchanging EF-hands domain 1,3 and 4 greatly reduced nNOS activity in all areas with the exception of 3TnC and 4Tnc mutants retaining substantial ability to transfer electrons from NADPH into the reductase domain as observed in their cytochrome c reduction activity comparable to wt CaM. Our binding data shows that all CaM-TnC mutants are able to associate and bind the NOS-CaM binding domain with reduced affinity compared

to wt CaM, with the exception of 4TnC, where replacing EF-hand 4 in CaM with the same domain from TnC stabilizes its overall binding interaction to the nNOS peptide. Changes to EF-hands 2, 3 and 4 show an increase in the rate of dissociation of the NOS-CaM complex (high relative k_{off}). This corroborates the idea from Newman et al. (2004) in that CaM-1TnC, CaM-3TnC and CaM-4TnC may make important contacts with sequence regions outside the nNOS CaM-binding domain that are important for nNOS activity and that elements within CaM EF-hand 2 aren't as important for nNOS activity. Furthermore, this explains how the observed increased affinity for CaM-4TnC for the CaM binding domain is not indicative of its ability to activate the full nNOS enzyme as we are only looking at specific binding of CaM proteins in terms of the CaM-binding domain.

With respect to TnC mutants binding to eNOS peptide, we see that replacing elements with the N-terminal domain of CaM with elements from TnC (TnC and 2TnC) increases its affinity for the eNOS CaM-binding domain, where the NOS-CaM complex is quite stable as seen by slow dissociation rate (high relative k_{off}) and low k_{on} : k_{off} ratio. This suggest that elements within the N-terminal domain of CaM aren't as important for eNOS peptide binding. On the other hand, replacing EF-hands within the C-terminal domain of CaM (3TnC and 4TnC) greatly diminishes the affinity of CaM proteins for the eNOS peptide (Figure 2.10). We can see that by removing these elements, the interaction is destabilized as seen with the great increase in dissociation of the NOS-CaM complex (low relative k_{off}). These results suggest that elements within the C-terminal domain of CaM are crucial for eNOS binding. CaM is believed to bind the NOS CaM-binding domain in an antiparallel fashion where elements within CaM-4TnC are closest to the oxygenase domain of NOS enzymes (Aoyagi, 2003). These results are consistent with a recent solution-state structural study of wt CaM binding to the eNOS peptide where they demonstrated this antiparallel binding and showed that the N-terminal domain of the NOS-CaM complex is more rigid and less dynamic than the C-terminal domain (Piazza et al., 2016). By replacing elements within the C-terminal domain of CaM, such as using 3TnC and 4TnC constructs, the important anchoring contacts and interactions CaM makes with the CaM-binding domain are disrupted, causing a decrease in binding affinity as seen in Figure 2.10 with regards to decreased relative binding in terms of affinity.

With respect to eNOS activation, TnC constructs showed a similar activation profile as previously seen with nNOS but the CaM mutations had less effect on the transfer of electrons within the reductase domain as demonstrated by the decrease in •NO production and increase in cytochrome c reduction and NADPH oxidation, similar to that seen with nNOS activation. By changing elements that help CaM anchor to the NOS CaM-binding domain, CaM is weakly bound to the peptide, lowering the rate of effective FMN to heme electron transfer and increasing the rate of cytochrome c

reduction. Similar to TnC binding and activation of nNOS, the amount of relative binding of TnC mutants to eNOS is not indicative of its ability to promote overall activation.

2.4.1.2 Analyzing the Binding Interactions Between CaM EF-Hand Pair Mutants and cNOS Peptides

Similar to the CaM TnC mutants, the EF-hand pair mutants look at the importance of EF-hand pairs but within their associated globular domains. Taking a look at the single EF-hand pairs, we were not able to determine appropriate binding kinetics of nCaM and cCaM to immobilized nNOS and eNOS peptides as the binding kinetics on the SPR resembled bulk shift effects. These results correlate well in that the single EF-hand pairs were not able to activate any substantial NOS activity with the exception of nCaM displaying 37% relative cytochrome c reduction activity in nNOS and 17% in eNOS enzymes. These results could suggest that the OpenSPR™ platform was not sensitive enough to distinguish minor binding interactions of the single EF-hand pairs but were otherwise detected in the activity assays. Furthermore, these results prove that both globular domains of CaM are important for CaM binding and activation (Spratt et al., 2006).

On the other hand, binding kinetics were observed for duplicate EF-hand pairs, CaMNN and CaMCC. CaMNN displayed greater relative binding for the nNOS peptide and comparable binding to wt CaM for the eNOS peptide. The k_{on}: k_{off} ratio of CaMNN was 2.4 for nNOS peptide and 3.2 for the eNOS peptide. Even though the CaMNN construct dissociates faster from the NOS-CaM complex compared to wt CaM, it is offset by its fast association for both cNOS peptides, thereby displaying high affinity. CaM CC displayed the opposite trend where it displayed significant greater binding for the eNOS peptide, with 2x greater affinity than wt CaM, and comparable binding to wt CaM for the nNOS peptide. With CaMCC, a k_{on}: k_{off} ratio of <1 is observed, signifying that elements of the CaM C-terminal domain stabilizes the NOS-CaM complex with its slow dissociation rate (high relative k_{off}). These results again corroborate the importance of elements within the CaM C-terminal domain and how these elements are crucial in CaM binding, especially in terms of eNOS binding (Piazza et al., 2016). These results reflect the trend we observed when we investigated the binding and activation of CaM 3TnC and 4TnC constructs, which exchanged CaM C-terminal EF-hand domains with those from TnC.

Taking a look at EF-hand pair activation of NOS activity, CaMNN was the only construct that showed substantial •NO production in both cNOS enzymes. Elements within the N-terminal region of CaM are most likely important in activating •NO production by facilitating the conformational change of NOS into the output state from the input state and thus improving efficiency of electron transfer from the FMN into the catalytic heme domain (Melody G Campbell et al., 2014; Spratt et al.,

2006). The N-terminal elements of CaM bind closer to the C-terminal domain of NOS and therefore these elements are most likely important in making important contacts with FMN that are needed for the activation of the conformational change (Aoyagi, 2003). In terms of electron transfer within the reductase domain of nNOS to cytochrome c, Newman et al (2004) previously stated that the CaM requirements for promotion of FMN domain release in eNOS are not as stringent as it is in nNOS as CaMCC was able to activate minor eNOS activity without having elements of the N-terminal domain. Our binding data shows that the CaMCC construct binds 2x as strong to the eNOS peptide than wt CaM, corroborating the suggestion by Spratt et al. (2006) that duplicate EF-hand pairs can in fact occupy the entire CaM-binding site, where the binding of one C-terminal domain of CaMCC can stabilize the interaction of the 2nd C-terminal domain with the N-terminal recognition site. These protein constructs were used to observe how the 2 globular domains within CaM affect NOS binding and activation. Overall, out of the 3 sets of mutants we investigated, the EF-hand mutants displayed the highest correlation of their binding profiles with their ability to activate NOS enzymes.

2.4.1.3 Analyzing the Binding Interactions Between Phosphomimetic CaM Mutants and cNOS Peptides

Unlike the CaM TnC and EF-Hand Pair mutants, CaM phosphomimetic mutants were studied to investigate natural *in vivo* regulations of CaM and how they affect NOS activation and binding. Due to the difficulty in individually phosphorylating single amino acids, single point mutations of known post-modified amino acids into glutamate and aspartate were done to mimic phosphorylation at the specified sites (Spratt et al., 2008).

In terms of central linker phosphomimetic mutants T79D, S81D and T79D/S81D nNOS peptide binding, we see that all 3 mutants showed less affinity for the peptide compared to wt CaM. Taking a closer look at the k_{on} : k_{off} ratios, we see varying ratios between the mutants (0.79, 1.29, 0.57 for respectively). There is no clear relationship on how the ratio explains the amount of relative affinity. In terms of eNOS peptide binding, we see a similar trend where all 3 mutants displayed lower affinity compared to wt CaM and relatively lower affinity compared to nNOS peptide binding. Looking at k_{on} : k_{off} ratios, we get a different trend where all ratios are <1 (0.72, 0.77 and 0.47, respectively). This does not correlate with our expected trend where having a slower dissociation rate (higher relative k_{off}) signifies a more stable affinity. Comparing the nNOS activities, we see that central linker phosphomimetic mutants displayed relatively similar rates of NADPH oxidation, increased rates of cytochrome c reduction but an overall decrease in •NO production compared to that of wt CaM. In contrast, for eNOS activation we see slightly higher relative activities of NADPH oxidation and •NO production with a decrease in electron transfer activity to cytochrome c from the

reductase domain. These results do not agree with Grief et al. (2004) where they demonstrate that phosphorylation of CaM proteins should attenuate overall eNOS activation. Therefore, our binding study does not correlate well with the activity study completed by Spratt et al. (2008).

With respect to S101D peptide binding, we see decreased affinity for both cNOS peptides. Similar to the CaM central linker phosphomimetic mutants, there is no observed trend by looking at the k_{on} : k_{off} ratio. Phosphorylation of S101 was previously reported to decrease eNOS activity (Greif et al., 2004). S101 is located in the loop region of EF-hand 3, which is located in the C-terminal domain of CaM. Like we saw with previous CaM mutants, changing interactions within the C-terminal domain decrease its level of binding to NOS. Our observed decrease in relative affinity of S101D mutant to cNOS peptides correlates with the previously observed decrease in not only eNOS activation (Spratt et al., 2008), but possibly with nNOS activation as well.

Lastly, with respect to Y99E, we see that the substitution of Y99 with a glutamic acid residue decreases the affinity of CaM for both nNOS and eNOS peptide. Structural studies have shown that the introduction of a negative charge at Y99 perturbs the binding interactions of CaM EF-hand and EF-hand 4 (Piazza et al., 2012). Once again, we see how crucial certain elements within the C-terminal domain of CaM are in terms of NOS binding and by changing these elements, we can greatly affect CaM affinity. Furthermore, it was previously reported that phosphorylation at this site induces hypoxia in newborn piglets due to increased nNOS activity. The activity study completed by Spratt et al. (2008) demonstrate a slight increase in nNOS activity for all 3 NOS assays and a decrease in both NADPH and overall •NO production in eNOS (Piazza et al., 2012). The slight increase in overall nNOS activity could be attributed to the increase in k_{on}.

Overall, using SPR, we determined the binding kinetics of CaM mutants to peptides for the canonical CaM-binding domains of NOS enzymes. With comparison of previously determined activity profiles for the same exact mutants, we saw varying results of how the different elements and structures of CaM affect activity. Notably, we saw a recurring trend where changing elements of the EF-hand domain found in the C-terminal of CaM greatly affected its level of binding to NOS peptides. Furthermore, we saw many variances in the amount of CaM binding affinity for NOS peptides compared to CaM activation of NOS enzymes. Once again, a caveat to this particular study is that we are specifically only looking at the binding interactions between CaM proteins and the canonical CaM-binding domain. This implies that the local binding interactions between CaM and the CaM binding domain do not sufficiently justify the mechanisms involved in the binding and activation of full NOS holoenzymes. We observed this frequently across all 3 CaM mutant constructs,

where elements of CaM that were not involved in forming the binding complex with the NOS peptide were in fact important in full activation of the enzyme. This correlates with findings from Venema et al, (1996) and Ishida and Vogel (2006). NOS is an extremely dynamic protein, and different elements of CaM that may not be involved in the NOS-CaM binding complex may interact with different segments of NOS that can either promote or inhibit activation of the enzyme. Despite this fact, it is still important to quantify the level of interaction of CaM proteins with the CaM-binding domain to understand the local interactions that are necessary or important for protein-protein interactions.

Chapter 3
Development of a Nitric Oxide Synthase Electrochemical Biosensor

3.1 Introduction

The study of NOS enzymes is important because they are integral proteins in human physiology. Due to their physiological relevance (Section 1.2.2), the pharmaceutical industry has a keen interest on finding NOS isoform-specific inhibitors. Coupled with the limited assay methods used currently to measure NOS activity, there is significant interests in developing a new bioelectronic system that can efficiently and accurately analyze NOS enzyme catalysis. Converting biological events, such as NOS catalysis, to an easily detectable and processed electrical signal can be a difficult process due to the intricacies of connecting an electronic device into a biological environment (Grieshaber et al., 2008). However, with recent advances over the past 2 decades in the fields of biosensing and bioelectrochemistry, electrochemical biosensors can now be confidently utilized to monitor electroactive proteins (Mehrotra, 2016). Developing a new technological platform with efficient, rapid and less expensive NOS activity detection would exponentially increase our understanding on the full mechanism of NOS by improving our ability to measure its activity. Furthermore, this technology could also speed up and simplify the drug development process needed in the pharmaceutical industry by expediting the screening process (Castrignanò et al., 2014), increasing the potential for new therapeutic compounds to be discovered that could be used to treat abnormal physiological NOS activity.

3.1.1 Electrochemical Biosensors

Electrochemical biosensors are analytical devices that can convert biological responses into a measurable electrical signal (Grieshaber et al., 2008; Thévenot et al., 2001). Remarkably, biosensor-related research has had exponential growth over the past few decades. The development of biosensors was pioneered by Clark and Lyons in the 1960's and their contributions has led to the current day use of various types of biosensing equipment, including enzyme-based, tissue-based and DNA-based biosensors as well as immunosensors and thermal and piezoelectric biosensors (Mehrotra, 2016). There is great demand for the development of an electrochemical NOS biosensor for its clinical relevance and the ability to study the biochemical regulation of NOS enzymes. A typical biosensor contains three main components: the bioregulatory element, a signal transducer and

lastly, a detector (Figure 3.1) (Thévenot et al., 2001). The main criteria a biosensor must have are (Schneider & Clark, 2013):

1. highly specificity
2. be independent of physical parameters such as pH, temperature and mechanical turbulence
3. accurate, precise and reproducible responses over the concentration range of interest; and lastly
4. be cheap, small, portable and easy to use for semi-skilled operators

3.1.1.1 Enzyme-based Electrochemical Biosensors

Enzyme-based biosensors are developed based on immobilization methods and bioelectrochemistry. With these types of biosensors, electroactive species, mostly redox enzymes, are typically immobilized onto an electrode surface using van der Waals forces, ionic bonds and/or covalent interactions (Castrignanò et al., 2014; Oku et al., 2004; Schneider & Clark, 2013; Sultana et al., 2007). Through the coupling of the enzyme with an electrical interface, the enzymatic activity of the redox protein can be measured as an electrical response.

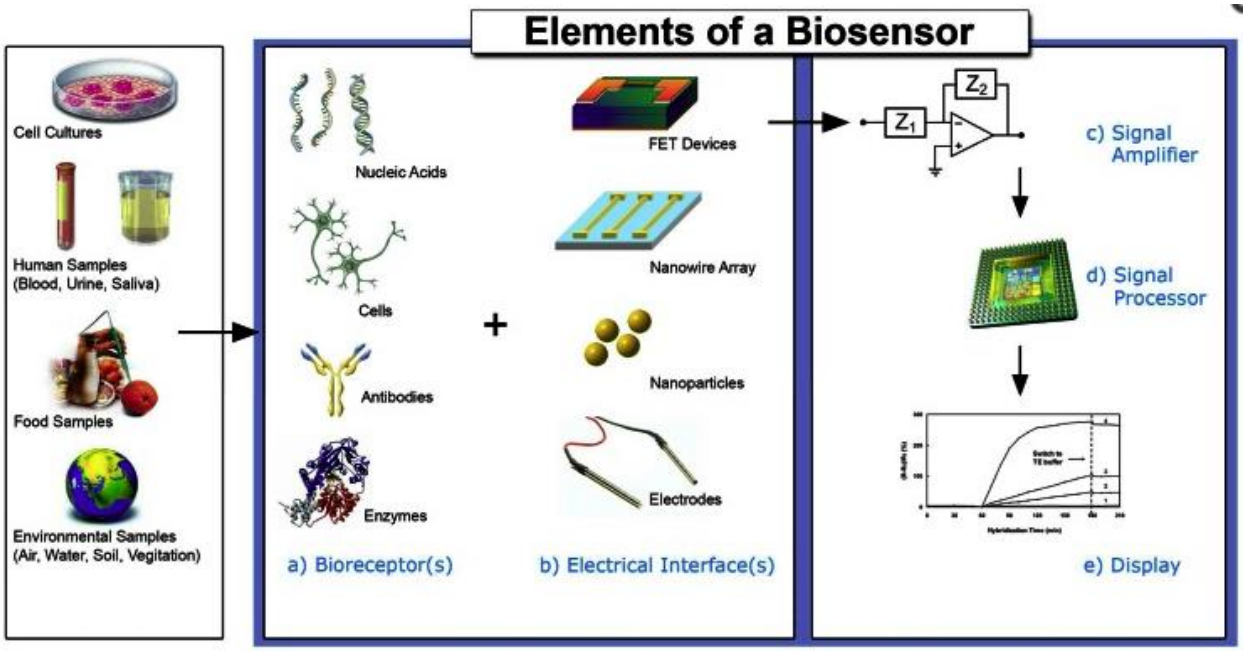

Figure 3.1 - Biosensor Component Requirements
Depicted on the left are 4 widely used bioregulatory elements and possible samples they can be attained from. Signal transducers take the biological response of the bioregulatory element and convert it into an electrical response that the detector can process. This figure was reprinted from *Sensors*. Switzerland, 8(3) Grieshaber, D.; MacKenzie, R.; Vörös, J.; Reimhult, E. Electrochemical Biosensors - Sensor Principles and Architectures, 1400–1458, 2008 [Open Source].

3.1.1.2 Electrochemical Detection of Enzyme-Based Biosensors

Electrochemical biosensors can either measure current (amperometric), potential or charge accumulation (potentiometric) or the conductive properties of a medium (conductometric) between electrodes. The measurable electrical signal is a result of the oxidation or reduction of the redox enzyme undergoing its biochemical reaction (Grieshaber et al., 2008). The majority of enzyme-based platforms use amperometric detection, where the current is measured at a constant potential, also known as amperometry. An increase in the current upon addition of an electrical potential is correlated with the catalytic activity of the redox enzyme against a candidate substrate (Schneider & Clark, 2013) . There are many types of amperometric methods, however the most widely used for enzyme-based platforms is cyclic voltammetry. Voltammetry is the measure of current as a result of varying the potential (Mabbott, 1983). With cyclic voltammetry, the voltage is swept between two fixed potentials at a fixed rate. When the voltage reaches one of the fixed potentials, the scan is reversed and the voltage is swept back to the original potential. It is a popular technique due to its usefulness in obtaining information about the redox potential and the chemical rate constant of analyte solutions(Grieshaber et al., 2008; Mabbott, 1983).

Additionally, since enzymes are immobilized onto electrodes, reactions occur in close proximity to the electrode surface. Therefore, the electrodes themselves play an important role in the performance of electrochemical detection. Based on the chosen function of a specific electrode, the electrode material, its dimensions and any surface modification can influence the detection ability of the enzyme (Mehrotra, 2016). Typically, electrochemical sensing requires a reference electrode, a counter or auxillary electrode and a working electrode. The enzyme is immobilized on the working electrode, which acts as the transducing element for the biochemical reaction. On the other hand, the counter electrode establishes a connection to the electrolytic solution so that a current can be applied to the working electrode. Lastly, the reference electrode, usually Ag/Ag/Cl, is kept away from the reaction site on the working electrode to maintain a known and stable potential. Electrodes are made of conductive and chemically stable materials, which are usually platinum, gold, carbon and silicon depending on the analyte being studied(Grieshaber et al., 2008) .

3.1.1.3 Cytochrome P450-Based Biosensors

To date, the most utilized and extensively researched redox enzymes for bioelectrochemistry applications are the family of cytochrome P450 (CYP or P450) enzymes, along with their redox

partners, the family of cytochrome P450 oxidoreductase (CYPOR) enzymes. CYP proteins are a family of heme-containing enzymes associated with the metabolism of xenobiotics and other endogenous chemicals within humans (Castrignanò et al., 2014) NOS enzymes share similarities with P450 enzymes in that they are also heme containing proteins found in almost all types of tissues. Both NOS and CYPs conduct electron transfer through flavin cofactors, with the difference of P450 enzymes being coupled with CYPOR enzymes, which are quite similar to the reductase domain of NOS enzymes and provide the reducing equivalents for heme catalysis (Schneider & Clark, 2013).

In the last ten years, there have been several reports of successful direct bioelectrochemical platforms using P450 enzymes adsorbed onto electrode surfaces to screen against drug candidates (Joseph et al., 2003). Past studies have designed novel CYP biosensors and have reported comparable kinetics to literature values and even having the ability to perform inhibitor studies (Newman et al., 2004). CYP biosensors have been used extensively in the pharmaceutical industry where lead compounds in drug development are screened against immobilized CYP enzymes as they are responsible for most of the drug metabolism within our bodies. Knowing the CYP profile of a drug allows principle investigators to predict possible harmful interactions that are caused by the inhibition or induction of a specific CYP isozyme(Joseph et al., 2003; Schneider & Clark, 2013).

Conversely, recent studies done have shown supporting evidence that immobilizing P450 enzymes directly onto electrodes can induce a conformational change of P450 enzymes into inactive cytochrome P420s by a process known as electrical fouling (Schneider & Clark, 2013). P450 enzyme species are characterized by absorption of the reduced heme at 420 nm, signifying a loss of the proximal cysteine ligand. Through analysis of the electrode surfaces after catalysis, the unstructured orientation of CYP enzymes during the immobilization step is has been found to be a major contributing factor to protein denaturation (Schneider & Clark, 2013).

3.1.1.4 Electrochemical Biosensor Advantages and Disadvantages

Overall, electrochemical biosensors are extremely useful tools because they can obtain intrinsic thermodynamic and kinetic properties of many protein-protein complexes. Furthermore, biosensor experiments are high throughput methods that can be developed for high specificity of virtually almost any substrate, even allowing the use of turbid samples such as whole cell extracts. They are highly repeatable, robust and faster than any conventional assay method used today. Lastly, other advantages come in the form of their miniaturization, excellent detection limits and small analyte volumes (Mehrotra, 2016; Shruthi et al., 2014).

Although there are many benefits, there are a few disadvantages, especially in regards to enzyme based-platforms. First, to develop these platforms can be expensive due to the source, extraction, isolation and purification of large amounts of active enzyme. Second, the adsorption of the purified enzyme onto the electrode surface is essentially irreversible. Harsh conditions are needed to reverse the immobilization process. Additionally, there can be potential issues with the deactivation of enzymes after a relatively short period of time, unless stored under proper conditions (Shruthi et al., 2014). Therefore, there is a limited shelf life for these applications. Last but not least, the viability of the biosensor is dependent on the ability of the bound enzyme to conduct redox reactions. The loss of activity can occur through the denaturation of the ligand by electrode fouling as seen in CYP biosensor examples (Schneider & Clark, 2013).

3.1.2 Developing a Nitric Oxide Synthase Electrochemical Biosensor

To reemphasise, there is high demand for the development of a NOS electrochemical biosensor for its clinical relevance and the need to still characterize NOS mechanisms. NOS enzymes are redox active proteins; therefore, they are highly suitable to be adapted for bioelectrochemical sensing platforms. Past experiments showing the viability of CYP biosensors shows the potential to adapt and develop a new NOS biosensor. The main objective of this chapter is to develop a new NOS-based electrochemical biosensor with the purpose of being able to measure NOS catalytic activity.

3.1.2.1 Initial Design Approach

Using the examples of previous CYP biosensors for inspiration, we attempted to design a new NOS sensing platform. The studies we conducted in Chapter 2 showed that we could immobilize NOS peptides (the biorecognition element) on a gold nanoparticle surface using the thiol-gold interaction, and observe CaM analyte binding (target molecule). Essentially, with our SPR method, we developed an optical CaM affinity biosensor where we could detect the specific binding of analyte CaM proteins to an immobilized biorecognition element. With proof that we could immobilize a NOS structure on a gold surface, we decided to immobilize NOS enzymes onto a gold electrode.

However, knowing about denaturation of electrode immobilized proteins as seen in the examples of CYP sensors, a prospective solution for a NOS sensor can be achieved by using a CaM protein tether (Figure 3.3). With this concept, instead of directly immobilizing the NOS enzyme directly on the surface, we could immobilize CaM, a stable protein that displays strong binding

affinity for NOS and is necessary for electron transfer within the enzyme (Section 1.4.1). Using this pseudo-sandwich format, CaM will act as the initial biorecognition element that will target NOS enzymes close to the surface of the electrode, NOS will be used as a secondary biorecognition element that will act as our electroactive catalyst. Utilizing the same thiol-gold chemistry that was used to bind NOS peptides to a gold nanoparticle surface (Section 2.3.2), CaM would be similarly modified with a cysteine group at one end of the protein. Due to known antiparallel binding of CaM to NOS enzymes (Aoyagi, 2003), 2 cysteine-modified CaM constructs were developed, yielding Nterm-Cys CaM and Cterm-Cys CaM constructs (Invitrogen, Life Technologies) (Figure 3.3). Testing both constructs could ensure proper binding orientation of NOS enzymes on the surface.

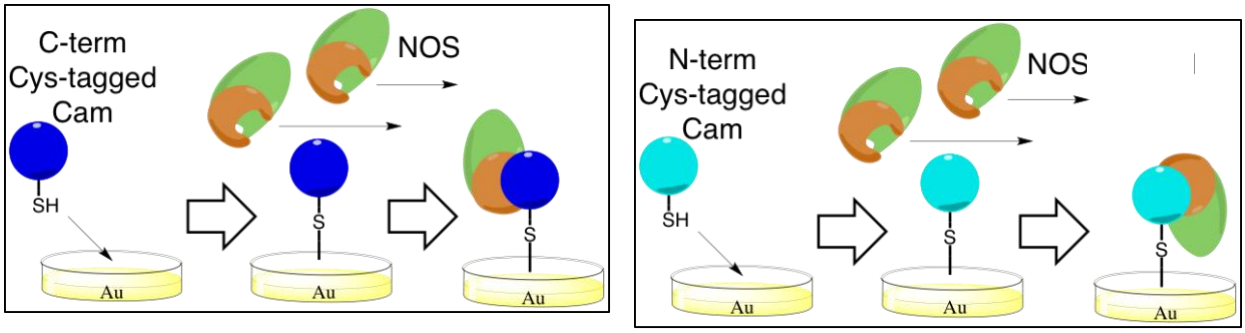

Figure 3.2 - Indirect-direct immobilization of NOS enzymes using a CaM protein tether
CaM will be immobilized on a gold surface using Cysteine-modified ends. Introduction of NOS enzyme will result in protein binding, indirectly immobilizing NOS to the surface.

Before applying our model onto a gold electrode platform, testing the viability of our constructs on a gold surface would be beneficial. L-SPR will be used to determine the optimal conditions for the immobilization of the protein tether. Furthermore, the affinity of the second recognition element, the NOS enzyme, will be determined using L-SPR analysis. Once we have optimized our binding methods, we hope to translate from an optical platform onto an electrical platform.

3.2 Experimental Procedures

3.2.1 Expression and Purification of Cysteine-modified C-terminal and N-terminal CaM

Synthesized human cysteine-modified C-terminal & N terminal CaM proteins were expressed in BL21 (DE3) *E.coli cells* transformed with pHuCaMCtermCys and pHuCaMNtermCys plasmids

(Invitrogen, Life Technologies) (Appendix A), as previously described for wild-type CaM (section 2.1.1).

Synthesized human cysteine-modified C-terminal & N terminal CaM proteins were purified as previously described for wild-type CaM (section 2.1.2).

3.2.2 Characterization of CaM and Cysteine-modified Terminal CaM

Both cysteine modified CaM proteins were characterized as previously described for wild-type CaM (Section 2.2.6)

3.2.3 NOS Enzymes

Purified bovine eNOS and human nNOSoxyFMN enzymes were a generous gift from Danica Estavillo and Dr. Mike Piazza (Guillemette Lab)

3.2.4 SPR Gold Chip Preparation

The interactions of all proteins used in this chapter were completed using a standard gold sensor chip. The gold sensor chip was prepared as previously described in Section 2.2.7.1.

3.2.5 SPR Protein Binding Kinetic Analysis of eNOS Holoenzyme and Immobilized Cysteine-modified Terminal CaM

The gold chip and Open SPR was prepared as previously described in Section 2.2.7, up until the equilibration of a new chip. The surface of the gold chip was primed with a 200 uL injection of a solution consisting of 6.25:1 cysteamine to cysteine modified-terminal CaM in PBS equilibration buffer. Several 200 uL injections of 1 mM cysteamine in PBS buffer were completed to saturate the rest of the surface and prevent NSB. After each injection, the equilibration buffer was pumped for at least 10 minutes or until the signal was stabilized. The buffer was switched to PBS analyte buffer as mentioned in Section 2.2.7.3. A range of NOS holoenzyme concentrations (500 nM, 300 nM, 200 nM, 150 nM, 100 nM, 50 nM) were prepared in PBS analyte buffer to inject into the OpenSPR individually and allowed to equilibrate. An injection of PBS regeneration buffer was done to regenerate the surface.

3.2.6 Reduction of Non-Specific Binding of NOS enzymes on the SPR

Preliminary experiments from Section 3.2.5 showed that strong non-specific binding occurs between NOS enzymes and the gold chip surface. Different running conditions and additives were tested to optimize the best running conditions for the binding of NOS enzymes to immobilized CaM and reduce and eliminate NSB. These methods include the use of surface blockers as well as protein and chemical additives and are described in the following sections below.

3.2.6.1 Reducing SPR Non-Specific Binding Through Surface Blockers

The gold chip and Open SPR was prepared as previously described in Section 2.2.7 and 2.2.8, up until the equilibration of a new chip on the OpenSPR. Three different surface blockers were tested: cysteamine, a neutral SPR-functional polyethylene glycol compound (PEG) (SH-PEG_{3000}-OMe) & a basic SPR-functional PEG compound (SH-PEG_{3000}-NH_2) PEG compounds were a generous gift from the Dieckmann lab. Each compound was tested separately on newly prepared chips. The same equilibration, analyte and regeneration buffers were used as previously described in Section 2.2.8.

The surface of the gold chip was primed with several 200 uL injections of the blocker being tested, prepared in PBS equilibration buffer, until no significant change in overall response on the sensogram was achieved, showing saturation of the gold surface. DTT was added into all PEG_{3000} injections to ensure the PEG was fully reduced. The buffer was swapped into PBS analyte buffer as described in Section 2.2.8. A 200 uL injection of 500 nM NOS holoenzyme in analyte buffer was done and allowed to equilibrate, followed with a 200 uL injection of PBS regeneration buffer to regenerate the surface.

3.2.6.2 Reducing SPR Non-Specific Binding Through Additives

The gold chip and Open SPR was prepared as previously described in Section 2.2.7 and 2.2.8, up until the equilibration of a new chip on the OpenSPR. The addition of bovine serum albumin (BSA) as a blocking protein as well as the use of the surfactant Tween 20 to reduce NSB were investigated. The same equilibration, analyte and regeneration buffers were used as previously described in Section 2.2.8 with the addition of 1% w/v BSA and 0.05% v/v Tween 20 into the analyte and regeneration buffers.

The surface of the gold chip was primed with several 200 μL injections of the cysteamine blocker prepared in equilibration buffer, until no significant change in overall response on the sensogram was achieved, showing saturation of the gold surface. The buffer was switched to the modified PBS analyte buffer. A 200 μL injection of 500 nM NOS holoenzyme in modified analyte buffer was done and allowed to equilibrate, followed with a 200 μL injection of modified regeneration buffer to regenerate the surface.

3.3 Results and Discussion

3.3.1 Protein Expression, Purification and Characterization

Both cysteine-modified C-term CaM and cysteine-modified N-term CaM were expressed and purified. The purified CaM proteins were analyzed by SDS-PAGE and were judged to be over 95%

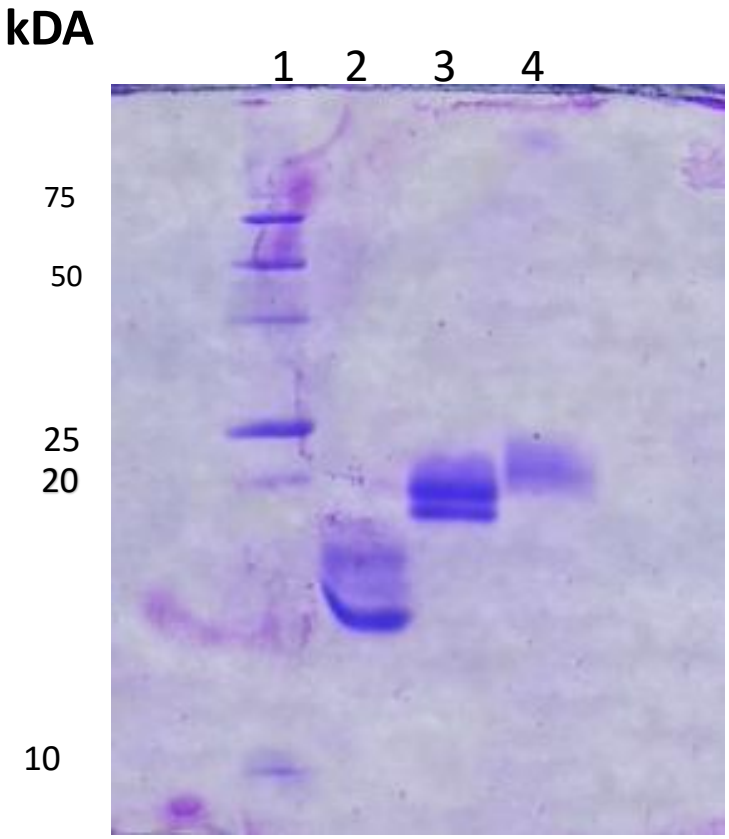

Figure 3.3 - SDS-PAGE of Cysteine-modified terminal CaM Proteins
The purified cysteine-modified CaM were run on a 15% SDS-polyacrylamide gel. 10 ug of each protein was loaded into an SDS buffer containing 5% BME. *Lane 1*: Low molecular mass protein standard (Bioshop); *Lane 2*: wt CaM; *Lane 3*: Cys-Modified Cterminal CaM ; *Lane 4*: Cys-Modified Nterminal CaM

CaM proteins were further verified using ESI-MS to rule out any modifications (Table 3.1). All CaM proteins were verified to be the correct size. UV-spectroscopy was used to calculate CaM protein as well as verify their identity through characteristic peaks.

Table 3-1 - UV-Spectroscopy and ESI-Mass Spectrometry Analysis of CaM proteins and NOS

CaM Protein	Mass (kDa) [a]		Concentration (uM)
	Theoretical [b]	Observed	
wt CaM	16.706	16.705	232 μM
Cterm Cys CaM	21.374	21.371	710 μM
Nterm Cys CaM	23.460	23.464	432 μM

(a) – Masses of deconvoluted ESI-MS spectra are accurate to within 4-5 Da.
(b) – Calculated mass based on amino acid sequence

3.3.2 SPR Protein Binding Kinetic Analysis of NOS Holoenzyme and Immobilized Cysteine Modified Terminal CaM

We verified that the cysteine-modified CaM protein could bind to the cNOS peptides with comparable kinetics to wt CaM proteins (results not shown). Strong immobilization of the of C-terminal cysteine-modified CaM onto the surface was achieved using a 6.25:1 ratio of cysteamine surface blocker and CaM protein (Figure 3.4.A). More injections of cysteamine were added to saturate the surface (Figure 3.4.B). We tested to see if a binding response would be detectable for the addition of eNOS peptide. Upon addition of peptide, a slight increase in signal was observed, bringing the baseline slightly higher (Figure 3.4.C). This indicated the binding of the peptide to the immobilized CaM. The small response is most likely due to the large difference in size between the ligand and the analyte in question. Addition of EDTA did not bring the signal down (Figure 2.4.D), indicating no dissociation of the CaM-eNOS complex. To test if this complex was formed, we added an injection of eNOS holoenzyme. eNOS enzyme should not be able to bind if the CaM-eNOS peptide complex was formed.

Upon injection of 200 nM eNOS holoenzyme, a strong binding response was observed (Figure 3.4.E). We tested to see if the interaction was specific. With addition of EDTA regeneration solution, the complex could not be dissociated (Figure 3.4.F). The sensogram showed no decrease in signal, showing only a bulk shift response. Subsequent additions of enzyme showed strong binding for each injection but with a decrease in wavelength response. This indicated that the addition of eNOS holoenzyme was non-specific binding (NSB), with each injection saturating the surface further.

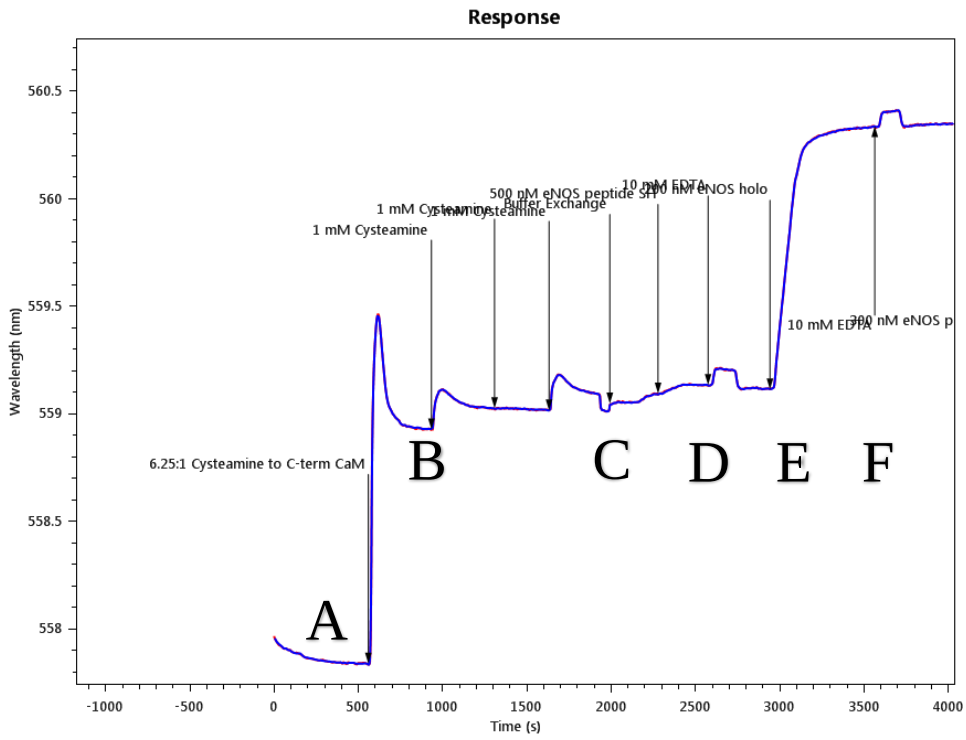

Figure 3.4 - Initial binding tests for Cys-modified C-terminal CaM
(A) Strong binding of C-terminal Cysteine Modified CaM. (B) Injection of cysteamine to block any remaining unbound surface. (C) injection of eNOS peptide displays a binding signal (D) EDTA injection does not dissociate the peptide from immobilized CaM (E) strong binding of eNOS holoenzyme even with bound peptide indicating non-specific binding (F) EDTA regeneration does not remove the enzyme from the surface.

Our initial test indicated that the interaction of the NOS enzymes were non-specific. To test this interaction, we injected eNOS holoenzyme in the absence of the Cys-modified CaM onto gold sensor chip. A strong binding response was observed, verifying the presence of NSB.

Non-specific binding is caused by the molecular forces, such as charge and hydrophobic interactions, between the analyte and the sensor surface. The non-specific binding of NOS enzyme onto the gold surface is most likely due to charge hydrophobic interactions.

We conducted a series of NSB tests to see if we could increase the specificity of our ligand and our enzyme analyte with the use of surface blockers and different buffer conditions.

3.3.2.1 Non-Specific Binding tests using Surface Blockers

The addition of surface blockers will saturate the reactive surface and will attempts to prevent analyte binding to the surface. We used cysteamine and different polyethylene glycol (PEG) units.

Full saturation of the gold surface was achieved by several injections of cysteamine. Saturation was judged when the addition of more cysteamine displayed a bulk shift response, indicating that no more binding could be achieved. However, upon injection of NOS enzyme, we see a large binding response, indicative that the enzyme is unaffected by cysteamine on the surface. NOS is a fairly large enzyme and we hypothesize that it can still interact with the gold surface in spite of cysteamine bound on the surface.

To prevent the reach of NOS enzyme to the surface, larger surface blockers were employed. Polyethylene glycol (PEG), is a polyether compound that has been used in mnay applications of biology. It has a structure that is expressed as $H\text{-}(O\text{-}CH_2\text{-}CH_2)_n\text{-}OH$. We used a 300-unit repeating PEG with both a neutral and basic reactive end:

(1) $SH\text{-}(O\text{-}CH_2\text{-}CH_2)_{300}\text{-}OME$

(2) $HS\text{-}(O\text{-}CH_2\text{-}CH_2)_{300}\text{-}ONH_3$

Similar to the cysteamine blocker, we first blocked the gold surface using 3000-PEG-OMe. The PEG was added until a bulk shift response was observed. We added a reducing agent, DTT, to ensure the PEG was fully reduced. Upon injection of wt CaM onto the surface, no binding response was observed. Upon addition of eNOS enzyme, we saw a similar binding profile seen with previous tests. A strong binding interaction is observed indicating NSB of the NOS.

Lastly, we attempted the use $HS\text{-}(O\text{-}CH_2\text{-}CH_2)_{300}\text{-}ONH_3$ to block the surface. Similar to the use of neutral PEG, the amino-PEG was added until a bulk shift response was observed. DTT was added to ensure full reduction of the PEG unit. Addition of wt CaM did not induce a binding response. Upon addition of eNOS enzyme, we saw a similar binding profile seen with previous tests.

3.3.2.2 Non-Specific Binding tests with Biological and chemical additives

To further test the reduction of NSB of NOS enzymes on the gold surface, we used a combination of biological and chemical additives. Bovine serum albumin (BSA) is a commonly used protein blocking agent that prevents non-specific protein-surface interactions. BSA is a globular protein with hydrophilic and hydrophobic subgroups. It naturally acts as a carrier protein in blood plasma. It can prevent NSB of a protein by encapsulating it, reducing its ability to interact.

In addition, chemical additives were employed. Tween 20 is a non-ionic surfactant that may disrupt hydrophobic interactions. It is commonly used in biological systems ranging from 0.005% v/V to 0.05% v/v and is commonly used in many protein SPR studies.

We systematically tested different buffer conditions with different combinations of the biological and chemical additives. NSB test conditions were done using the following running buffers:

1. PBS, pH 7.5 + 0.1% w/v BSA
2. PBS, pH 7.5 + 1.0% w/v BSA
3. PBS, pH 7.5 + 0.05% v/v Tween 20
4. PBS, pH 7.5 + 1.0% w/v BSA + 0.05% v/v Tween 20

NOS enzyme was diluted into each running buffer and with each test, the same result occurred, a strong binding response of the NOS enzyme.

A possible explanation for what seems to be happening in regards with NOS enzymes and binding interactions on the surface is that the enzyme is too large. Proteins are naturally sticky and upon injection of NOS enzyme onto the surface, it sits on top of the surface. Upon attaching to the surface, it promotes aggregation of other NOS enzymes to non-specifically bind. This is indicated by the binding signals with subsequent injections of NOS enzyme. There is possible interaction of the NOS enzyme with the CaM ligand, however upon binding, it sterically blocks the other immobilized CaM proteins with binding. The surface becomes inaccessible and is possibly why addition of EDTA regeneration solution cannot dissociate the interaction.

3.3.3 Summary

Our goal for this chapter was to develop an electrochemical biosensor with the concept of directly immobilizing NOS enzyme onto a gold electrode, which could provide the reducing equivalents to activate NOS catalytic activity. Previous studies have implicated that direct immobilization of redox enzymes are prone to denaturation due to electrode fouling. We decided to adapt the standard direct electrochemistry method and hypothesized that we could circumvent the known fouling of our enzyme by immobilizing CaM first onto the surface to act as a protein tether, and use it to indirectly immobilize NOS onto the electrode surface, but still close enough for efficient electron transfer.

We were able to express and purify our CaM protein and we tested the immobilization of our construct onto a gold surface with the use of SPR. However, NOS enzymes non-specifically bind onto the gold surface, possibly due to its relative size compared to the CaM bound on the surface. We ran

systematic tests to remove the non-specific binding, however, we were not yet able to a find a solution.

Overall, the development of new technology for assaying NOS activity is of great importance, especially in the field of medicine due to the physiological implications of NOS. Enzyme-based electrochemical biosensors and the direct immobilization of NOS enzymes shows a lot of promise for this new adaptive technology.

Chapter 4
Future Work

4.1 Binding Kinetics for CaM Mutant Proteins Interacting with the iNOS Peptide

To improve our results, more statistical data must be determined. Binding kinetics will be repeated for mutant CaM proteins binding with cNOS peptides. Duplicates were completed for all constructs but conducting more trials can help solidify the experimentally determined values for binding kinetics and affinities.

Other methods to observe the binding interactions of mutant CaM proteins with iNOS peptide are being explored. A prospective surface being used in sensing technology is gold self-assembled monolayers with covalent attachment of the molecule of interest. Another commonly used surface is the use of an activated dextran matrix monolayer. Immobilization of a protein can be achieved through the covalent attachment of the primary amine. Both surfaces have shown stability in harsh pH conditions (Schneider & Clark, 2013)

Furthermore, it would be useful to validate the binding affinities determined by L-SPR and compare them to other binding affinity methods such as ITC.

4.2 Developing a NOS Electrochemical Biosensor

Our methods to immobilize NOS enzymes onto a gold surface using a CaM protein tether to specifically bind NOS enzymes was without success. We are currently exploring different methods to help increase the signal to response with the immobilization of CaM and specific interactions with NOS enzymes.

Once we have established the proper running parameters and optimized the binding interaction of immobilized CaM and NOS enzymes, we can verify that using a protein tether can be a viable immobilization method for direct electrochemistry of NOS enzymes for a new NOS optical biosensor. We hope to translate from working under this SPR optical platform and attempt immobilization of our protein constructs on a working gold electrode.

Letter of Copyright Permission

Permission for Figure 1.6 & Figure 1.7

PNAS Permissions

to John

Permission is granted for your use of the figures as described in your message. Please list a full citation for each PNAS article when re-using its material. Because this material published after 2008, a copyright note is not needed. There is no charge for this material, either. Let us know if you have any questions.

Best regards,
Kay McLaughlin for
Diane Sullenberger
Executive Editor
PNAS

Article #1: Figure 1-B & Figure 7 from http://www.pnas.org/content/111/35/E3614.full
Article #2: Figure 1-A from http://www.pnas.org/content/110/38/E3577.full

From: John Lape [mailto:jelape@uwaterloo.ca]
Sent: Tuesday, October 03, 2017 12:24 PM
To: PNAS Permissions
Subject: Permission to Reuse Material

To Wom It May Concern,

I would like to request to use a total 3 Figures from 2 of your papers for my dissertation. Here is the requested information you've asked for:

1. **Your full name, affiliation, and title**

John Edmond Lape
Univeristy of Waterloo
Candidate for Masters in Chemistry

2. **Your complete mailing address, phone number, and email**

3197 Eclipse Ave, Mississauga, ON
(647) 889 - 5273
john.edmond.lape@gmail.com

3. **PNAS volume number, issue number, and issue date**

Article #1:
Volume 111
Issue 38
Issued August 14, 2014

Bibliography

Alderton, W. K., Cooper, C. E., & Knowles, R. G. (2001). Nitric oxide synthases: structure, function and inhibition. *Biochemical Journal*, *357*(3), 593. https://doi.org/10.1042/0264-6021:3570593

Aoyagi, M. (2003). Structural basis for endothelial nitric oxide synthase binding to calmodulin. *The EMBO Journal*, *22*(4), 766–775. https://doi.org/10.1093/emboj/cdg078

Armstrong, F. a., Hill, H. A. O., & Walton, N. J. (1988). Direct electrochemistry of redox proteins. *Accounts of Chemical Research*, *21*, 407–413. https://doi.org/10.1021/ar00155a004

Babu, Y. S., Bugg, C. E., & Cook, W. J. (1988). Structure of calmodulin refined at 2.2 Å resolution. *Journal of Molecular Biology*, *204*(1), 191–204. https://doi.org/10.1016/0022-2836(88)90608-0

Bachetti, T., Comini, L., Curello, S., Bastianon, D., Palmieri, M., Bresciani, G., Callea, F., & Ferrari, R. (2004). Co-expression and modulation of neuronal and endothelial nitric oxide synthase in human endothelial cells. *Journal of Molecular and Cellular Cardiology*, *37*(5), 939–945. https://doi.org/10.1016/j.yjmcc.2004.07.006

Bayley, P. M., Findlay, W. a, & Martin, S. R. (1996). Target recognition by calmodulin: dissecting the kinetics and affinity of interaction using short peptide sequences. *Protein Science : A Publication of the Protein Society*, *5*(7), 1215–1228. https://doi.org/10.1002/pro.5560050701

Brenman, J. E., Chao, D. S., Gee, S. H., McGee, A. W., Craven, S. E., Santillano, D. R., Wu, Z., Huang, F., Xia, H., Peters, M. F., Froehner, S. C., & Bredt, D. S. (1996). Interaction of nitric oxide synthase with the postsynaptic density protein PSD-95 and a1-syntrophin mediated by PDZ domains. *Cell*, *84*(5), 757–767. https://doi.org/10.1016/S0092-8674(00)81053-3

Campbell, M. G., Smith, B. C., Potter, C. S., Carragher, B., & Marletta, M. a. (2014). Molecular architecture of mammalian nitric oxide synthases. *Proceedings of the National Academy of Sciences*, *111*(35), E3614–E3623. https://doi.org/10.1073/pnas.1413763111

Campbell, M. G., Smith, B. C., Potter, C. S., Carragher, B., & Marletta, M. A. (2014). Molecular architecture of mammalian nitric oxide synthases. *Proceedings of the National Academy of Sciences*, *111*(35), E3614–E3623. https://doi.org/10.1073/pnas.1413763111

Castrignanò, S., Ortolani, A., Sadeghi, S. J., Di Nardo, G., Allegra, P., & Gilardi, G. (2014). Electrochemical Detection of Human Cytochrome P450 2A6 Inhibition: A Step toward Reducing Dependence on Smoking. *Analytical Chemistry*, *86*(5), 2760–2766. https://doi.org/10.1021/ac4041839

Chattopadhyaya, R., Meador, W. E., Means, A. R., & Quiocho, F. A. (1992). Calmodulin structure refined at 1.7 Å resolution. *Journal of Molecular Biology*, *228*(4), 1177–1192. https://doi.org/10.1016/0022-2836(92)90324-D

Chou, J. J., Li, S., Klee, C. B., & Bax, a. (2001). Solution structure of Ca(2+)-calmodulin reveals flexible hand-like properties of its domains. *Nature Structural Biology*, *8*(11), 990–997. https://doi.org/10.1038/nsb1101-990

Daff, S. (2010). NO synthase: Structures and mechanisms. *Nitric Oxide*, *23*(1), 1–11. https://doi.org/10.1016/j.niox.2010.03.001

Fallon, J. L., & Quiocho, F. A. (2003). A closed compact structure of native Ca2+ calmodulin. *Structure*, *11*(10), 1303–1307. https://doi.org/10.1016/j.str.2003.09.004

Fang, J., Ji, H., Lawton, G. R., Xue, F., Roman, L. J., & Silverman, R. B. (2009). L337H mutant of rat neuronal nitric oxide synthase resembles human neuronal nitric oxide synthase toward inhibitors. *Journal of Medicinal Chemistry*, *52*(14), 4533–4537. https://doi.org/10.1021/jm900380j

Finn, B. E., & Forsén, S. (1995). The evolving model of calmodulin structure,function and activation. *Structure*, *3*(1), 7–11. https://doi.org/10.1016/S0969-2126(01)00130-7

Fischmann, T. O., Hruza, a, Niu, X. D., Fossetta, J. D., Lunn, C. a, Dolphin, E., Prongay, a J., Reichert, P., Lundell, D. J., Narula, S. K., & Weber, P. C. (1999). Structural characterization of nitric oxide synthase isoforms reveals striking active-site conservation. *Nature Structural Biology*, *6*(3), 233–242. https://doi.org/10.1038/6675

Förstermann, U., & Münzel, T. (2006). Endothelial nitric oxide synthase in vascular disease: From marvel to menace. *Circulation*, *113*(13), 1708–1714. https://doi.org/10.1161/CIRCULATIONAHA.105.602532

Garcin, E. D., Bruns, C. M., Lloyd, S. J., Hosfield, D. J., Tiso, M., Gachhui, R., Stuehr, D. J., Tainer, J. A., & Getzoff, E. D. (2004). Structural Basis for Isozyme-specific Regulation of Electron Transfer in Nitric-oxide Synthase. *Journal of Biological Chemistry*, *279*(36), 37918–37927. https://doi.org/10.1074/jbc.M406204200

Geller, D. a, & Billiar, T. R. (1998). Molecular biology of nitric oxide synthases. *Cancer Metastasis Reviews*, *17*(1), 7–23. https://doi.org/10.1023/A:1005940202801

George, S. E., Su, Z., Fan, D., & Means, A. R. (1993). Calmodulin-cardiac troponin C chimeras. Effects of domain exchange on calcium binding and enzyme activation. *Journal of Biological*

Chemistry, *268*(33), 25213–25220. Retrieved from http://www.ncbi.nlm.nih.gov/pubmed/8227086

Ghosh, Dipak, K. (2003). Nitric oxide synthases: domain structure and alignment in enzyme function and control. *Frontiers in Bioscience*, *8*(1–3), d193. https://doi.org/10.2741/959

Ghosh, D., & Salerno, J. (2003). Nitric oxide synthases: domain structure and alignment in enzyme function and control. *Front Biosci*, *8*(24), 193–209. https://doi.org/10.2741/959

Greif, D. M., Sacks, D. B., & Michel, T. (2004). Calmodulin phosphorylation and modulation of endothelial nitric oxide synthase catalysis. *Proceedings of the National Academy of Sciences of the United States of America*, *101*(5), 1165–1170. https://doi.org/10.1073/pnas.0306377101

Grieshaber, D., MacKenzie, R., Vörös, J., & Reimhult, E. (2008). Electrochemical Biosensors - Sensor Principles and Architectures. *Sensors*, *8*(3), 1400–1458. https://doi.org/10.3390/s8031400

Guo, F. H., De Raeve, H. R., Rice, T. W., Stuehr, D. J., Thunnissen, F. B., & Erzurum, S. C. (1995). Continuous nitric oxide synthesis by inducible nitric oxide synthase in normal human airway epithelium in vivo. *Proceedings of the National Academy of Sciences*, *92*(17), 7809–7813. https://doi.org/10.1073/pnas.92.17.7809

Haes, A. J., & Van Duyne, R. P. (2004, August 28). A unified view of propagating and localized surface plasmon resonance biosensors. *Analytical and Bioanalytical Chemistry*. Springer-Verlag. https://doi.org/10.1007/s00216-004-2708-9

Hegyi, G., Kardos, J., Kovács, M., Málnási-Csizmadia, A., Nyitray, L., Pál, G., Radnai, L., Reményi, A., & István VenekeiKardos, J. (2013). *Introduction to Practical Biochemistry - Chapter 8: Protein-ligand interactions*. (J. Kardos, Ed.). Budapest: Eötvös Loránd University. Retrieved from http://elte.prompt.hu/sites/default/files/tananyagok/IntroductionToPracticalBiochemistry/index.html

Homola, J., Yee, S. S., & Gauglitz, G. (1999). Surface plasmon resonance sensors: review. *Sensors and Actuators B: Chemical*, *54*(1–2), 3–15. https://doi.org/10.1016/S0925-4005(98)00321-9

Ikura, M., & Ames, J. B. (2006). Genetic polymorphism and protein conformational plasticity in the calmodulin superfamily: two ways to promote multifunctionality. *Proceedings of the National Academy of Sciences of the United States of America*, *103*(5), 1159–1164. https://doi.org/10.1073/pnas.0508640103

Joseph, S., Rusling, J. F., Lvov, Y. M., Friedberg, T., & Fuhr, U. (2003). An amperometric biosensor with human CYP3A4 as a novel drug screening tool. *Biochemical Pharmacology*, *65*(11), 1817–1826. https://doi.org/10.1016/S0006-2952(03)00186-2

Joubert, J., & Malan, S. F. (2011). Novel nitric oxide synthase inhibitors: a patent review. *Expert Opinion on Therapeutic Patents*, *21*(4), 537–560. https://doi.org/10.1517/13543776.2011.556619

Karlsson, R., & Fält, A. (1997). Experimental design for kinetic analysis of protein-protein interactions with surface plasmon resonance biosensors. *Journal of Immunological Methods*, *200*(1–2), 121–133. https://doi.org/10.1016/S0022-1759(96)00195-0

Kelm, M., Dahmann, R., Wink, D., & Feelisch, M. (1997). The nitric oxide/superoxide assay. Insights into the biological chemistry of the NO/O-2. interaction. *The Journal of Biological Chemistry*, *272*(15), 9922–32.

Kroncke, K., Fehsel, K., & Kolb-Bachofen, V. (1998). Inducible nitric oxide synthase in human diseases. *Clinical and Experimental Immunology*, *113*(2), 147–156. https://doi.org/10.1046/j.1365-2249.1998.00648.x

Kuboniwa, H., Tjandra, N., Grzesiek, S., Ren, H., Klee, C. B., & Bax, A. (1995). Solution structure of calcium-free calmodulin. *Nature Structural Biology*, *2*(9), 768–776. https://doi.org/10.1038/nsb0995-768

Leferink, N. G. H., Hay, S., Rigby, S. E. J., & Scrutton, N. S. (2014). Towards the free energy landscape for catalysis in mammalian nitric oxide synthases. *FEBS Journal*, *282*(16), 3016–29. https://doi.org/10.1111/febs.13171

Li, H., Raman, C. S., Martásek, P., Masters, B. S., & Poulos, T. L. (2001). Crystallographic studies on endothelial nitric oxide synthase complexed with nitric oxide and mechanism-based inhibitors. *Biochemistry*, *40*(18), 5399–406.

Mabbott, G. A. (1983). An introduction to cyclic voltammetry. *Journal of Chemical Education*, *60*(9), 697. https://doi.org/10.1021/ed060p697

Matter, H., Kumar, H. S. A., Fedorov, R., Frey, A., Kotsonis, P., Hartmann, E., Fr??hlich, L. G., Reif, A., Pfleiderer, W., Scheurer, P., Ghosh, D. K., Schlichting, I., & Schmidt, H. H. H. W. (2005). Structural analysis of isoform-specific inhibitors targeting the tetrahydrobiopterin binding site of human nitric oxide synthases. *Journal of Medicinal Chemistry*, *48*(15), 4783–4792. https://doi.org/10.1021/jm050007x

Meffert, M. K., Premack, B. A., & Schulman, H. (1994). Nitric oxide stimulates Ca(2+)-independent synaptic vesicle release. *Neuron*, *12*(6), 1235–44. https://doi.org/10.1016/0896-6273(94)90440-5

Mehrotra, P. (2016). Biosensors and their applications - A review. *Journal of Oral Biology and Craniofacial Research*. https://doi.org/10.1016/j.jobcr.2015.12.002

Mishra, O. P., Ashraf, Q. M., & Delivoria-Papadopoulos, M. (2010). Mechanism of increased tyrosine (Tyr99) Phosphorylation of calmodulin during hypoxia in the cerebral cortex of newborn piglets: The role of nNOS-derived nitric oxide. *Neurochemical Research*, *35*(1), 67–75. https://doi.org/10.1007/s11064-009-0031-8

Nathan, C. F., & Hibbs, J. B. (1991). Role of nitric oxide synthesis in macrophage antimicrobial activity. *Current Opinion in Immunology*, *3*(1), 65–70. https://doi.org/10.1016/0952-7915(91)90079-G

Newman, E., Spratt, D. E., Mosher, J., Cheyne, B., Montgomery, H. J., Wilson, D. L., Weinberg, J. B., Smith, S. M. E., Salerno, J. C., Ghosh, D. K., & Guillemette, J. G. (2004). Differential activation of nitric-oxide synthase isozymes by calmodulin-troponin C chimeras. *Journal of Biological Chemistry*, *279*(32), 33547–33557. https://doi.org/10.1074/jbc.M403892200

Nieba, L., Nieba-Axmann, S. E., Persson, A., Hämäläinen, M., Edebratt, F., Hansson, A., Lidholm, J., Magnusson, K., Karlsson, Å. F., & Plückthun, A. (1997). BIACORE Analysis of Histidine-Tagged Proteins Using a Chelating NTA Sensor Chip. *Analytical Biochemistry*, *252*(2), 217–228. https://doi.org/10.1006/abio.1997.2326

Nishida, C. R., & de Montellano, P. R. O. (1998). Electron Transfer and Catalytic Activity of Nitric Oxide Synthases: Chimeric constructs of the neuronal, inducible and endothelial isoforms. *Journal of Biological Chemistry*, *273*(10), 5566–5571. https://doi.org/10.1074/jbc.273.10.5566

O'Shannessy, D. J., & Winzor, D. J. (1996). Interpretation of deviations from pseudo-first-order kinetic behavior in the characterization of ligand binding by biosensor technology. *Analytical Biochemistry*, *236*(2), 275–283. https://doi.org/10.1006/abio.1996.0167

Oku, Y., Ohtaki, A., Kamitori, S., Nakamura, N., Yohda, M., Ohno, H., & Kawarabayasi, Y. (2004). Structure and direct electrochemistry of cytochrome P450 from the thermoacidophilic crenarchaeon, Sulfolobus tokodaii strain 7. *Journal of Inorganic Biochemistry*, *98*(7), 1194–1199. https://doi.org/10.1016/j.jinorgbio.2004.05.002

Pattnaik, P. (2005). Surface Plasmon Resonance: Applications in Understanding Receptor–Ligand

Interaction. *Applied Biochemistry and Biotechnology*, *126*(2), 079–092. https://doi.org/10.1385/ABAB:126:2:079

Persechini, A., Blumenthal, D. K., Jarrett, H. W., Klee, C. B., Hardy, D. O., & Kretsinger, R. H. (1989). The effects of deletions in the central helix of calmodulin on enzyme activation and peptide binding. *Journal of Biological Chemistry*, *264*(14), 8052–8058. Retrieved from http://www.ncbi.nlm.nih.gov/pubmed/2542260

Persechini, A., Gansz, K. J., & Paresi, R. J. (1996). Activation of myosin light chain kinase and nitric oxide synthase activities by engineered calmodulins with duplicated or exchanged EF hand pairs. *Biochemistry*, *35*(1), 224–228. https://doi.org/10.1021/bi952383x

Persechini, A., McMillan, K., & Leakey, P. (1994). Activation of myosin light chain kinase and nitric oxide synthase activities by calmodulin fragments. *Journal of Biological Chemistry*, *269*(23), 16148–16154. Retrieved from http://www.ncbi.nlm.nih.gov/pubmed/7515878

Piazza, M., Dieckmann, T., & Guillemette, J. G. (2016). Structural Studies of a Complex between Endothelial Nitric Oxide Synthase and Calmodulin at Physiological Calcium Concentration. *Biochemistry*, *55*(42), 5962–5971. https://doi.org/10.1021/acs.biochem.6b00821

Piazza, M., Futrega, K., Spratt, D. E., Dieckmann, T., & Guillemette, J. G. (2012). Structure and dynamics of calmodulin (CaM) bound to nitric oxide synthase peptides: Effects of a phosphomimetic CaM mutation. *Biochemistry*, *51*(17), 3651–3661. https://doi.org/10.1021/bi300327z

Piazza, M., Taiakina, V., Dieckmann, T., & Guillemette, J. G. (2017). Structural Consequences of Calmodulin EF Hand Mutations. *Biochemistry*, *56*(7), 944–956. https://doi.org/10.1021/acs.biochem.6b01296

Piliarik, M., Vaisocherová, H., & Homola, J. (2009). Surface plasmon resonance biosensing. *Methods in Molecular Biology (Clifton, N.J.)*. Humana Press. https://doi.org/10.1007/978-1-60327-567-5_5

Quadroni, M., James, P., & Carafoli, E. (1994). Isolation of phosphorylated calmodulin from rat liver and identification of the in vivo phosphorylation sites. *Journal of Biological Chemistry*, *269*(23), 16116–16122. Retrieved from http://www.ncbi.nlm.nih.gov/pubmed/8206911

Raman, C. S., Li, H., Martasek, P., Kral, V., Masters, B. S. S., & Poulos, T. L. (1998). Crystal structure of constitutive endothelial nitric oxide synthase: A paradigm for pterin function involving a novel metal center. *Cell*, *95*(7), 939–950. https://doi.org/10.1016/S0092-

8674(00)81718-3

Rhoads, a R., & Friedberg, F. (1997). Sequence motifs for calmodulin recognition. *The FASEB Journal : Official Publication of the Federation of American Societies for Experimental Biology*, *11*(5), 331–340. https://doi.org/0892-6638/97/0011-0331

Roe, N. D., & Ren, J. (2012). Nitric oxide synthase uncoupling: A therapeutic target in cardiovascular diseases. *Vascular Pharmacology*, *57*(5–6), 168–172. https://doi.org/10.1016/j.vph.2012.02.004

Roman, L. J., & Masters, B. S. S. (2006). Electron transfer by neuronal nitric-oxide synthase is regulated by concerted interaction of calmodulin and two intrinsic regulatory elements. *Journal of Biological Chemistry*, *281*(32), 23111–23118. https://doi.org/10.1074/jbc.M603671200

Schmidt, H. H. H. W., & Walter, U. (1994). NO at work. *Cell*, *78*(6), 919–25. https://doi.org/10.1016/0092-8674(94)90267-4

Schmidt, H. H., Lohmann, S. M., & Walter, U. (1993). The nitric oxide and cGMP signal transduction system: regulation and mechanism of action. *Biochimica et Biophysica Acta*, *1178*(2), 153–75.

Schneider, E., & Clark, D. S. (2013). Cytochrome P450 (CYP) enzymes and the development of CYP biosensors. *Biosensors and Bioelectronics*, *39*(1), 1–13. https://doi.org/10.1016/j.bios.2012.05.043

Schreier, T., Kedes, L., & Gahlmann, R. (1990). Cloning, structural analysis, and expression of the human slow twitch skeletal muscle/cardiac troponin C gene. *Journal of Biological Chemistry*, *265*(34), 21247–21253. Retrieved from http://www.ncbi.nlm.nih.gov/pubmed/2250022

Shruthi, G., Amitha, C., & Mathew, B. B. (2014). Biosensors: A Modern Day Achievement. *Journal of Instrumentation Technology*, *2*(1), 26–39. https://doi.org/10.12691/JIT-2-1-5

Sia, S. K., Li, M. X., Spyracopoulos, L., Gagné, S. M., Liu, W., Putkey, J. A., & Sykes, B. D. (1997). Structure of cardiac muscle troponin C unexpectedly reveals a closed regulatory domain. *Journal of Biological Chemistry*, *272*(29), 18216–18221. https://doi.org/10.1074/jbc.272.29.18216

Smith, B. C., Underbakke, E. S., Kulp, D. W., Schief, W. R., & Marletta, M. A. (2013). Nitric oxide synthase domain interfaces regulate electron transfer and calmodulin activation. *Proceedings of the National Academy of Sciences of the United States of America*, *110*(38), E3577-86. https://doi.org/10.1073/pnas.1313331110

Spratt, D. E., Israel, O. K., Taiakina, V., & Guillemette, J. G. (2008). Regulation of mammalian nitric

oxide synthases by electrostatic interactions in the linker region of calmodulin. *Biochimica et Biophysica Acta - Proteins and Proteomics*, *1784*(12), 2065–2070. https://doi.org/10.1016/j.bbapap.2008.09.002

Spratt, D. E., Newman, E., Mosher, J., Ghosh, D. K., Salerno, J. C., & Guillemette, J. G. (2006). Binding and activation of nitric oxide synthase isozymes by calmodulin EF hand pairs. *FEBS Journal*, *273*(8), 1759–1771. https://doi.org/10.1111/j.1742-4658.2006.05193.x

Stevens-Truss, R., & Marletta, M. A. (1995). Interaction of calmodulin with the inducible murine macrophage nitric oxide synthase. *Biochemistry*, *34*(48), 15638–45.

Su, Z., Blazing, M. A., Fan, D., & George, S. E. (1995). The calmodulin-nitric oxide synthase interaction: Critical role of the Calmodulin latch domain in enzyme activation. *Journal of Biological Chemistry*, *270*(49), 29117–29122. https://doi.org/10.1074/jbc.270.49.29117

Sultana, N., Schenkman, J. B., & Rusling, J. F. (2007). Direct electrochemistry of cytochrome P450 reductases in surfactant and polyion films. *Electroanalysis*, *19*(24), 2499–2506. https://doi.org/10.1002/elan.200704014

Thévenot, D. R., Toth, K., Durst, R. A., & Wilson, G. S. (2001). Electrochemical biosensors: Recommended definitions and classification. *Biosensors and Bioelectronics*, *16*(1–2), 121–131. https://doi.org/10.1016/S0956-5663(01)00115-4

Venema, R. C., Sayegh, H. S., Kent, J. D., & Harrison, D. G. (1996). Identification , Characterization , and Comparison of the Calmodulin-binding Domains of the Endothelial and Inducible Nitric Oxide Synthases *, *271*(11), 6435–6440.

Volkmann, N., Martásek, P., Roman, L. J., Xu, X.-P., Page, C., Swift, M., Hanein, D., & Masters, B. S. (2014). Holoenzyme structures of endothelial nitric oxide synthase – An allosteric role for calmodulin in pivoting the FMN domain for electron transfer. *Journal of Structural Biology*, *188*(1), 46–54. https://doi.org/10.1016/j.jsb.2014.08.006

Willets, K. A., & Van Duyne, R. P. (2007). Localized Surface Plasmon Resonance Spectroscopy and Sensing. *Annual Review of Physical Chemistry*, *58*(1), 267–297. https://doi.org/10.1146/annurev.physchem.58.032806.104607

Wu, G., Berka, V., & Tsai, A. L. (2011). Binding kinetics of calmodulin with target peptides of three nitric oxide synthase isozymes. *Journal of Inorganic Biochemistry*, *105*(9), 1226–1237. https://doi.org/10.1016/j.jinorgbio.2011.06.003

Xue, F., Li, H., Fang, J., Roman, L. J., Martásek, P., Poulos, T. L., & Silverman, R. B. (2010).

Peripheral but crucial: a hydrophobic pocket (Tyr(706), Leu(337), and Met(336)) for potent and selective inhibition of neuronal nitric oxide synthase. *Bioorganic & Medicinal Chemistry Letters*, *20*(21), 6258–61. https://doi.org/10.1016/j.bmcl.2010.08.096

Yap, K. L., Kim, J., Truong, K., Sherman, M., Yuan, T., & Ikura, M. (2000). Calmodulin target database. *Journal of Structural and Functional Genomics*, *1*(1), 8–14. https://doi.org/10.1023/A:1011320027914

Yonzon, C. R., Jeoung, E., Zou, S., Schatz, G. C., Mrksich, M., & Van Duyne, R. P. (2004). A comparative analysis of localized and propagating surface plasmon resonance sensors: The binding of Concanavalin A to a monosaccharide functionalized self-assembled monolayer. *Journal of the American Chemical Society*, *126*(39), 12669–12676. https://doi.org/10.1021/ja047118q

Zhang, J., Martasek, P., Paschke, R., Shea, T., Siler Masters, B. S., & Kim, J.-J. P. (2001). Crystal Structure of the FAD/NADPH-binding Domain of Rat Neuronal Nitric-oxide Synthase: COMPARISONS WITH NADPH-CYTOCHROME P450 OXIDOREDUCTASE. *Journal of Biological Chemistry*, *276*(40), 37506–37513. https://doi.org/10.1074/jbc.M105503200

Zhang, L., Dawson, V. L., & Dawson, T. M. (2006). Role of nitric oxide in Parkinson's disease. *Pharmacol Ther*, *109*(1–2), 33–41. https://doi.org/10.1016/j.pharmthera.2005.05.007

Zhou, L., & Zhu, D.-Y. (2009). Neuronal nitric oxide synthase: structure, subcellular localization, regulation, and clinical implications. *Nitric Oxide*, *20*(4), 223–230. https://doi.org/10.1016/j.niox.2009.03.001

Zoche, M., Bienert, MichaelMichael Beyermann, § and, & Koch, K.-W. (1996). Distinct Molecular Recognition of Calmodulin-Binding Sites in the Neuronal and Macrophage Nitric Oxide Synthases: A Surface Plasmon Resonance Study†. https://doi.org/10.1021/BI960445T

Zoche, M., Bienert, M., Beyermann, M., & Koch, K. W. (1996). Distinct molecular recognition of calmodulin-binding sites in the neuronal and macrophage nitric-oxide synthases - a surface-plasmon resonance study. *Biochemistry*, *35*(26), 8742–8747. Retrieved from http://pubs.acs.org/doi/pdf/10.1021/bi960445t

Appendix A

List of CaM Plasmids Used

The plasmid constructs used to transfect E.*coli* for this study are listed here with a description specifying the protein sequence and the vector the sequence was contained in

pET9dCaM – wt CaM cloned in pET9D plasmid (p229)

pnCaMChlor – nCaM cloned in pACMIP plasmid (p

pcCaMKan – cCAM cloned in pET28a (p278)

pCaMNNKan – CAMNN cloned in pET28a (p281)

pCaMCCkan – CAMCC cloned in pET28a (p282)

pCaM-1TNCKan – CAM-1TnC cloned in pET28a (p247)

pCaM-2TNCKan – CAM-2TnC cloned in pET28a (p237)

pCaM-3TNCKan – CAM-3TnC cloned in pET28a (p248)

pCaM-4TNCKan – CAM-4TnC cloned in pET28a (p301)

pHuCaMCtermCys – Cysteine-modified C-terminal CaM cloned in pRSETA plasmid (p529)
)
pHuCaMNtermCys – Cysteine-modified N-terminal CaM cloned in pRSETA plasmid (p530)

Appendix B

OpenSPR™ By Nicoya Lifesciences Inc.

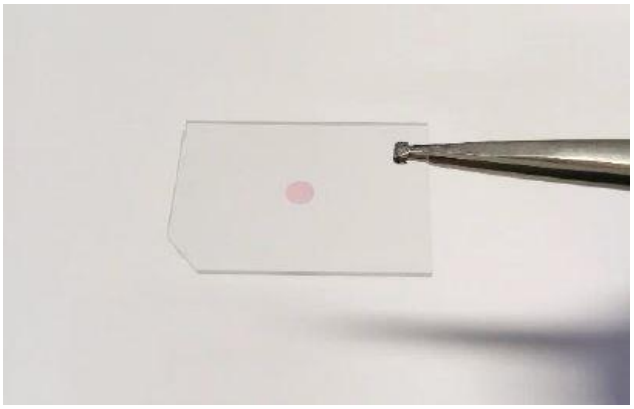

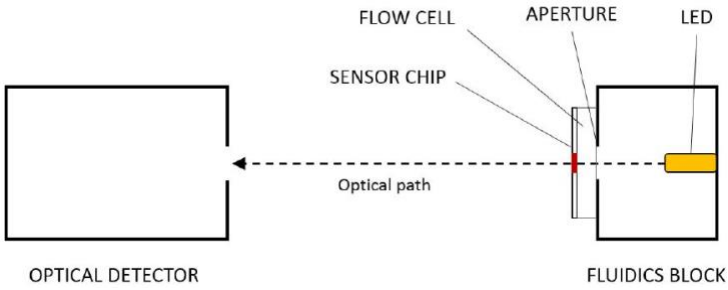

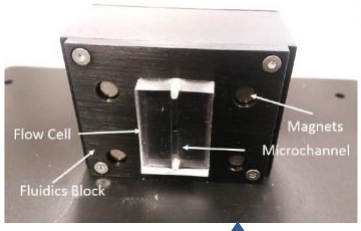

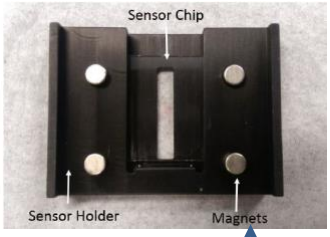

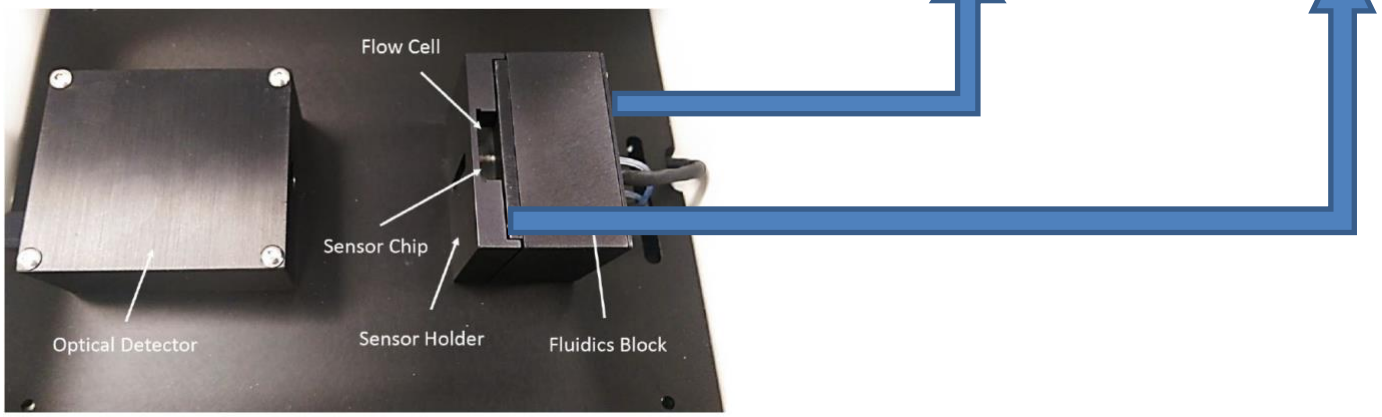

B. 1 – The OpenSPR™.
Highlighting the OpenSPR™ machine, displaying the different parts of the apparatus. Displayed with permission from John Dick, Nicoya Lifesciences Inc.

Appendix C

SPR Raw Data

Table C.1 - Binding Kinetics of CaM-TnC chimeric mutants with cNOS peptides

CaM Protein	nNOS Peptide			eNOS Peptide		
	K_{on} (10^4 $M^{-1}s^{-1}$)	K_{off} (10^{-4} s^{-1})	K_D (nM)	K_{on} (10^4 $M^{-1}s^{-1}$)	K_{off} (10^{-4} s^{-1})	K_D (nM)
wt CaM	9.77 ± 0.03	14 ± 0.003	14.4 ± 0.09	15.8 ± 0.02	18.9 ± 0.01	12.0 ± 0.17
1TnC	5.02 ± 5.20	16.4 ± 3.80	15.6 ± 1.80	9.11 ± 0.93	10.0 ± 0.27	11.1 ± 0.78
2TnC	14.8 ± 5.90	28.0 ± 9.10	19.3 ± 1.60	13.6 ± 1.90	4.13 ± 5.80	6.91 ± 1.90
3TnC	16.2 ± 1.40	35.9 ± 19.00	21.8 ± 9.80	27.7 ± 0.21	31.4 ± 1.80	19.0 ± 6.20
4TnC	26.0 ± 2.00	27.8 ± 1.50	10.7 ± 0.28	17.7 ± 3.90	69.6 ± 43.0	37.8 ± 16.0

Table C.2 - Binding kinetics of CaM EF-hand pair mutants with cNOS peptides

CaM Protein	nNOS Peptide			eNOS Peptide		
	K_{on} (10^4 $M^{-1}s^{-1}$)	K_{off} (10^{-4} s^{-1})	K_D (nM)	K_{on} (10^4 $M^{-1}s^{-1}$)	K_{off} (10^{-4} s^{-1})	K_D (nM)
wt CaM	9.77 ± 0.03	14 ± 0.003	14.4 ± 0.09	15.8 ± 0.02	18.9 ± 0.001	12.0 ± 0.17
nCaM [(a)]	NAB [(b)]	NAB	NAB	NAB	NAB	NAB
cCaM [(a)]	NAB	NAB	NAB	NAB	NAB	NAB
CaM NN	17.6 ± 2.20	18.3 ± 4.80	10.2 ± 1.5	30.5 ± 15.3	31.6 ± 0.04	10.4 ± 0.06
CaM CC	5.05 ± 7.10	23.8 ± 17.0	14.9 ± 8.9	20.9 ± 2.00	12.5 ± 3.70	6.07 ± 2.40

(a) These constructs were fit against a 1:2 binding model
(b) No apparent binding

Table C.3 - Binding Kinetics of CaM Phosphomimetic mutants with cNOS peptides

CaM Protein	nNOS Peptide			eNOS Peptide		
	K_{on} (10^4 $M^{-1}s^{-1}$)	K_{off} (10^{-4} s^{-1})	K_D (nM)	K_{on} (10^4 $M^{-1}s^{-1}$)	K_{off} (10^{-4} s^{-1})	K_D (nM)
wt CaM	9.77 ± 0.03	14 ± 0.003	14.4 ± 0.09	15.8 ± 0.02	18.9 ± 0.001	12.0 ± 0.17
T79D	6.19 ± 0.58	16.2 ± 1.70	26.1 ± 0.57	10.7 ± 2.80	20.5 ± 3.10	19.7 ± 2.00
S81D	10.5 ± 2.40	16.9 ± 3.40	16.2 ± 0.60	9.64 ± 2.60	23.9 ± 7.70	24.6 ± 2.50
T79D/S81D	5.97 ± 3.20	13.1 ± 5.30	22.8 ± 3.30	6.74 ± 13.0	20.9 ± 0.14	31.1 ± 0.32
S101D	8.79 ± 0.005	19.1 ± 0.01	21.7 ± 1.40	7.54 ± 5.60	21.4 ± 19.0	26.6 ± 4.90
Y99E	11.9 ± 1.70	30.7 ± 1.30	26.1 ± 2.60	9.17 ± 7.10	13.5 ± 10.0	14.9 ± 0.28